

Constraining the hydrology of intrusion-related ore deposits with fluid inclusions and numerical modeling

Maximilian Korges

Kumulative Dissertation

zur Erlangung des akademischen Grades
"doctor rerum naturalium"
(Dr. rer. nat.)
in der Wissenschaftsdisziplin Geochemie

eingereicht an der
Mathematisch-Naturwissenschaftlichen Fakultät
Institut für Geowissenschaften
der Universität Potsdam

Potsdam, den 26. März 2019

Supervisors:

PD Dr. Philipp Weis

GFZ German Research Centre for Geosciences, Potsdam, Germany

Prof. Dr. Jörg Erzinger

University of Potsdam, Institute of Earth and Environmental Science, Germany

Referees:

1. Referee **PD Dr. Philipp Weis**

GFZ German Research Centre for Geosciences, Potsdam, Germany

2. Referee **apl. Prof. Dr. Uwe Altenberger**

University of Potsdam, Institute of Earth and Environmental Science, Germany

3. Referee **Prof. Mag.rer.nat. Dr.mont. Frank Melcher**

Montanuniversität Leoben, Institute of Geology and Economic Geology, Austria

Published online at the

Institutional Repository of the University of Potsdam:

<https://doi.org/10.25932/publishup-43484>

<https://nbn-resolving.org/urn:nbn:de:kobv:517-opus4-434843>

*“Advice is a dangerous gift,
even from the wise to the wise,
and all courses may run ill.”*

*„Ratschläge sind eine gefährliche Gabe,
selbst von den Weisen an die Weisen,
und alle Wege mögen in die Irre führen.“*

J.R.R Tolkien

Declaration of Authorship

I hereby confirm that the thesis entitled „ Constraining the hydrology of intrusion-related ore deposits with fluid inclusions and numerical modeling” I am submitting is entirely my own original work without use of others than the indicated sources. I am aware of the University's regulations concerning plagiarism, including those regulations concerning disciplinary actions that may result from plagiarism. Any use of the works of any other author, in any form, is properly acknowledged at their point of use. I further declare that I have not submitted this thesis at any other institution in order to obtain a degree. This work was accomplished during the PhD candidature at the University of Potsdam.

Date, Signature:

26.03.2019, Maximilian Korges

Acknowledgement

This PhD was financed within the project “GRAMM –Quantifizierung lagerstättenbildender Prozesse an granitischen Intrusionen für Explorationsmodelle wirtschaftsstrategischer Spurenmetalle“ (033R149) which received founding over the r4 initiative “Innovative Technologien für Ressourceneffizienz – Bereitstellung wirtschaftsstrategischer Rohstoffe“ which was launched by the German Federal Ministry of Education and Research (BMBF – Bundesministerium für Bildung und Forschung).

My first and biggest thank goes to Dr. Philipp Weis who not only received the founding for this project but also installed the group at the GFZ Potsdam with its incredible opportunities. Philipp was the best imaginable supervisor for this PhD and without him, this entire thesis would not have been possible. Thanks for your incredible patience, guidance (especially with the companies) and the hours and hours of your time spent on discussion about few fluid inclusions or few lines of code. Additionally, thank again for trust in me when I became father and your understanding when I had to come late and leave early.

My next big thank goes to Dr. Volker Lüders for the introduction and the help in the fluid inclusion analysis and to Dr. Oscar Laurent for his help with the LA-ICP-MS and his enthusiasm when I shot my first fluid inclusion. Both of them had been a great help when I struggled with the data and its interpretation. Further thanks for thin section preparation at the GFZ to Elke Lewerenz and Uwe Dittmann as well as Christine Fischer from the University of Potsdam. Additional thank to Franziska Wilke for her guidance with the EPMA and to the many other people who helped me with various analytical possibilities (sometimes useful, sometimes not), e.g. Christian Schmidt with the Raman, Ilona Schäpan with the CL at the SEM and Prof. Uwe Altenberger with the hot CL. Further, I want to acknowledge the G.E.O.S. Freiberg Ingenieurgesellschaft mbH and Saxore Bergbau GmbH which made the sampling in the mines possible.

My last work related thanks goes to my two office and GRAMM fellows Marta Codeço and Christine Andersen who both helped with numerous discussions regarding geochemistry, fluid inclusions or code. It was a lot of fun sharing an office and thanks that both of you always had an open ear to my problems. Further, big personal thanks go to my both fellow PhD sufferers Matthias Wolf and Philipp Rieger who always had an open ear, an open bear, a cigarette when I needed one or time to listen to my complains when I thought everything goes wrong. I never thought that I will find such exceptional friends at GFZ.

The last person I want to acknowledge is my fiancée and future wife Lydia. I would have not been able to do it without you and our little daughter and sunshine Yuna.

Abstract

Magmatic-hydrothermal fluids are responsible for numerous mineralization types, including porphyry copper and granite related tin-tungsten (Sn-W) deposits. Ore formation is dependent on various factors, including, the pressure and temperature regime of the intrusions, the chemical composition of the magma and hydrothermal fluids, and fluid rock interaction during the ascent. Fluid inclusions have potential to provide direct information on the temperature, salinity, pressure and chemical composition of fluids responsible for ore formation. Numerical modeling allows the parametrization of pluton features that cannot be analyzed directly via geological observations.

Microthermometry of fluid inclusions from the Zinnwald Sn-W deposit, Erzgebirge, Germany / Czech Republic, provide evidence that the greisen mineralization is associated with a low salinity (2-10 wt.% NaCl eq.) fluid with homogenization temperatures between 350°C and 400°C. Quartzes from numerous veins are host to inclusions with the same temperatures and salinities, whereas cassiterite- and wolframite-hosted assemblages with slightly lower temperatures (around 350°C) and higher salinities (ca. 15 wt. NaCl eq.). Further, rare quartz samples contained boiling assemblages consisting of coexisting brine and vapor phases. The formation of ore minerals within the greisen is driven by invasive fluid-rock interaction, resulting in the loss of complexing agents (Cl⁻) leading to precipitation of cassiterite. The fluid inclusion record in the veins suggests boiling as the main reason for cassiterite and wolframite mineralization. Ore and coexisting gangue minerals hosted different types of fluid inclusions where the beginning boiling processes are solely preserved by the ore minerals emphasizing the importance of microthermometry in ore minerals. Further, the study indicates that boiling as a precipitation mechanism can only occur in mineralization related to shallow intrusions whereas deeper plutons prevent the fluid from boiling and can therefore form tungsten mineralization in the distal regions.

The tin mineralization in the Hämmerlein deposit, Erzgebirge, Germany, occurs within a skarn horizon and the underlying schist. Cassiterite within the skarn contains highly saline (30-50 wt% NaCl eq.) fluid inclusions, with homogenization temperatures up to 500°C, whereas cassiterites from the schist and additional greisen samples contain inclusions of lower salinity (~5 wt% NaCl eq.) and temperature (between 350 and 400°C). Inclusions in the gangue minerals (quartz, fluorite) preserve homogenization temperatures below 350°C and sphalerite showed the lowest homogenization temperatures (ca. 200°C) whereby all minerals (cassiterite from schist and greisen, gangue minerals and sphalerite) show similar salinity ranges (2-5 wt% NaCl eq.). Similar trace element contents and linear trends in the chemistry

of the inclusions suggest a common source fluid. The inclusion record in the Hämmerlein deposit documents an early exsolution of hot brines from the underlying granite which is responsible for the mineralization hosted by the skarn. Cassiterites in schist and greisen are mainly forming due to fluid-rock interaction at lower temperatures. The low temperature inclusions documented in the sphalerite mineralization as well as their generally low trace element composition in comparison to the other minerals suggests that their formation was induced by mixing with meteoric fluids.

Numerical simulations of magma chambers and overlying copper distribution document the importance of incremental growth by sills. We analyzed the cooling behavior at variable injection intervals as well as sill thicknesses. The models suggest that magma accumulation requires volumetric injection rates of at least $4 \times 10^{-4} \text{ km}^3/\text{y}$. These injection rates are further needed to form a stable magmatic-hydrothermal fluid plume above the magma chamber to ensure a constant copper precipitation and enrichment within a confined location in order to form high-grade ore shells within a narrow geological timeframe between 50 and 100 kyrs as suggested for porphyry copper deposits. The highest copper enrichment can be found in regions with steep temperature gradients, typical of regions where the magmatic-hydrothermal fluid meets the cooler ambient fluids.

Zusammenfassung

Magmatisch-hydrothermale Fluide sind verantwortlich für zahlreiche Mineralisationstypen, wie porphyrische Kupferlagerstätten und granitgebundene Zinn-Wolfram (Sn-W) Lagerstätten. Die Lagerstättenbildung ist abhängig von unterschiedlichen Faktoren, z.B. dem Druck- und Temperaturregime der Intrusion, der chemischen Zusammensetzung des Magmas und der hydrothermalen Fluide sowie den Fluid-Gesteinsreaktionen während des Aufstiegs der Fluide. Flüssigkeitseinschlüsse haben das Potential, direkte Informationen zur Temperatur, zum Salzgehalt, zum Druck und der Chemie der Fluide, welche für die Lagerstättenbildung verantwortlich sind, zu liefern. Außerdem erlauben numerische Modellierungen die Parametrisierung der Plutoneigenschaften, die nicht direkt anhand von geologischen Beobachtungen analysiert werden können.

Mikrothermometrie von Flüssigkeitseinschlüssen der Zinnwald Sn-W Lagerstätte zeigen, dass die Vergreisung an ein schwach salzhaltiges (2-10 wt.% NaCl eq.) Fluid gebunden ist, das zwischen 350°C und 400°C homogenisiert. Quarze der diversen Gänge beinhalten Einschlüsse mit den gleichen Temperaturen und Salzgehalten, wohingegen Kassiterit und Wolframit Einschlüsse mit niedrigeren Temperaturen (um 350°C) und höheren Salzgehalten zeigen (ca. 15 wt. NaCl eq.). Seltene Quarzproben enthalten kochende Einschluss-Ansammlungen, die aus koexistierenden salzreichen Lösungen und gasreichen Phasen bestehen. Die Bildung der Erzminerale des Greisens entsteht durch tiefgreifende Fluid-Gesteinsreaktionen, die den Verlust des Komplexbildners (Cl⁻) zur Folge haben, wodurch Kassiterit ausgefällt wird. Die Einschlüsse in den Gängen verdeutlichen, dass kochende Fluide der Hauptgrund für die Kassiterit- und Wolframit-Mineralisation sind. Erz- und benachbarte Gangminerale beinhalten unterschiedliche Einschlusstypen, wobei die beginnende Phasenseparation ausschließlich in den Erzmineralen erhalten ist, wodurch die Bedeutung der Mikrothermometrie in Erzmineralen hervorgehoben wird. Die Studie verdeutlicht weiterhin, dass Phasenseparation als Ausfällungsmechanismus nur in Lagerstätten gefunden werden können, die an flache Intrusionen gebunden sind, wohingegen tiefsitzende Granite die Phasenseparation verhindern. Dies hat zur Folge, dass eine Wolfram-Vererzung eher distal zur Intrusion auftritt.

Die Zinn-Mineralisation der Hämmerlein Lagerstätte tritt sowohl in einem Skarn-Horizont als auch im darunterliegenden Schiefer auf. Fluideinschlüsse in Kassiteriten des Skarns enthalten Fluide mit hohem Salzgehalt (30-50 wt% NaCl eq.) und Homogenisierungstemperaturen von bis zu 500°C, wohingegen Kassiterite des Schiefers (und von zusätzlichen Greisenproben) Einschlüsse mit geringerem Salzgehalt (~5 wt% NaCl eq.)

und geringeren Temperaturen (zwischen 350 und 400°C) enthalten. Einschlüsse in Gangmineralen (Quarz, Fluorit) zeigen Homogenisierungstemperaturen von unter 350°C und Einschlüsse in Sphaleriten konservieren die niedrigsten gemessenen Temperaturen (ca. 200°C). Allerdings haben Flüssigkeitseinschlüsse in allen Mineralen (Kassiterite der Schiefer und Greisen, Gangminerale und Sphalerit) einen annähernd gleichen Salzgehalt (2-5 wt% NaCl eq.). Ähnliche Spurenelementgehalte und lineare Trends in der Chemie der Einschlüsse deuten auf ein gemeinsames Ursprungsfluid hin. Die Einschlüsse in der Hämmerlein-Lagerstätte dokumentieren eine frühe Entmischung von heißen Fluiden mit hohem Salzgehalt aus dem darunterliegenden Granit, die für die Mineralisation im Skarn verantwortlich ist. Die Kassiterite der Schiefer und der Greisen formen sich hauptsächlich durch Fluid-Gesteinsreaktionen bei niedrigeren Temperaturen. Die Niedrigtemperatureinschlüsse in Sphalerit und die im Vergleich zu den anderen Mineralen niedrigen Spurenelementgehalte deuten auf eine Bildung aufgrund von Mischungsprozessen mit meteorischen Fluiden hin.

Numerische Simulationen von Magmenkammern und deren darüber gelegenen Kupferverteilungen dokumentieren die Wichtigkeit des schrittweisen Wachstums einer Intrusion durch Sills. Wir untersuchten das Abkühlungsverhalten bei unterschiedlichen Injektionsintervallen sowie bei unterschiedlicher Mächtigkeit des Sills. Die Modelle deuten darauf hin, dass für die Bildung der Magmakammer eine Injektionsrate von mindestens ca. $4 \times 10^{-4} \text{ km}^3/\text{y}$ benötigt wird. Solche Raten sind ebenfalls nötig um eine kontinuierliche Bildung von magmatisch-hydrothermalen Fluiden zu garantieren, denn nur dann können sich hoch vererzte Bereiche in einem kurzen geologischen Zeitraum von 50.000 bis 100.000 Jahren bilden, so wie es für porphyrische Kupferlagerstätten angenommen wird. Die höchsten Kupfergehalte bilden sich in Regionen mit steilem Temperaturgradient, also vor allem in Bereichen, wo das magmatisch-hydrothermale Fluid auf kältere meteorische Fluide trifft.

Contents

Declaration of Authorship	I
Acknowledgement.....	II
Abstract	III
Zusammenfassung.....	V
1 Introduction	1
1.1 Constraining the fluid evolution of two Sn (-W) deposits in the Erzgebirge	2
1.1.1 Geology of the Erzgebirge.....	2
1.1.2 Fluid inclusions analysis.....	7
1.1.3 Fluids in tin deposits.....	9
1.2 Constraining the magma and fluid evolution of porphyry copper deposits.....	9
1.2.1 Porphyry copper deposits	10
1.2.2 Numerical modeling of porphyry copper deposits	10
1.3 Outline of this thesis.....	11
2 Depressurization and boiling of a single magmatic fluid as a mechanism for tin-tungsten deposit formation	14
Abstract	15
2.1 Introduction	16
2.2 The Zinnwald Sn-W Deposit.....	16
2.3 Results	18
2.4 Fluid Evolution.....	19
2.5 Ore Precipitation.....	20
2.6 Conclusions	23
2.7 Appendix	23
2.7.1 Additional Geological Background	23
2.7.2 Sample Origin.....	26
2.7.3 Methods	27
2.7.4 Additional fluid chemistry data	29
3 Skarn-hosted Sn mineralization by unusually hot brines: insights from fluid inclusions in ore and gangue minerals from the polymetallic Hämmerlein deposit, Erzgebirge, Germany	34
Abstract	35
3.1 Introduction	36
3.2 The polymetallic Hämmerlein deposit	37
3.3 Samples	39

Contents

3.4 Methods	42
3.5 Results	44
3.5.1 Fluid inclusion petrography and microthermometry	44
3.5.2 Fluid compositions	48
3.5.3 Chlorite compositions.....	50
3.6 Discussion	51
3.6.1 Variations in fluid compositions	51
3.6.2 Fluid evolution	53
3.6.3 Implications	56
3.7 Conclusions	57
4 Incremental magma chamber growth and its significance for ore precipitation in porphyry copper deposits.....	59
Abstract	60
4.1 Introduction	61
4.2 Methods.....	62
4.2.1 Sill injection and magmatic fluid production	62
4.2.2 Multi-phase fluid flow and dynamic permeability	64
4.2.3 Simulation Setup	66
4.3 Results	67
4.3.1 Magma chamber growth.....	67
4.3.2 The influence of the hydrothermal system on magma chamber growth	67
4.3.3 The influence of magma chamber growth on the hydrothermal system	71
4.3.4 Copper enrichment	74
4.4 Discussion	76
4.5 Conclusions	78
5 Thesis conclusion and outlook	79
5.1 The magmatic-hydrothermal evolution of Sn deposits.....	79
5.2 IR- Microthermometry	80
5.3 Modeling	81
Bibliography	83
Appendices	96
Data Zinnwald	96
Data Hämmerlein	96
Curriculum Vitae.....	97

1 Introduction

Many of the world's ore deposits are the result of enrichment processes mediated by the circulation of hydrothermal fluids (Edwards 2012). The impact of hydrothermal fluids can be seen in a wide spectrum of environments, ranging from igneous to sedimentary, and at pressures and temperatures from shallow to deep in the lithosphere (Robb 2004). Interactions between magmatic rocks and hydrothermal fluids are relevant for numerous ore types, including porphyry copper, polymetallic skarn, granite-related Sn–W and epithermal Au–Ag–(Cu) deposit types (Edwards 2012). Ore-forming processes are particularly relevant at shallow to moderate crustal levels where both, magma and fluid are spatially and genetically related (Robb 2004). Hydrous felsic magmas typically exsolve substantial quantities of water (several wt%) either as vapor, liquid or a homogenous supercritical phase (+/- carbon dioxide). Water is particularly important, as it may contain significant concentrations of anions (e.g. Cl⁻, F⁻) capable of transporting metals (Roedder 1984). Many metals strongly partition into the fluid phase, resulting in alteration and mineralization of the host rock within or external to the intrusion (Ridley 2013; Robb 2004).

The work presented in this thesis primarily focuses on granite-related tin-(tungsten) mineralization, together with porphyry copper mineralization, both of which are styles of intrusion-related ore systems. Fluid inclusions (FIs) from two Sn (-W) deposits in the Erzgebirge were studied, (1) Zinnwald, located in the eastern Erzgebirge and, (2) Hämmerlein, in the western Erzgebirge. The Zinnwald mineralization consists of irregular cassiterite-bearing greisen bodies and horizontal cassiterite- and wolframite-bearing quartz veins within the endocontact of the Zinnwald granite (Stemprok 1965; Stemprok 1971). Although the granite is geochemically well constrained, the formation of the ore minerals and especially the relation of greisen and veins are debated (Breiter et al. 2017; Forster et al. 2011; Stemprok 1965). Fluid inclusions within the ore and gangue minerals were analyzed by microthermometry and laser ablation – inductively coupled plasma – mass spectrometry (LA-ICP-MS) in order to compare the different mineralization types and to find the triggering factor for ore precipitation.

The Hämmerlein Sn deposit is also host to ores of Zn and In, and is currently under exploration. The ore mineralization is mainly hosted by a skarn horizon with units of varying mineralogy, and additionally preserves elevated ore grades in the underlying schist unit (Schuppan and Hiller 2012). The main ore mineral is cassiterite and can be found in both lithologies. The formation of the skarn units and its relation to the mineralizing fluids is still under debate. Currently, various studies have analyzed the geochemical composition of the

skarn itself (Kern et al. 2018; Lefebvre et al. 2018). However, fluid composition, together with the precipitation mechanism, remains elusive. Fluid inclusions were analyzed (microthermometry and LA-ICP-MS) in ore and gangue minerals hosted by the schist and by the skarns, in order to compare both mineralization types and find a possible connection between them. The main gangue minerals were quartz, fluorite and chlorite. Even though chlorite does not contain fluid inclusions, its chemical composition was determined by electron probe micro analysis (EPMA) in order to apply mineral thermometry and compare it with the intergrown ore minerals.

Numerical simulations were performed with the goal to identify magmatic emplacement rates necessary for incremental growth of a magma chamber using the Complex System Modeling Platform (CSMP++) software. We developed a new functionality which allows the episodic input of sills with varying dimensions at different time intervals. Numerical simulations were conducted in order to analyze the influence of an incrementally growing magma chamber on potential copper ore formation. Furthermore, we compared the results from the incremental growth setups with simulations of a single large cooling magma chamber.

1.1 Constraining the fluid evolution of two Sn (-W) deposits in the Erzgebirge

The following subchapter provides additional information on the fluid inclusion studies of the two ore deposits in the Erzgebirge and includes a general overview of the relevant geology of the Erzgebirge, a short introduction to fluid inclusions and fluids in tin mineralization. The results and interpretations of the ore-forming processes are described in detail in chapters 2 and 3.

1.1.1 Geology of the Erzgebirge

The evolution of the Erzgebirge is a history of diverse geological settings, ranging from an active continental margin over rifting to a continent-continent collision (resulting in metamorphism and magmatism). These various contexts are preserved in the complex geology of the Erzgebirge, which consists of 75% of metamorphic rocks, especially gneisses (Sebastian 2013). A majority of the metamorphic rocks formed during the Variscan orogeny reached up to ultra-high pressure and ultra-high temperature conditions (Kroner et al. 2007). The protoliths are magmatic and sedimentary rocks of Cadomian and Ordovician age. The Erzgebirge is, similar to other Variscan massifs (e.g. Cornwall, Massif Central and parts of the Iberian Mountains), a metallogenetic fertile region known for granite-related Sn-W

deposits (Romer and Kroner 2015). The formation of Sn-W deposits is related to the post-Variscan magmatism focused in the eastern and western part of the Erzgebirge (Romer and Kroner 2016).

1.1.1.1 Granites of the Variscan orogeny

Variscan magmatic rocks form the second largest part of the Erzgebirge (Sebastian 2013). The collision of Laurussia and Gondwana resulted in thickening of the crust, which lead to the formation of granites that are the most common igneous rocks, similar to other continent-continent collisions (Linnemann and Romer 2010; Sebastian 2013). All the granites in the Erzgebirge represent crustal melts, with geochemical compositions reflecting the lithological diversity among the metamorphosed volcano-sedimentary rocks that characterize the granite source (Kroner et al. 2007). The granites are located along two zones (Fig. 1-1) in the eastern and western Erzgebirge and have been mostly emplaced between 327 and 318 Ma (Romer et al. 2012). In the western Erzgebirge the majority of granites have been emplaced at a deeper level than those of the eastern Erzgebirge (Romer et al. 2012).

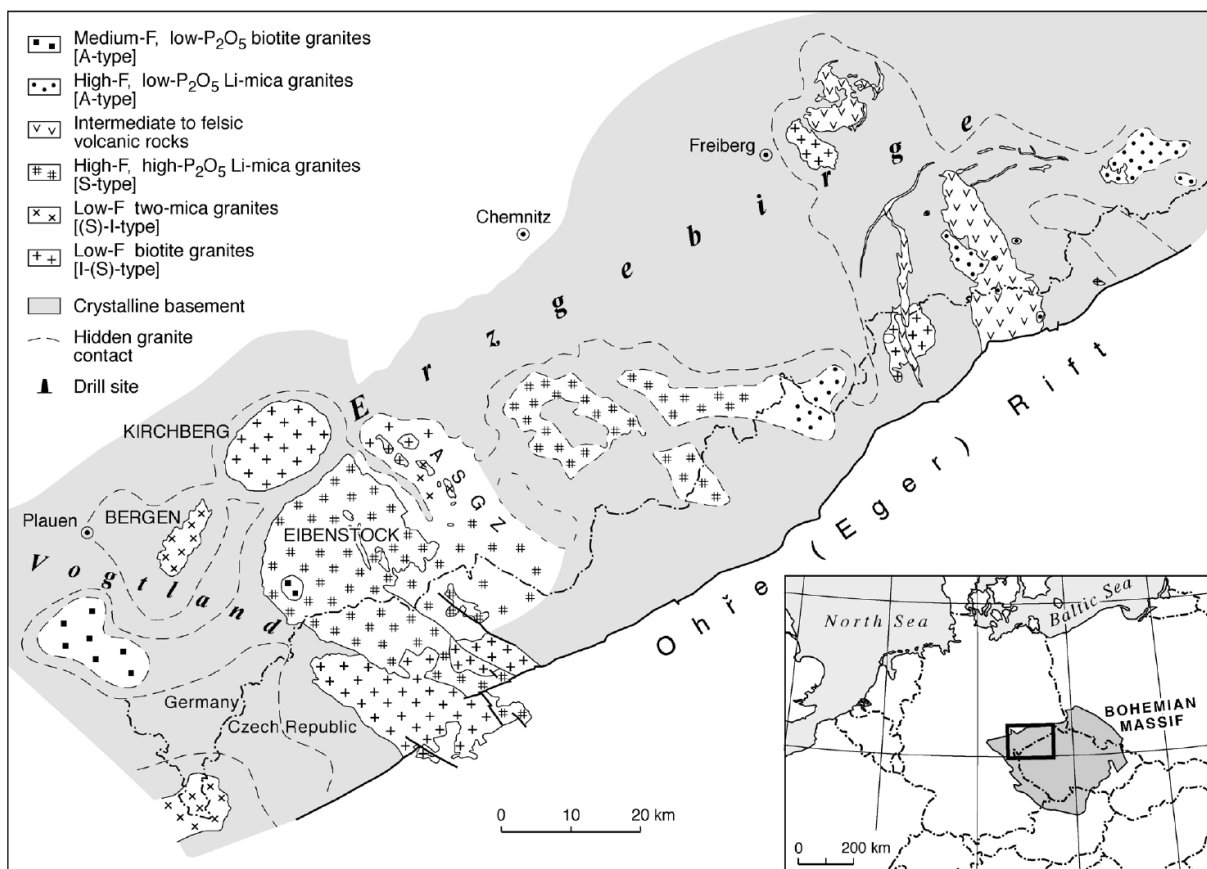


Fig. 1-1 Geological overview map of the Erzgebirge–Vogtland Zone with the different granite types (Förster 2012)

The Erzgebirge granites can be subdivided into five groups of magmatic suites, according to chemical composition and mineralogy (Förster et al. 1998; Förster et al. 1999; Förster and Romer 2010). These groups can also be an indication of the ore-forming potential of the granites. The two groups that are mainly related to Sn-W mineralization are the Li-rich mica granites of the (1) Eibenstock group and the (2) Schellerhau group. Group (1) granites are rich in fluorine and P_2O_5 , and are thereby defined as S-type. The protoliths of the S-type granites were Paleozoic sediments and Cadomian crust (mainly greywackes and granodiorites). These S-type granites can be found in the eastern and central Erzgebirge. Group (2) is defined by low P_2O_5 and high F contents and is mainly located in the eastern Erzgebirge. The Zinnwald granite is part of this group, which is further defined as A-type (anorogenous). The biotite granites of the Gottesberg group (3) and the Kirchberg group (4) as well as the two-mica granites of the Bergen group (5) show less relationship to any mineralization. Groups (4) and (5) are P_2O_5 and fluorine poor and are defined as I-(S)-type granites. Group (3) shows medium F and low P_2O_5 contents, is predominantly located in the western Erzgebirge and has an A-I type signature.

The overall chemical diversity of the Variscan granites in the Erzgebirge can be explained by melting of a heterogeneous, layered crust, which is exposed by the Saxo-Thuringian basement (Förster et al. 1999). The character of the granites is caused by a combination of various characteristics of the source (Förster and Romer 2010): (1) low degrees of melting; (2) wide distribution of fertile lithologies; (3) interlayering with less fertile but Sn-W-rich micaceous metapelites and; (4) mantle-derived intermediate to mafic rocks (whereby both interlayers can be a major source of fluid). These features of the source can explain the large quantities of granites and the high S-W content of Variscan granites in the Erzgebirge.

1.1.1.2 Eastern Erzgebirge

The eastern Erzgebirge was highly influenced by late- and post-orogenic Variscan uplift and exhumation, along with intense felsic magmatism that formed the eastern Erzgebirge volcano-plutonic complex (Stemprok et al. 2003). This complex is dominated by the 630 km² Altenberg-Teplice caldera, which has an elliptical structure that is 18x35 km across. The caldera stage is followed by several topaz-bearing rare-metal intrusions, including several small granites (e.g. Zinnwald, Sadisdorf) and the Schellerhau granite complex (Müller and Seltmann 2012). The intrusions of the igneous rocks of the eastern Erzgebirge started

with the Niederbobritzsches granites at 320 ± 6 Ma and continued over the following 25 Ma ending with the intrusions of the Schönfeld complex (Müller and Seltmann 2012).

The Altenberg-Sadisdorf-Zinnwald area (Fig. 1-2) is the biggest tin district in the Erzgebirge, and mineralization is related to small Li-mica granites (Sebastian 2013). The deposits are mainly located at the endocontact or exocontact of the granite (Seifert et al. 2011) where they form vein-like and/or greisen mineralization, which has mostly been mined for cassiterite, along with copper, molybdenum and tungsten. However, the eastern Erzgebirge has not been actively mined since the 1990s, despite the granitic complexes hosting large amounts of various metals (Lehmann 2006; Sebastian 2013). Current exploration mainly focuses on Li in the Zinnwald granite body, although the Altenberg as well as the Sadisdorf granite are currently explored for Sn and W.

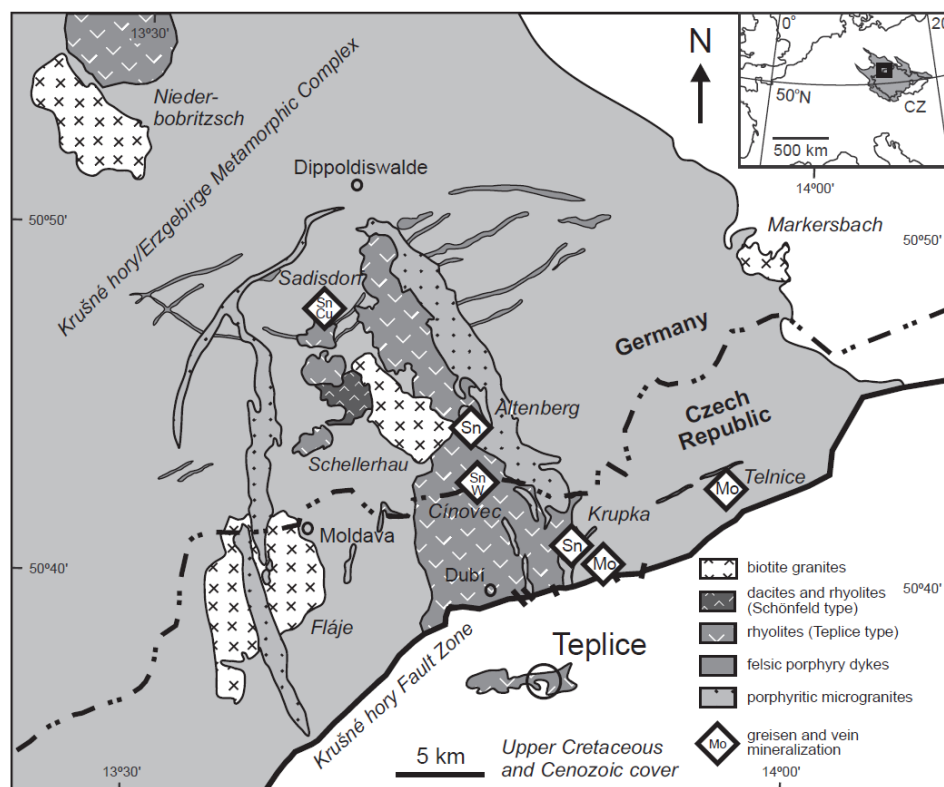


Fig. 1-2 Geological units of the Eastern Erzgebirge and the location of the Čínovec/Zinnwald, Krupka and Altenberg Sn–W–Mo deposits (Dolejš and Stemprok 2001)

1.1.1.3 Western Erzgebirge

The western Erzgebirge is host to three large granitic complexes (Fig. 1-3). The Eibenstock granite is the biggest pluton in the entire Erzgebirge and covers an area of 850 km^2 (Sebastian 2013). The smaller Kirchberger granite has a surface area of 107 km^2 but is still the second largest granite. The smallest and westernmost granite is the Bergener granite with an

1.1.2 Fluid inclusions analysis

Paleo-processes of fluid-rock interaction, especially those at high pressure and temperature, cannot be observed in an outcrop or drillcore (Bakker 2016). Although the initial and final rock may be preserved, the initial and final bulk fluids have vanished. Thermodynamic modeling allows some fluid properties to be calculated from the rock, but many parameters cannot be estimated (Roedder 1984). Fortunately, some minerals trap fluid inclusions (FIs) that provide the only direct source of information on paleo-fluids in the crust (Bodnar 2003). The favorability of the mineral host to trap FIs depends on the wetting properties during the initial fluid trapping (Bodnar 2003). Moreover, inclusions can only be trapped if the crystal has imperfect cleavage and if it does not recrystallize during its post-entrapment history (Van den Kerkhof and Hein 2001). Excellent hosts for fluid inclusion analysis are quartz, fluorite, calcite and anhydrite and (under good conditions) also other carbonates, halites, sulphides and oxides (Roedder 1984).

Three formation mechanisms for fluid inclusions can be distinguished with respect to growth of the host crystal (Goldstein 2003):

- (1) Primary fluid inclusions were trapped during the crystal growth and nucleated on surface imperfections. Hereby, fast crystal growth rates favor inclusion entrapment. Those FIs represent fluids in which the host crystal was growing.
- (2) Secondary FIs are trapped after the host crystal has finished growing, and are therefore younger than the fluid in which the host crystal grew. They form in fractures within minerals whereby the fractures heal afterwards due to the property of minerals to minimize the surface free energy. Such healing processes are particularly fast under high-temperature conditions (e.g. days at 600°C) and slower and often incomplete at low temperatures.
- (3) Pseudosecondary FIs are trapped during the deformation of the growing host crystal and have the same formation mechanism as secondary inclusions but can have the same geological significance as primary inclusions, if the trails clearly terminate at growth zones and are absent in the youngest parts of the same crystal.

Fluid inclusions can preserve several characteristics that are crucial in order to understand the fluid system. The fluid composition can be directly analyzed using LA-ICP-MS (Bodnar 2003). Furthermore, fluid inclusions are the only direct source of the paleo-fluid density or the molar volume, and also preserve the fluid state during trapping (1, 2, 3 etc. phases), providing valuable indications for phase separation processes, potentially important for ore formation (Bodnar 2003). Fluid inclusion assemblages further record the temperature and pressure conditions of entrapment (Van den Kerkhof and Hein 2001). Homogenous fluid

inclusion assemblages (= a group of cogenetic inclusions as proven by petrographic evidence) indicate minimal temperatures and pressures in contrast to heterogeneously entrapped assemblages, which give exact T and P values of the entrapment condition (Moncada et al. 2017). Several generations of FIs can preserve the evolution of the various parameters through time (Bakker 2016).

Fluid inclusions are primarily analyzed by microthermometry (Fig. 1-4). In order to determine the homogenization temperatures and the salinity of individual inclusions, the FIs are heated and frozen (Bodnar 2003; Samson et al. 2003; Roedder 1984). During heating, the most common water-rich two-phase (liquid and vapor) inclusions homogenize by disappearance of one component, mostly of the vapor phase (Samson et al. 2003). Freezing of those inclusions results in ice nucleation. If inclusions are heated again after freezing, it leads to melting of the ice within the FIs (Samson et al. 2003). The melting temperature of the ice is a direct proxy for the salinity of the liquid within the FI (Bodnar 2003; Goldstein 2003). Highly saline FIs contain salt crystals that dissolve during heating experiments. The melting temperature of the salt crystal provides information on the salinity (Samson et al. 2003) of the inclusion during entrapment (considering that the FIs are trapped as a homogenous fluid).

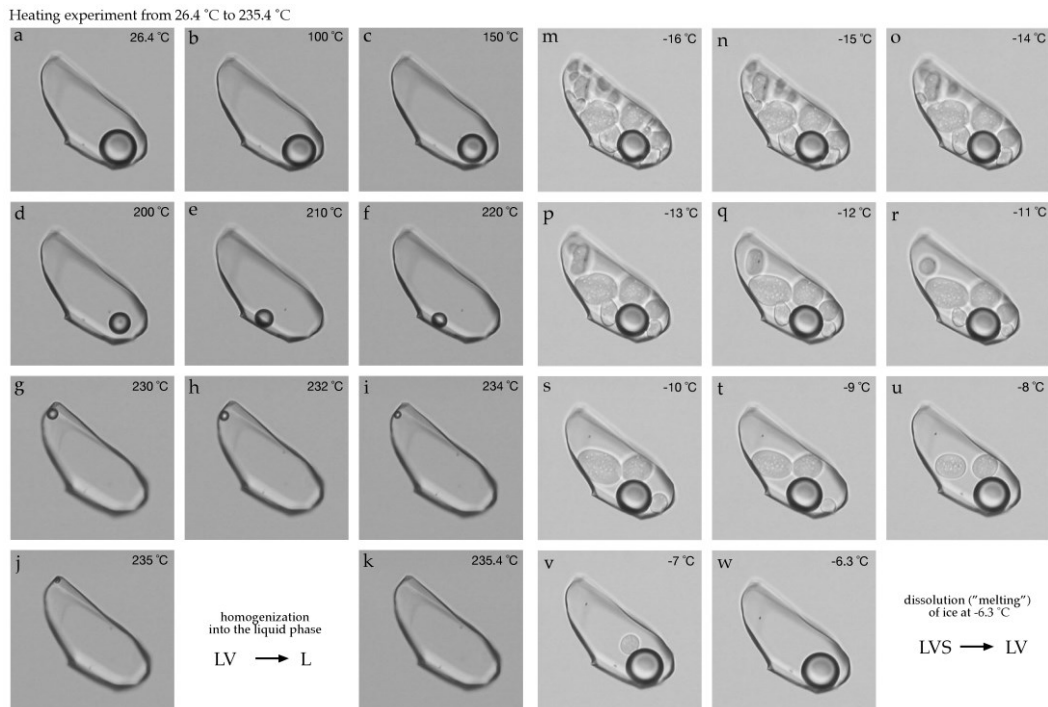


Fig 1-4 Synthetically produced fluid inclusions showing the principle measurement methods for analysis of fluid inclusions (Bakker 2016)

1.1.3 Fluids in tin deposits

Tin deposits are commonly forming by saline fluids that are initially equilibrated with a high-temperature (Naumov et al. 2011) granitic source. Ore forming fluids then react irreversibly with rocks and/or fluids in a cooler depositional environment (Heinrich 1990). High tin concentrations (hundreds of possibly thousands of ppm) can be transported as complexes (mostly with Cl) to lower temperature (<400°C) depositional environments (Durisova et al. 1979). Recent studies by Schmidt (2018) showed that the HCl molality is the crucial parameter for hydrothermal Sn transport. Therefore, the precipitation of Sn seems to be mostly independent of the oxidation state, pH or pressure, and directly bound to the availability of Cl (Schmidt 2018). Cassiterite thus precipitates if the activity of HCl decreases (if Sn loses its Cl ligand), e.g. by reaction with wall rocks (greisenization/skarn formation), by dilution (mixing with ambient fluid) or by boiling (Schmidt 2018).

Numerous studies on fluid inclusions in tin deposits have shown that the typical formation temperature of gangue and ore minerals lies between of 300 and 500°C with most determinations ranging from 300 to 400°C (Naumov et al. 2011). Pressure estimations of those fluids mainly range between 50 and 150 MPa but can vary from 10 MPa to 640 MPa, with most inclusions showing salinities below 10 wt.% NaCl eq. (Naumov et al. 2011). Few studies have analyzed the fluid inclusion record of ore minerals due to their (mostly) opaque appearance (Lüders 1996; Lüders and Ziemann 1999; Kouzmanov et al. 2010). Infra-red microscopy and microthermometry is therefore a powerful tool to investigate the ore-forming fluid directly in ore minerals, rather than coexisting gangue minerals (Campbell and Panter 1990). Fluid inclusions measured via IR-microthermometry have to be treated carefully due to the radiative heating of the sample during analysis (Casanova et al. 2018). Only very low light intensities should be applied in order to minimize the error. Furthermore, the low optical resolution at such wavelength and the dark appearance of the fluid inclusion walls are a big challenge during measurements (Wilkinson 2001). Nevertheless, the information revealed by FIs in opaque/less transparent ore minerals can give new insights in the deposition processes.

1.2 Constraining the magma and fluid evolution of porphyry copper deposits

The interaction between pluton and ore is still highly debated in all magmatic-hydrothermal derived ore types. Most studies which analyze this interaction focus on porphyry copper deposits due to their economic importance. The better constraints obtained by geochemistry, geological observations, fluid inclusions and other simulations are the reasons for the application of the new developed functionalities to porphyry copper deposits. Numerical

simulations were processed in order to understand the magma growth and behavior as well as the fluid evolution above the magma chamber which form porphyry copper deposits. Ongoing development of the software can possibly allow the implantation to Sn-W deposits during a later stage of the research. Currently, it is not possible to simulate the behavior of Sn and W within the fluid because the precipitation is not only dependent on the temperature (as for Cu) but is based on various features (as presented in the following chapters of this thesis).

1.2.1 Porphyry copper deposits

Globally, porphyry deposits are forming our most important Cu resource, as well as 20% of Au, half of Mo and important sources for Pb, Zn and Ag (Sillitoe 2010). The mineralization itself can be divided into a deeper part, which mainly hosts Cu-Mo-Au and possible skarns, and an upper part that can contain hydrothermal Au-Ag-Cu ores (Wilkinson 2013). The ore minerals are associated with numerous quartz veins, which form during multiple cycles of magmatic-hydrothermal fluid influx (Landtwing et al. 2005). The fluid exsolving magma chamber typically has a granitoid composition, batholithic dimensions and consists of equigranular, multiphase intrusions (Sillitoe 2010). They can be the source for single deposits (Mount Polley, British Columbia) as well as for clusters (El Abra, Chile; Highland Valley, British Columbia) of several discrete deposits (Fraser et al. 1995; Sillitoe 2010). The parental magma chambers are not directly accessible due to their typical intrusion depth of ca. 5 km (Chiaradia and Caricchi 2017; Sillitoe 1973), unless post-mineralization tectonic uplift leads to exposure close to the earth surface, e.g. Yerington district, Nevada (Dilles 1987; Dilles and Proffett 1995; Sillitoe 2010). The formation of porphyry copper systems requires the accumulation of magma while allowing large quantities of fluids to exsolve from the crystallizing magma/melt (Burnham and Ohmoto 1980; Chiaradia and Caricchi 2017; Cline and Bodnar 1991; Dilles 1987). The hydrothermal fluid outflow is focused by geological structures and/or self-organization by convection and transports the ore-forming elements to shallow depths (Fournier 1999). A detailed summary of the formation of porphyry copper deposits can be found in Sillitoe (2010).

1.2.2 Numerical modeling of porphyry copper deposits

Numerical simulations are performed because plutonic rocks are only rarely exposed (e.g. Yerington district, Nevada), and direct analysis is only possible in a limited number of cases (Sillitoe 2010). Numerical simulations, therefore, provide a powerful tool for understanding the development of magma chambers responsible/important for the formation

of porphyry copper deposits. Modeling of magmatic-hydrothermal fluid flow, however, requires fluid properties ranging from magmatic to ambient temperatures and pressures as well as fluid-vapor-salt phase relations. Importantly, multiphase fluid flow can be calculated using the Complex System Modeling Platform (CSMP++), which is able to combine these crucial parameters with accurate equations of state for the H₂O-NaCl system (Driesner and Heinrich 2007; Driesner 2007). Although fluid producing magma chambers have been analyzed by various numerical modeling studies, most approaches have included a large magma chamber at the beginning of the simulations with hundreds of km³ of magma being instantaneously emplaced in a cold host rock (Cathles et al. 1997; Norton and Knight 1977; Steinberger et al. 2013; Weis 2015). Geochronological data, however, suggest that the emplacement of a pluton resulted from step by step agglomeration of discrete pulses of sills (de Saint Blanquat et al. 2011; Menand 2008; Michel et al. 2008; Pasquarè and Tibaldi 2007) over several million years (Coleman et al. 2004; Matzel et al. 2006), whereas the Cu mineralization itself developed only over a short period of 50.000 to 100.000 years (Chelle-Michou et al. 2015; Gilmer et al. 2017; Tapster et al. 2016; Von Quadt et al. 2011).

1.3 Outline of this thesis

The thesis consists of five chapters. Chapter 1 provides a general introduction to the various topics of the manuscripts, including, a background for the regional geology of the Erzgebirge; a short introduction to fluid inclusions; fluid chemistry in tin (-tungsten) deposits and; a short background of the numerical modeling approaches in porphyry copper deposits. Chapter 5 ends the thesis with a discussion of the outcomes of the presented work. Chapter 2 – 4 are written as stand-alone manuscripts for publication in peer-reviewed scientific journals. Chapter 2 has been published in *Geology*, the manuscript of chapter 3 has been submitted to *Mineralium Deposita* and is currently under revision after receiving positive reviews, and the manuscript of chapter 4 is currently in preparation for submission to *Earth and Planetary Sciences Letters* or *Geochemistry, Geophysics, Geosystems*.

Chapter 2: “Depressurization and boiling of a single magmatic fluid as a mechanism for tin-tungsten deposit formation” has been published in *Geology* in January 2018. Maximilian Korges is the first author of this study. The chapter shows the importance of fluid inclusion analysis in opaque ore minerals, which were key for understanding the precipitation processes (boiling) in the veins of the Zinnwald deposit. The start of the phase separation within the veins was only preserved in cassiterite/wolframite and was absent in the coexisting gangue minerals (mainly quartz). Inclusions in quartz mainly document a precipitation regime before

the boiling processes occur and only rarely show heterogeneously entrapped fluid inclusion assemblages, which occurred in the successive boiling process.

Sampling was done by Maximilian Korges and supported by the co-authors as well as the team of the Zinnwald visitor mine “Vereinigt Zwitterfeld zu Zinnwald”. Further samples were contributed by the mineral collections Federal Institute for Geosciences and Natural Resources (BGR), the Humboldt University Berlin and the ETH Zurich. The preparation of thin sections was carried out by E. Lewerenz and W. Dittmann at GFZ Potsdam, as well as Christine Fischer from the University of Potsdam. Microthermometry and LA-ICP-MS work was done by Maximilian Korges with technical guidance of V. Lüders and O. Laurent respectively. Evaluation and interpretation of the data were done together with P. Weis and V. Lüders. Maximilian Korges has written the paper which was edited by the co-authors.

Chapter 3: “Skarn-hosted Sn mineralization by unusually hot brines: insights from fluid inclusions in ore and gangue minerals from the polymetallic Hämmerlein deposit, Erzgebirge, Germany” has been submitted to *Mineralium Deposita* and received positive reviews. Inclusions entrapped in cassiterite provide evidence of two ore-forming events. The first mineralization stage occurred during the beginning of the magmatic-hydrothermal evolution and is documented by high saline inclusions forming at around 500°C, which were mainly entrapped in the cassiterites of the skarn horizon. The second mineralization stage occurred at lower temperatures and intermediate salinities and can be found especially within schists which occur below the skarn units.

Maximilian Korges is the first author of this manuscript. Sampling was done by Maximilian Korges and supported by P. Weis as well as M. Rocher (Saxore Bergbau) for guidance within the mine. The preparation of thin sections was carried out by E. Lewerenz and W. Dittmann at GFZ Potsdam, as well as Christine Fischer from the University of Potsdam. Microthermometry and LA-ICP-MS work was done by Maximilian Korges. EPMA analysis was done by Franziska Wilke and evaluated by Maximilian Korges. Evaluation and interpretation of the data were done together with P. Weis and V. Lüders. Maximilian Korges has written the paper which was edited by the co-authors. The readers must be aware of potential differences between the future publication and this chapter.

Chapter 4: “Incremental magma chamber growth and its significance for ore precipitation in porphyry copper deposits” is written as a manuscript for submission to *Earth and Planetary Sciences Letters* or *Geochemistry, Geophysics, Geosystems*. The manuscript compares various numerical simulations setups of incremental magma growth and its influence for a potential copper precipitation. It is further highlighted that a volumetric magmatic emplacement rate of

at least ca 4×10^{-4} km³/y is needed for formation of a magma chamber and additionally comparing the setups to intrusion of only one big magma chamber at the beginning of the simulation.

Maximilian Korges is the first author of this manuscript. The functionality which was added in the CSMP++ code was written by Maximilian Korges and completed by P. Weis who also edited other parts of the code for this specific setup. Evaluation and interpretation of the data were done together with P. Weis and C. Andersen. Maximilian Korges has written the manuscript, which was edited by the co-authors. The readers must be aware of potential differences between the future publication and this chapter.

2 Depressurization and boiling of a single magmatic fluid as a mechanism for tin-tungsten deposit formation

Maximilian Korges¹, Philipp Weis¹, Volker Lüders¹, and Oscar Laurent²

¹*GFZ German Research Centre for Geosciences, Telegrafenberg, 14473 Potsdam, Germany*

²*ETH Zurich, Institute of Geochemistry and Petrology, 8092 Zurich, Switzerland*

Published in *Geology* (2018):46, 1, pp. 75-79.

The chapter is completed by additional information regarding the regional geology, methods and chemical data. Due to space limitations these information were also not in the original manuscript but were included in the supplementary files.

Abstract

Tin (Sn) and tungsten (W) mineralization are often associated with each other in relation to highly evolved granites, but economical ore grades are restricted to rare global occurrences and mineralization styles are highly variable, indicating different mechanisms for ore formation. The Sn-W Zinnwald deposit in the Erzgebirge (Germany/Czech Republic) in the roof zone of a Variscan Li-F granite hosts two contrasting styles of mineralization: 1) cassiterite (Sn) in greisen bodies and 2) cassiterite and wolframite (W) in predominantly sub-horizontal quartz-rich veins. The relative timing and causes for ore formation remain elusive. Studies of fluid inclusion assemblages in wolframite, cassiterite and quartz samples from greisen and veins by conventional and infrared microthermometry and LA-ICP-MS analyses have revealed compelling evidence that all elements required for the formation of the Zinnwald Sn-W deposit were contained in a single parental magmatic-hydrothermal fluid that underwent two main processes: 1) fluid-rock interaction during Sn-greisen formation and 2) depressurization and vapor loss leading to ore precipitation in quartz-Sn-W veins. The results also show that fluid inclusion assemblages in ore minerals can document fluid processes that are absent in the fluid inclusion record of gangue minerals. The study further highlights the role of phase separation in the formation of W-rich Sn-deposits and indicates that W-deposits in distal parts of evolved granites may be restricted to fluids derived from deeper-seated plutons.

2.1 Introduction

Natural enrichments of tin (Sn) and tungsten (W) to economic grades are typically associated with evolved A- or S-type granites in major orogenic settings (e.g. Romer and Kroner (2016) and references therein). Sn, W or Sn-W mineralization are hosted in metasomatized roof zones (greisen) and/or hydrothermal veins, which can be located proximal within the intrusion, e.g., Erzgebirge, Germany/Czech Republic (Stemprok 1967) and East Kemptville, Canada (Halter et al. 1998), or may extend to more distal parts into the surrounding rocks, e.g., Panasqueira, Portugal (Kelly and Rye 1979) and Pasto Bueno, Peru (Landis and Rye 1974). However, fluid sources and pathways as well as their temporal and spatial evolution which lead to Sn-W ore precipitation often remain debated.

Within the same deposit, precipitation of cassiterite, wolframite and other ore minerals have occurred contemporaneously or successively, indicating that several geologic controls can trigger ore deposition. Formation of Sn-greisens has mainly been attributed to alteration of feldspars to quartz and mica by magmatic fluids (Stemprok 1987; Stemprok and Sulcek 1969). Sn-vein formation at Mole Granite, Australia (Audétat et al. 2000) and W-Sn-vein formation at Vaulry, France (Vallance et al. 2001) are related to mixing of magmatic and meteoric fluids. W-mineralization at Panasqueira has been attributed to fluid-rock reactions of W-rich, Fe-poor magmatic fluids with Fe-rich metasedimentary host rocks (Lecumberri-Sanchez et al. 2017). Phase separation has further been identified as a potential mechanism for ore deposition, albeit with a subordinate efficiency to form an economic ore deposit (Heinrich 1990). About half of the global W production comes from vein, stockwork, breccia, and porphyry deposits and only 5% from disseminated greisen mineralization, which in contrast is the main source for Sn (Pitfield et al. 2011).

Infrared microthermometry and LA-ICP-MS analyses of fluid inclusion assemblages (FIA) in ore minerals such as cassiterite and wolframite can provide direct insights to temperature, salinity and chemistry of ore-forming fluids (Lüders 2017), but LA-ICP-MS analyses of ore-hosted fluid inclusions (FIs) require a very precise documentation of the location of fluid inclusions prior to ablation (Kouzmanov et al. 2010).

2.2 The Zinnwald Sn-W Deposit

The Zinnwald/Cínovec deposit is located on both sides of the German/Czech border in the eastern part of the Erzgebirge, which is part of the Saxothuringian Zone of the Variscan Orogeny (Fig. 2-1). The deposit is related to the evolved Li-F Zinnwald granite (Förster et al. 1998) and hosts two mineralization styles: 1) Sn in greisen (Fig. 2-1B) and 2) proximal Sn-W-

veins (Fig. 2-1D) within the metasomatized roof zone of the granitic intrusion. Fluid inclusion microthermometry in quartz and cassiterite from tin-tungsten deposits in the Erzgebirge showed a predominance of intermediate-density fluids and temperatures between 360 and 400 °C for ore formation (Thomas 1982). Studies of wolframite-hosted fluid inclusions from the Zinnwald deposit yielded homogenization temperatures between 300 and 360 °C and variable salinity (Lüders 1996). Few LA-ICP-MS measurements of fluid inclusions in quartz from the Zinnwald Sn-W deposit have been performed in rare boiling assemblages at higher temperatures of ca. 470 °C (Heinrich et al. 1999). However, the fluid evolution in Zinnwald and ore formation remains debated.

For this study, we collected samples from quartz veins from the German part of the mine at the northern flank of the granite (Fig. 2-1A). Additional historic samples containing euhedral crystals of cassiterite, wolframite and quartz were provided from mineral collections. Fluid inclusion in 25 selected samples of quartz and ore minerals were studied by microthermometry (convectonal and infrared), isotope ratio mass spectrometry and LA-ICP-MS.

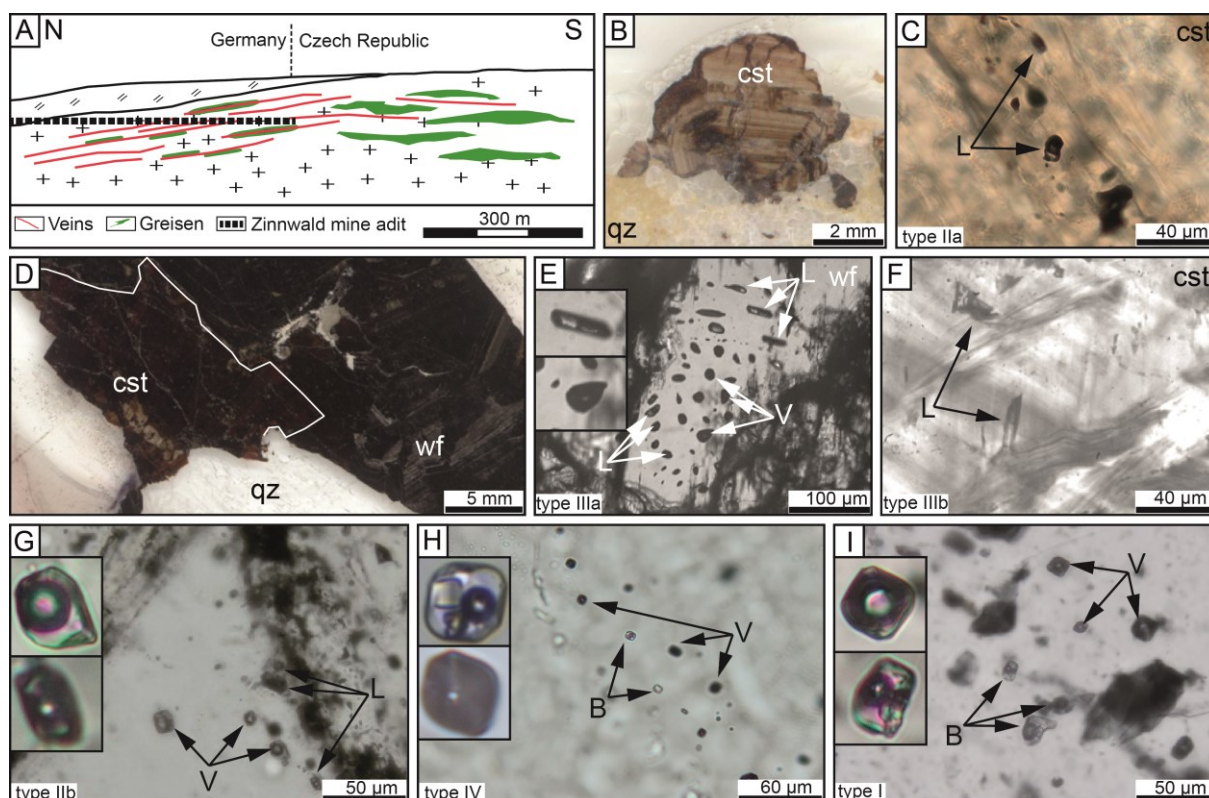


Fig. 2-1 A: Schematic cross section through the roof zone of the Zinnwald granite showing the sampling area (adit) with greisen and vein-type mineralization. B + C: Greisen sample with quartz (qz) and cassiterite (cst) showing growth zones with primary liquid-rich (L) inclusions. D: Wolframite (wf) intimately intergrown with cassiterite indicating contemporaneous deposition in the vein. E: Wolframite with a boiling assemblage of liquid-rich and vapor-rich (V) inclusions. F: Cassiterite with

intermediate density inclusions orientated along growth zones. G: Fluid inclusion assemblage in the wake of a quartz growth zone showing different homogenization behavior: L to liquid, V to vapor. H: Trail of a boiling assemblage with pseudosecondary brine-type inclusions (B) in quartz. I: High-temperature boiling assemblage in a quartz growth zone with hypersaline brines

2.3 Results

The studied quartz samples are often recrystallized and host abundant secondary fluid inclusions. Rare primary and pseudosecondary fluid inclusions and fluid inclusion assemblages hosted in quartz, cassiterite and wolframite were classified after Roedder (1984) and define four different inclusion types (Fig. 2-2A). Type I high-temperature brine inclusions from boiling assemblages hosted in a re-analyzed quartz sample from Heinrich et al. (1999) and in one quartz sample from the BGR collection yield salinities of ca. 40 wt.% NaCl equiv. and homogenization temperatures between 420 and 490 °C (Fig. 2-1I). The most common primary fluid inclusions (type II) decorate growth zones and are aqueous two-phase inclusions with liquid to vapor ratios of ~1:1. They are hosted in greisen (quartz and cassiterite: type IIa; Fig. 2-1C) as well as in vein quartz (type IIb; Fig. 2-1G). Type II inclusions commonly homogenize into the liquid phase between 350 °C and 410 °C, but in rare FIAs they homogenize either into the liquid or vapor phase (Fig. 2-1G) or even show critical homogenization. Salinities of type II inclusions range between 1 and 8.5 wt.% NaCl equiv. Type III inclusions are aqueous two-phase inclusions hosted in wolframite (type IIIa; Fig. 2-1E) and cassiterite (type IIIb; Fig. 2-1F) in veins. Most type IIIa inclusions are liquid-rich, have homogenization temperatures between 340 and 350 °C and salinities of 10 – 12 wt.% NaCl equiv. Type IIIa inclusions are locally found in boiling assemblages (Fig. 2-1E). Type IIIb inclusions in cassiterite have lower homogenization temperatures of ca. 335 °C and higher salinities of ~14 wt.% NaCl equiv. even though cassiterite is intimately intergrown with wolframite. Type III inclusions are not contained in quartz, not even in quartz intergrown with wolframite (Fig. 2-1D). Rare type IV fluid inclusion low-temperature boiling assemblages were observed in two samples from a quartz vein (Fig. 2-1H). The samples host abundant small vapor-rich inclusions besides brine inclusions which mostly contain two to three solid phases and have salinities around 30 wt.% NaCl equiv. and homogenization temperatures of ca. 300 °C.

LA-ICP-MS analyses show that all elements necessary for the formation of cassiterite (Sn) and wolframite (Mn, Fe, W) can be detected in all inclusion types (Fig. 2-2B). Sn contents are slightly higher in the boiling assemblages (I, IV) than in type IIb inclusions. Wolframite has higher traces of Sn, but some type IIIa inclusions have detectable Sn contents

of up to 2400 ppm. Relevant metals for the formation of wolframite are more enriched in brine-type inclusions and have similar contents in greisen (IIa) and vein quartz (IIb).

The different fluid inclusion types show a strong similarity in chemical compositions, suggesting a common source fluid, with variations mainly depending on different salinities due to phase separation and fractionation. A single fluid source is best documented by various almost linear positive correlations, e.g., Cs/Na versus Rb/Na ratios and As versus Cs contents (Fig. 2-3A + B) and homogeneous $\delta^{13}\text{C}_{\text{CO}_2}$ values of fluid inclusions in quartz and cassiterite between -5.5 and -7 ‰, which is consistent with a magmatic fluid source (e.g. Fuex and Baker (1973)). The geochemical data further show that fluid inclusions in all type II inclusions have similar element contents whereas the FI from boiling assemblages (type I, III, IV) form a distinct cluster of high element concentrations.

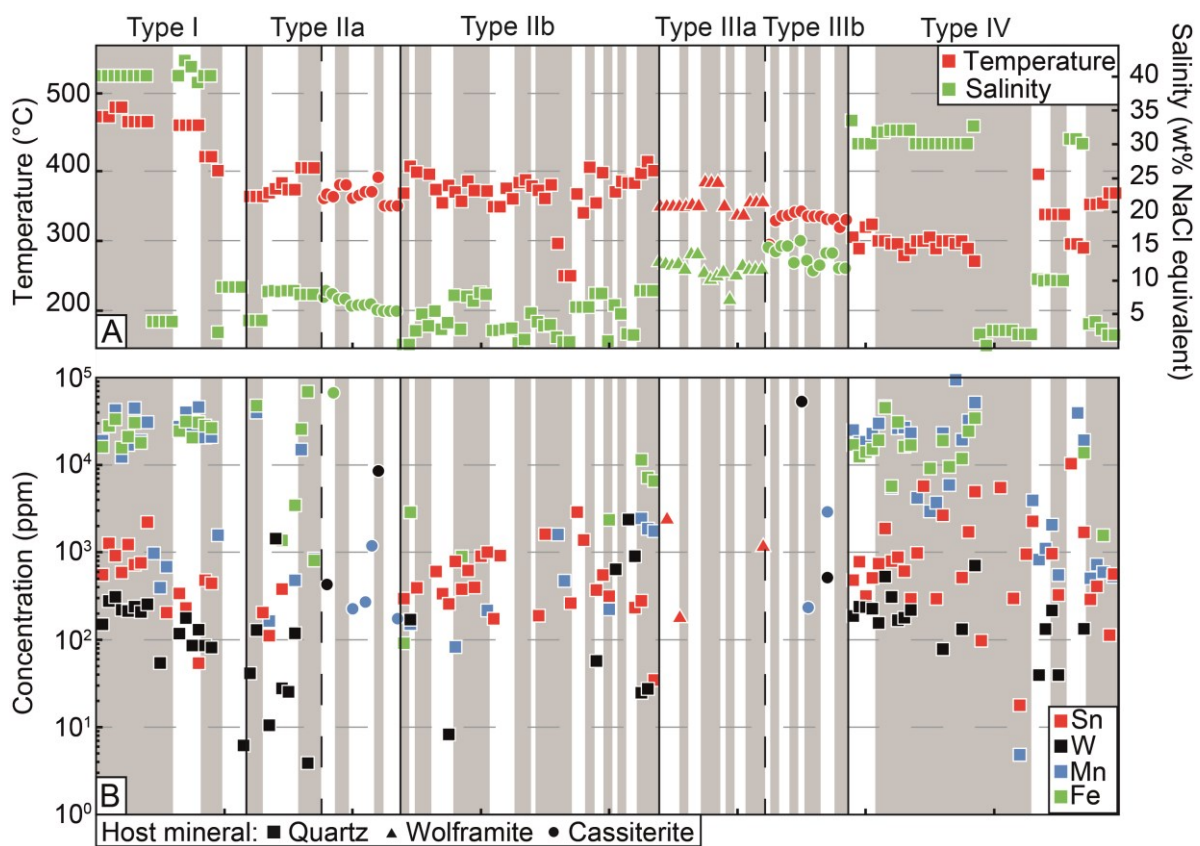


Fig. 2-2 A: Homogenization temperatures and salinities of different fluid inclusion types (I – IV) in quartz (squares), cassiterite (circles) and wolframite (triangles). Grey and white fields group individual fluid inclusion assemblages. B: Element contents in fluid inclusions by LA-ICP-MS

2.4 Fluid Evolution

Type IV FIA allow a direct estimate of the fluid pressures during vein formation because they are tied to the two-phase liquid-vapor (LV) coexistence curve, yielding fluid pressures of $\sim 60 - 100$ bar (Fig. 2-3C). Type IIb inclusions with variable salinities lack

boiling assemblages and yield minimum entrapment pressures between 150 and 330 bar. Their variable homogenization behavior indicate that they were also likely trapped at or near the LV-coexistence and that the salinity variations of 1 – 10 wt.% NaCl equiv. reflect gentle boiling. Since all sampled veins represent a similar depth level (Fig. 2-1A) and type II and IV inclusions occur in the same vein, the pressure variation with a factor 1.5 – 5.5 can best be explained by transition from a (nearly) lithostatic to a (nearly) hydrostatic pressure regime, suggesting a paleodepth of ~1 - 2km in agreement with estimates for the granite intrusion depth (Dolejš and Stempok 2001). Lithostatic fluid pressure conditions have been inferred as a possible mechanism for the formation of sub-horizontal veins by hydraulic fracturing during fluid exsolution from a crystallizing magma chamber (Breiter et al. 2017; Foxford et al. 2000).

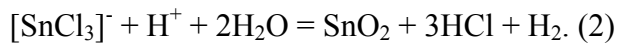
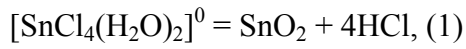
Type I inclusions hosted in historic quartz samples yield higher pressure conditions between 250 and 450 bar during fluid entrapment, suggesting a sample origin from deeper parts of the deposit. The high temperatures partially narrow the temperature gap between an assumed solidus temperature of the granite of ~650°C (Johannes 1984) and the average mineralization temperature of 380 °C.

2.5 Ore Precipitation

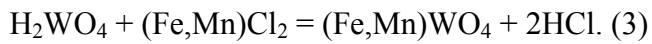
The type III inclusions in ore minerals from vein mineralization follow the same trend of decreasing pressures and temperatures and increasing salinities along the two-phase coexistence field. Their entrapment conditions are positioned in the middle between the inclusions representing the lithostatic (type II) and the hydrostatic (type IV) endmembers of the fluid evolution in the veins. This interpretation is confirmed by the presence of boiling FIAs in wolframite (type IIIa) and their geochemical similarities to other boiling FIAs. The FIA in the intergrown wolframite-cassiterite sample form slightly different types (IIIa and IIIb, respectively), which suggests a rapid, dynamic process during ore deposition, such as depressurization during fracture opening. A transient pressure drop from nearly-lithostatic to sub-hydrostatic conditions leads to partial loss of the high-enthalpy vapor phase, resulting in cooling and salinity increase of the remaining brine.

The similarities in chemical composition and partial overlap of fluid inclusions types IIa (greisen) and IIb (vein quartz) suggest a simultaneous formation of vein and greisen in Zinnwald, which is in line with geological observations at the mine where quartz veins can be hosted by greisen, granite (not greisenized) or partially by granite and greisen.

Our interpretation suggests two contrasting processes of Sn-W deposition for greisen and vein mineralization: 1) fluid-rock reaction and 2) phase separation. Sn can be transported as Sn(II) or Sn(IV) by complexation with Cl^- in the fluid whereas W is in solution as WO_4^{2-} . Therefore, SnO_2 (cassiterite) can be precipitated by lowering the HCl activity in the fluid system (Schmidt 2018):



Wolframite precipitation needs additional cations (here, Fe and Mn) which are also mostly transported as complexes with Cl^- (Heinrich 1990):



Greisenization (alteration of feldspars and biotite) moves the Sn-reactions (1, 2) to the right and can therefore precipitate cassiterite, whereas W can still stay in solution, e.g., if Fe and Mn are consumed for the formation of zinnwaldite (Tischendorf et al. 1997). During fluid phase separation volatile elements (e.g., HCl, Cl^- , H^+) preferentially partition into the vapor phase (Bischoff et al. 1996; Simonson and Palmer 1993) which can readily leave the system due to its low density, leading to a change in the chemical composition of the fluid and therefore to cassiterite and simultaneous wolframite precipitation (Heinrich 1990).

Phase separation during vein opening may be episodic, but the presence of a brine phase and the absence of pure vapor inclusions exclude extreme pressure drops during flashing events (Clark and Williams-Jones 1990; Moncada et al. 2017). Ore precipitation due to phase separation with the proposed mechanism will be most efficient at relatively low pressures where the vapor phase has a very low density. This relation suggests that greisen deposits with Sn-W-rich veins are more favorably associated with shallow intrusions, while fluids exsolved from deeper intrusions may be capable of avoiding wolframite precipitation by phase separation and allow metal transport to more distal parts, where fluids can interact with the surrounding rocks (e.g. Polyá (1989)).

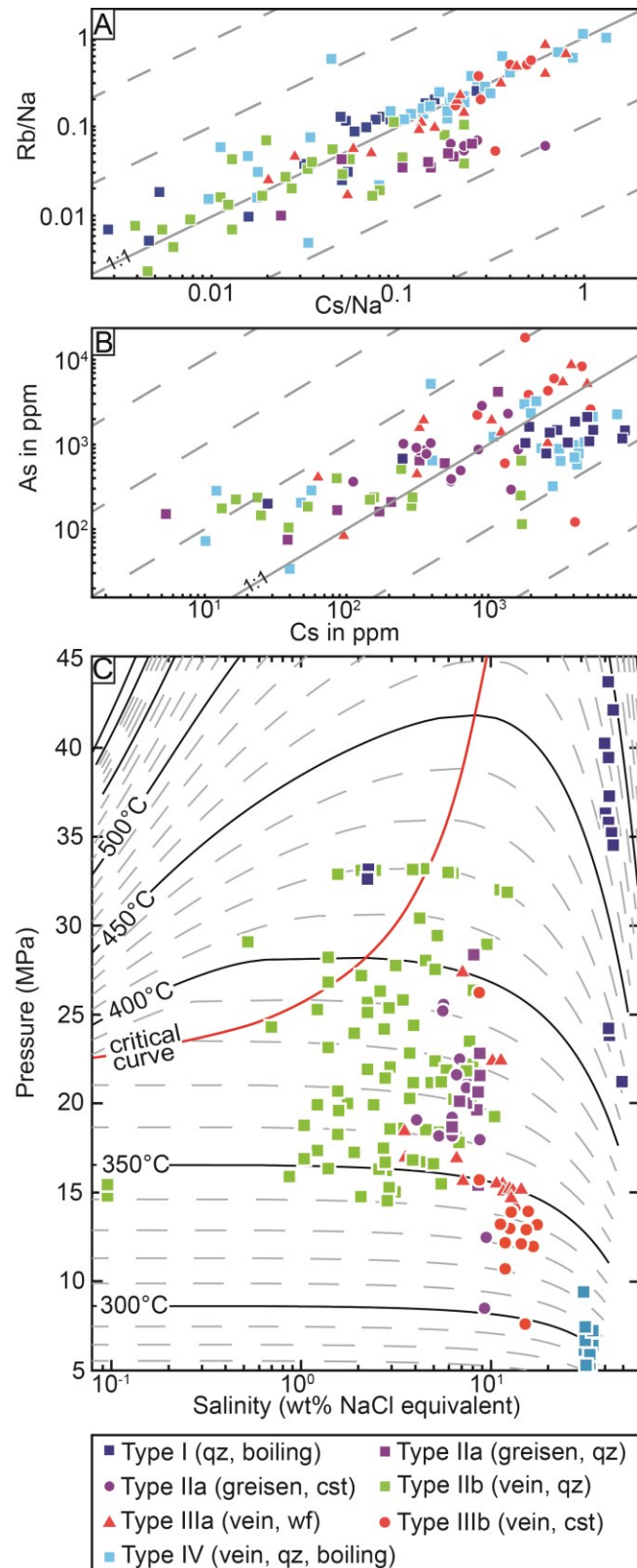


Fig. 2-3 A + B: Cs/Na versus Rb/Na ratios and Cs versus As contents of different fluid inclusion types showing near-linear trends. C: Pressure estimates from homogenization temperatures and salinities. Fluid inclusions of type IIa in Greisen overlap with type IIb inclusions. Fluid inclusions of type IIIa and IIIb in vein wolframite and cassiterite form a distinct field between type II and type IV brine inclusions. Fluid pressures, phase relations and isotherms are calculated after Driesner and Heinrich (2007)

2.6 Conclusions

Our fluid inclusion study suggests that contrasting mineralization styles at the Sn-W Zinnwald deposit, Erzgebirge formed from a single magmatic fluid:

1. Fluid-rock interaction in the roof of an evolved granitic intrusion leads to the formation of cassiterite-bearing greisen bodies.

2. Transient changes of the pressure regime from lithostatic to (sub-)hydrostatic conditions due to vein opening leads to phase separation and vapor loss, triggering coeval precipitation of wolframite and cassiterite in quartz veins within the greisenized cupola.

The fluid inclusion data, together with geological observations at the mine, suggest that both precipitation mechanisms happen roughly at the same time. The results of this study also show that fluid inclusion assemblages in ore minerals can form distinct compositional fields, which may be overlooked or not even documented in primary growth zones in coexisting vein quartz, highlighting the importance of fluid inclusion analyses in ore minerals as direct evidence for ore formation in dynamic hydrothermal systems.

2.7 Appendix

2.7.1 Additional Geological Background

The Zinnwald granite is hosted by the Teplice rhyolite and has an elliptical shape of ca. 1.4 km x 0.3 km at the surface (Fig. 2-4) (Monecke et al. 2007). The granite widens at depth with dips between 20° and 70°. Drill cores document a minimum depth of 1.6 km (Stemprok 1965; Stemprok 1971; Stemprok and Sulcek 1969), but the exact vertical extent of the pluton is unknown.

The Zinnwald granite intruded into the Altenberg-Teplice caldera (Stemprok et al. 2014) which forms the predominant structure of the eastern Erzgebirge magmatic complex. The Caldera was formed by two extrusive events at 326.8 ± 4.3 and 308.8 ± 4.9 Ma, represented by different ignimbrites (Hoffmann et al. 2013) whereas the granite intruded the Teplice rhyolite between 312.6 ± 2.1 and 314.9 ± 2.3 Ma (Seifert et al. 2011). However, the dating of granites in the eastern Erzgebirge remains problematic due to their high hydrothermal overprint (Gerstenberger 1989; Stemprok et al. 2014). Geochemically, it has been interpreted as a highly fractionated A-type (Breiter et al. 1999; Breiter and Škoda 2012; Sebastian 2013) similar to the granites at Altenberg and Sadisdorf, which are all characterized by a subvolcanic setting with distinct hydraulic fracturing (Breiter 2012; Seltmann 1994). The formation of enriched Sn-granites capable of forming economic deposits may require assimilation of pre-concentrated sedimentary rocks during melting (Romer and Kroner 2015;

Romer and Kroner 2016). The Zinnwald granite itself is internally complex and can be divided into three different textural types with increasing depth: 1) fine-grained lepidolite-albite granite at the top (Cocherie et al. 1991; Stemprok and Sulcek 1969); 2) medium-grained zinnwaldite-albite granite (Johan and Johan 2004; Rub et al. 1998) with irregular bodies of fine-grained porphyritic zinnwaldite microgranite; 3) porphyritic medium-grained protolithionite granite, which is the main unit of the Zinnwald granite (Johan et al. 2012; Rub et al. 1998).

Sn mineralization mainly occurs in greisen bodies at the endo-contact (Fig. 2-5) in the lepidolite-albite granite, which is an equigranular, whitish rock with quartz, albite, potassic feldspar, mica and accessory minerals such as topaz and fluorite (Monecke et al. 2007). The greisen ore bodies have irregular shapes from vertical pipes to horizontal lying bodies, and consist mainly of quartz, mica and topaz (Monecke et al. 2007). Greisenized zones can also be traced to deeper parts of the granite but become less frequent with increasing depth (Neßler et al. 2011; Webster et al. 2004). They can be associated with flat-lying veins but also occur as independent bodies with thicknesses of several tens of meters (Webster et al. 2004).

In contrast to the central greisen-dominated zone, the German part at the northern flank of the mineralized granite is dominated by flat-lying quartz veins (“Flöze”) and sub-vertical veins (“Morgengänge”), which contain considerable amounts of wolframite besides cassiterite.

The veins predominantly occur in the upper part of the granite (to 220m depth) and can extend into the Rhyolite (Monecke et al. 2007). Both types (Morgengänge and Flöze) mainly consist of quartz, zinnwaldite and topaz. The horizontal veins are on average 20 to 50 cm thick, but can locally be up to 4 m. The vertical veins are thinner with thicknesses between 10 and 20 cm, but their general mineralogical composition is the same. They trend in NE-SW direction and are formed (or at least reactivated) simultaneously to the horizontal ones (Monecke et al. 2007).

Sn and W from the horizontal and vertical veins have both been historically mined as the main ore at the German part of the mine (which we refer to as the Zinnwald deposit in this paper, because the Czech part is called Cinovec). The predominance of the high ore grades within the horizontal veins is documented by the orientation and naming of the historical mining tunnels which basically followed their extent (Fig. 2-4). The mineralization is localized and heterogeneous, with high grade parts next to barren quartz veins. Greisen bodies around the veins have mostly limited dimensions of a few cm to several m and are more irregular in their spatial expansion in comparison to the independent greisen bodies (Fig. 2-5).

The relationship of joints and mineralized veins in the Zinnwald granite is still discussed. We briefly summarize the main aspects here and the reader is referred to Stemprok et al. (1994) and Breiter et al. (2017) for further details.

The flat-lying veins in Zinnwald dip into NE direction and are subparallel to the granite-rhyolite surface. They are occurring together with greisen bodies for which, in the southern part, a relation to irregular steep joints has been reported (Breiter et al. 2017). This joint system is explained by hydraulic fracturing due to fluid exsolution from the crystallizing magma chamber. However, in the northern part the influence of steep fluid pathways is limited and the veins and greisens are related to more flat-lying joints (Breiter et al. 2017), which are indicative for a formation under near lithostatic pressure. At Panasqueira, the formation of sub-horizontal veins has been attributed to episodic pressure decreases during vein formation due to hydraulic valving (cycles of fluid injection) (Foxford et al. 2000). Episodic injection of fluid may also be documented in the Zinnwald veins by growth zones around coarse grained quartz (Bons et al. 2012) and multiple fluid pulses have been inferred by Breiter et al. (2017). Further, the heterogeneous distribution of the ore could be indication for dynamic fluid pulses.

Some parts of the horizontal veins show a high amount of zinnwaldite at their selvages and these occurrences are currently explored as a possible Li resource (Neßler et al. 2011; Neßler et al. 2014). There are a few analyses of fluid inclusions in Zinnwald but with less focus in the detailed precipitation mechanism itself (Durisova et al. 1979; Graupner et al. 2005; Thomas 1982; Thomas and Baumann 1980). The fluid evolution and the relative timing of formation of greisen, veins and ores remain unclear.

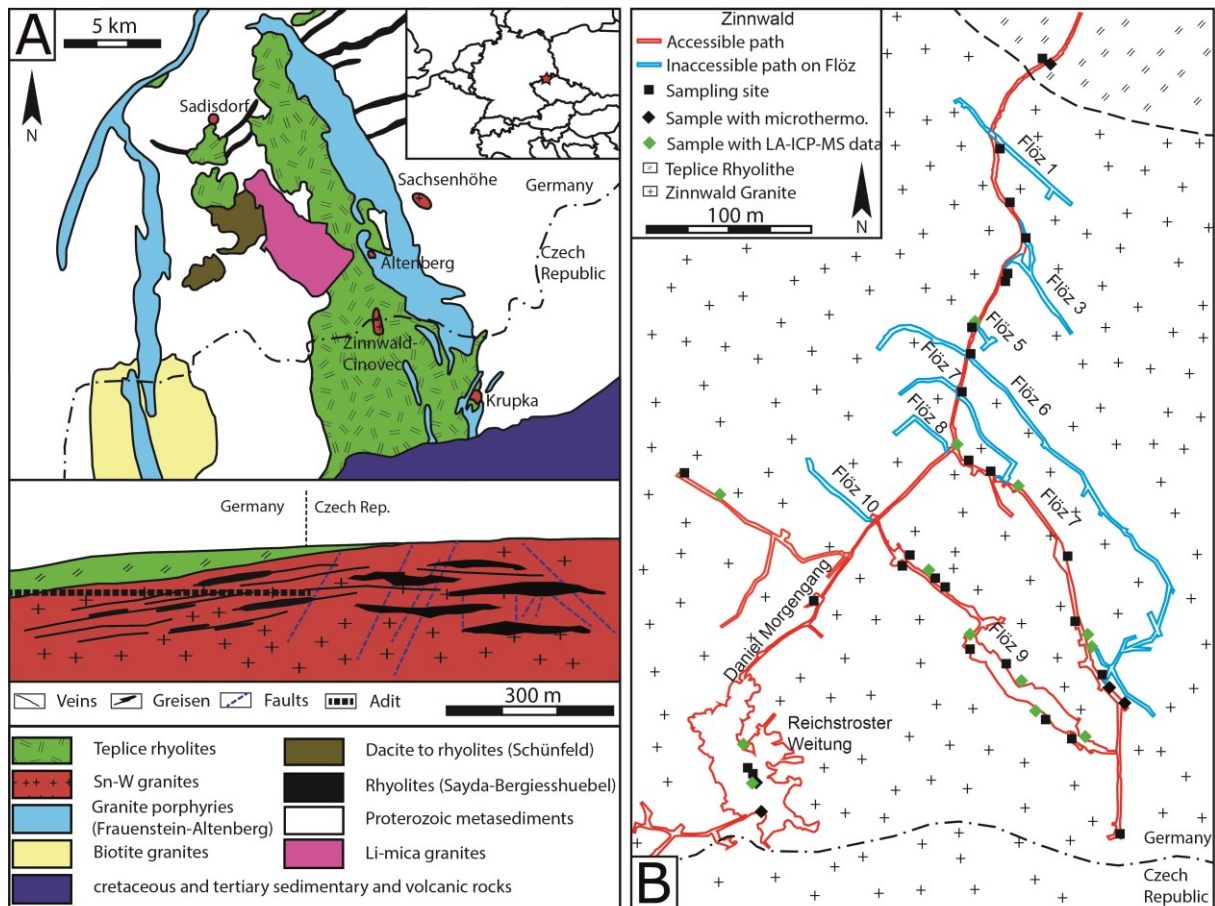


Fig. 2-4 A: Geological map of the Zinnwald area (after Dolejš and Stempok (2001) with schematic geological cross section through the granite cupola (after Stempok et al. (1994), the sampling area “Tiefer Büнау Stollen” (adit entrance: 5413041(E) 5623549(N)) is located in the German part of the deposit. B: Sampling points in the adit along the accessible parts of the formerly mined veins (Flöße). Symbols indicate the different used analytical techniques

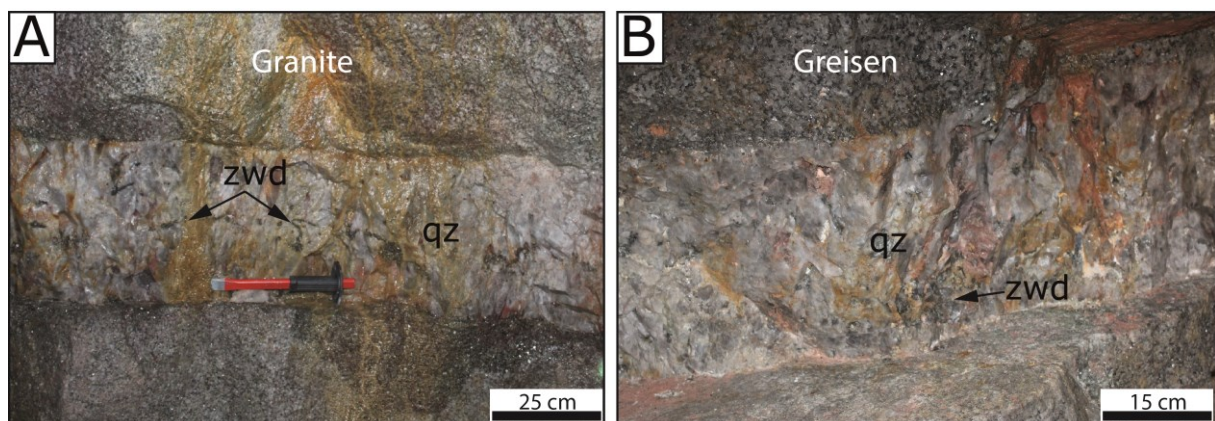


Fig. 2-5 Flöz 9 quartz (qz) vein with zinnwaldite (zwd) in contact with granite (A) and greisen (B)

2.7.2 Sample Origin

The Zinnwald deposit is partially accessible, because of its use as a historical visitors mine and for Li exploration. We systematically sampled the horizontal and vertical quartz veins being exposed in the deposit (Fig. 2-4). The vein quartz shows highly variable (often

chevron) textures, ranging from clear to milky with signs for recrystallization. The sample suite from the mine comprises a total of 50 quartz samples, from which 17 were used for microthermometry and a subset of 13 for chemical analyses with LA-ICPMS.

Ore specimens are almost absent in the remaining underground exposures because of the extensive past mining activities. Therefore, we obtained additional 28 samples containing crystals of cassiterite, wolframite and quartz from mineral collections of the Federal Institute for Geosciences and Natural Resources (BGR), the Humboldt University Berlin and the ETH Zurich. The old labels and sample descriptions are not detailed enough to perfectly locate the samples, but all labels related to Zinnwald, Sachsen (Saxony), can most likely be attributed to the German part of the mine.

A subset of eight samples was used for microthermometry and LA-ICPMS (Tab. 1), providing data from wolframite, cassiterite and quartz. One vein sample included intergrown cassiterite and wolframite together with quartz (ZWD B9), showing coeval precipitation of the two ore minerals. Other crystals from vein samples included pure wolframite or wolframite intergrown with quartz. A further sample contains vein-hosted cassiterite with quartz (HU8). One greisen sample (HU 4) contains small quartz grains intergrown with cassiterite of reddish to brown color. We further analyzed quartz crystals from the BGR archive (ZWD B12) and re-analyzed a euhedral crystal from ETH Zurich (Zinw 1) (Heinrich et al. 1999).

Tab. 1 Samples of ore and gangue minerals from collections

Collection	Mineral	Sample number	Type	Measured FI in
BGR	Qz	ZWD B2	Vein	Qz
BGR	Qz, Wf	ZWD B5	Vein	Wf
BGR	Qz, Wf, Cst	ZWD B9	Vein	Wf, Cst
BGR	Wf	ZWD B10	Vein	Wf
BGR	Qz	ZWD B12	Vein	Qz
Humboldt University	Qz, Cst	HU 4	Greisen	Qz, Cst
Humboldt University	Qz, Cst	HU 8	Vein	Qz, Cst
ETH Zurich	Qz	Zinw 1	Vein	Qz

2.7.3 Methods

Fluid inclusions in quartz were studied in transmitted light using a FLUID INC. adapted USGS heating/freezing stage with an Olympus BX 50 microscope. Fluid inclusions hosted in wolframite were analyzed with a Linkham THMS 600 system with an Olympus BHSM-IR microscope. The infrared image is transmitted to a monitor by a QCam-IR camera. For calibration, synthetic fluid inclusions standards by Synflinc were used. Cassiterite showed varying transmittance and was therefore studied in transmitted light and near-infrared light.

However, IR and transmitted light always revealed the same homogenization and ice melting temperatures. As CO₂ concentrations are generally very low, pressure estimates were calculated using the phase relations of the H₂O-NaCl system as described in Driesner and Heinrich (2007) and Driesner (2007).

LA-ICP-MS measurements were performed at ETH Zurich using a GeoLas system (LambaPhysik-Coherent, Germany) equipped with a 193 nm ArF-Excimer laser ablation system coupled to a Perkin Elmer Elan 6100 DRC quadrupole IC mass spectrometer for multi-element analysis (see Günther et al. (1998) for a detailed description). The samples were analyzed either in a ca. 1 cm³ rhomb-shaped, stainless steel cell (cassiterite- and wolframite-hosted inclusions); or a ca. 5 cm³ round glass cell (quartz-hosted inclusions). The cell was fluxed with carrier gas consisting of high-purity (5.0 grade) He (1.1 L.min⁻¹), to which H₂ was added (5 mL.min⁻¹) to enhance sensitivity for heavy elements (Guillong and Heinrich 2007). Sample gas consisting of 6.0 grade Ar (ca. 0.8 L.min⁻¹) was admixed downstream of the ablation cell prior to injection in the plasma. The ICP-MS was tuned for maximum sensitivity and low oxide rate formation (248ThO⁺/232Th⁺ <1%). The glass standard NIST SRM 610 was used as the primary reference material (using conventional standard bracketing) and analyzed with 40 µm pit size, repetition rates of 10 Hz and ca. 1 min measurement consisting of 30 s gas blank + 30 s ablation. FI in quartz were analyzed by slowly incrementing the spot size using an opening aperture (Gagnon et al. 2003). Depending on the behavior of the host quartz, repetition rates of 10 or 20 Hz with laser output energies between 110 and 170 mJ (corresponding to energy densities on sample of ca. 14 to 18 J.cm⁻²) were applied. Cassiterite and wolframite were analyzed with a repetition rate of 10 Hz and output energies of 40 – 60 mJ (energy densities of ca. 5 to 7 J.cm⁻²). Fluid inclusions in wolframite could not be relocated directly with the given LA-ICP-MS setup and were therefore retrieved via a documentation of IR, coupled IR and reflected light, and reflected light photomicrographs. In total, we measured 25 elements (7Li, 11B, 23Na, 39K, 55Mn, 57Fe, 65Cu, 66Zn, 75As, 85Rb, 97Mo, 118Sn, 133Cs, 182W, 208Pb, 88Sr, 29Si, 43Ca, 93Nb, 107Ag, 121Sb, 181Ta, 197Au, 238U, 209Bi) and subsequently reduced the data with the SILLS software (Guillong et al. 2008), using the salinity (wt.% eq. NaCl) determined by microthermometry as internal standard.

Despite the small amount of CO₂ stable carbon isotopic compositions in fluid inclusions could be measured using a sample crusher connected via a gas chromatography column to an elemental analyzer isotope ratio mass spectrometry system. This analytical setup allows online simultaneous measurements of stable isotope ratios of N₂, CH₄, and CO₂ in

natural gas mixtures released by crushing of fluid inclusions. For details see Lüders et al. (2012) and Plessen and Lüders (2012).

2.7.4 Additional fluid chemistry data

Despite their different properties, the chemical data obtained by LA-ICP-MS reveal many similarities between the different FI types. Measurements of Sn concentrations by LA-ICP-MS were difficult due to the high background (Schlöglova et al. 2017). However, Sn could be detected in some type IIb inclusions but was rarely measured in IIa inclusions (Fig. 2-6). The Sn content is relatively constant with ca. 380 ppm and maximum values of up to 2900 ppm. The average Sn contents in type I brine inclusions is about 710 ppm and 1500 ppm for type IV FI. Wolframite has higher backgrounds for Sn, but some IIIa FIs have detectable Sn contents of up to 2400 ppm.

The Mn contents in brines of type I and IV are similar with average values of 28000 ppm and 24000 ppm, respectively. Fe concentrations have the same range like Mn in type I (25000 ppm) but lower values in type IV (15000 ppm), whereas the W contents are comparable in both brine generations (176 ppm and 168 ppm). In some type II inclusions, Fe was above the limit of detection (2000 – 10000 ppm,) resulting in contents of up to tens of thousands ppm in some greisen FI and up to 11000 ppm in the quartz veins. The rare FI with measurable W peaks had average contents of 92 ppm in the greisen (IIa) and 105 ppm in the quartz veins (IIb).

The most abundant elements in the FI besides Na are Cs and Rb, which were detected in almost all different inclusion generations independent of the host. Their contents depend on salinity with up to 9000 ppm of Cs and 15 000 ppm of Rb in brine-type inclusions of types I and IV, in contrast to the type IIb inclusions with averages of 170 ppm Cs and 240 ppm Rb. Type IIa and III have higher contents of both elements, due to their slightly higher salinity (300 ppm Rb, 620 ppm Cs in the greisen (IIa) and 2500 ppm Rb, 2000 ppm Cs in ore mineral-hosted type III FI). Pb and Zn show low contents in the type II but are higher in brines-type inclusions of type I and IV.

High saline inclusions of I, IV and III also contain high amounts of K, sometimes with even higher contents than Na, while K contents are lower or below the detection limit in type IIb. The contents of trace elements such as Li, B and As are relatively constant in all different FI generations in quartz (I, II, IV), mainly varying between 300 and 1000 ppm, but are generally higher in FIs hosted in ore minerals (III).

The almost linear relation between some elements shown in the study is further documented by an almost linear positive correlation between Cs and Rb with Cs:Rb ratios between 1:1 and 1:2. A similar correlation is also given in the Cs:Na plot for type IIa and IIb but not for higher saline FIs of type III, IV and I, showing relatively constant Na contents but varying Cs contents (Fig. 2-7). Linear correlation patterns are also visible in other element ratios, e.g. by replacing Cs with K (Fig. 2-7). Replacing Rb by Pb (Fig. 2-7) suggests that Pb concentrations in type III FI are reduced compared to those in FIs in quartz, which is also visible when plotting As vs. Pb (Fig. 2-7). These lower contents can be explained by different compatibilities of Pb in ore minerals in contrast to quartz, which can modify the FI contents after entrapment (James and MacNaughton 1977). The linear correlation of elements shown in Fig. 2-7 between all fluid inclusions types is further confirmed by other elements such as Mn and Zn, which are not particularly related geochemically and support the interpretation of a single source fluid (Fig. 2-7). These trends are independent of the origin of the samples (from the mine or from collections) and are, together with the homogeneous element content within one inclusion type (especially for vein quartz from the mine and the collection) and their similar appearance (L-V-ratio, salinity, homogenization), an important confirmation for the validity of the samples from the mineral collections.

Further, the geochemical data show that fluid inclusions in all type II (both in vein quartz and greisen) have similar element contents (Fig. 2-7) whereas the FI from boiling assemblages (type I, III, IV) form a distinct cluster of high element concentrations. The samples in boiling FIA from the archives (type I and III) show the same behavior as the boiling assemblages from Flöz 9 (type IV). This association is also documented by opposing trends in the Na vs. Cs plot, showing a positive correlation at low concentrations in type II inclusions, whereas type I, III and IV inclusions indicate a slight decrease in Cs for the highest Na concentration. These similar trends between the distinct boiling FIAs in the quartz (I, IV) and the FI in the ore (II) are not only visible in the several diagrams; they are also distinct by comparing the medians and means of the elements with each other. Here, the data further proves the same ranges of these different mineralogical generations (summarized in Fig. 2-8). This supports the observation that the type III assemblages, consisting of liquid and vapor rich inclusions, represent boiling assemblages. The described relation between type I, III and IV can also be detected in the linear trends but are furthermore visible in additional x-y diagrams. Certain elements seem to undergo an enrichment/depletion process during boiling which is preserved only in those plots.

LA ICP-MS data reveal that there are two trends visible in Fig. 2-7: 1) the linear trend supporting the interpretation of a single magmatic fluid and 2) the high amount of overlap between type I, III and IV in contrast to the inclusions of II as a second indication for boiling of type III fluid inclusions.

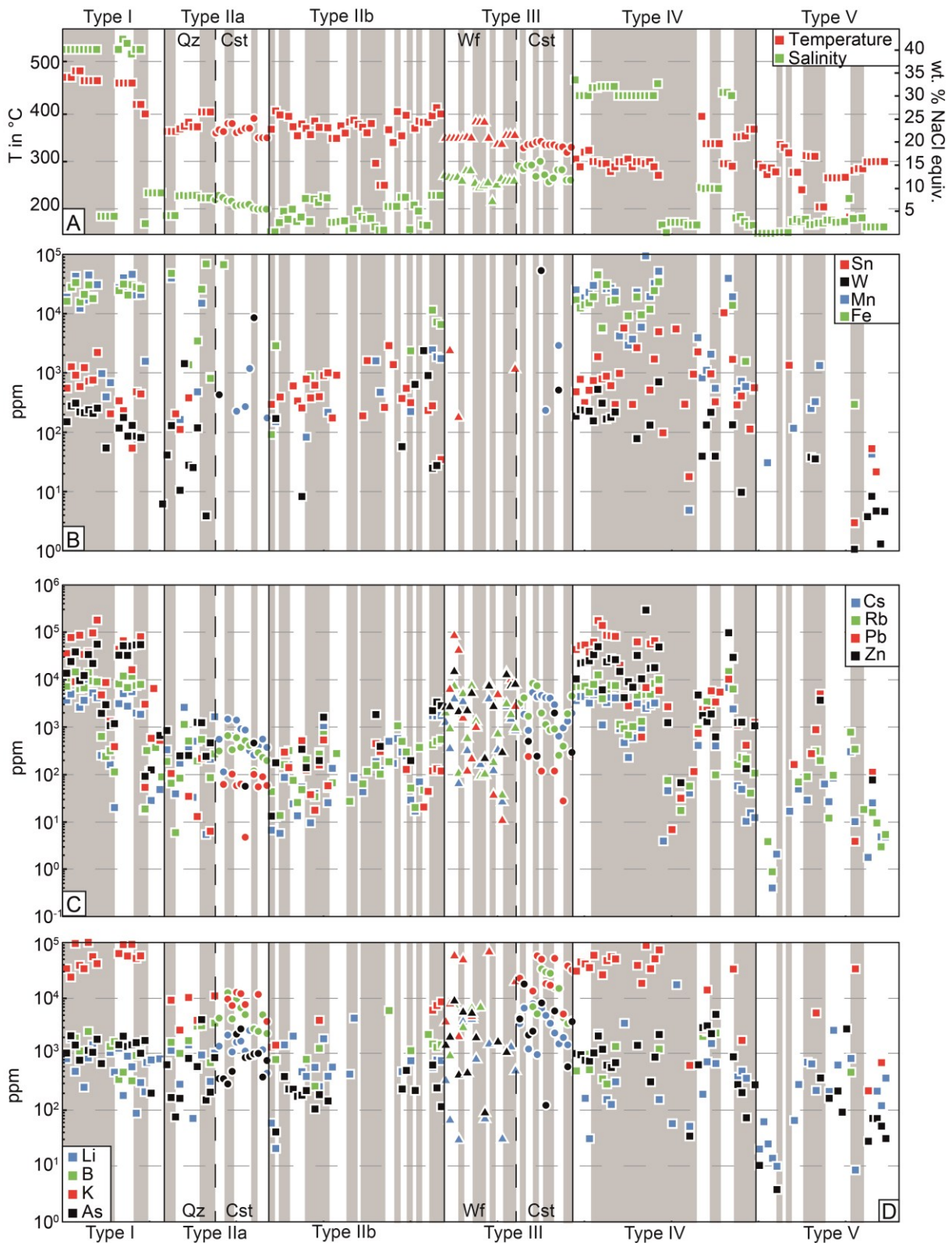


Fig. 2-6 (previous page) A: Homogenization temperature and salinity of fluid inclusions with added secondary inclusions (type V) B-D: Element contents in fluid inclusions hosted in quartz (squares), cassiterite (circles) and wolframite (triangles) (LA-ICP-MS analyses). Grey and white areas indicate fluid inclusion assemblages. Shapes of the symbols indicate the host mineral

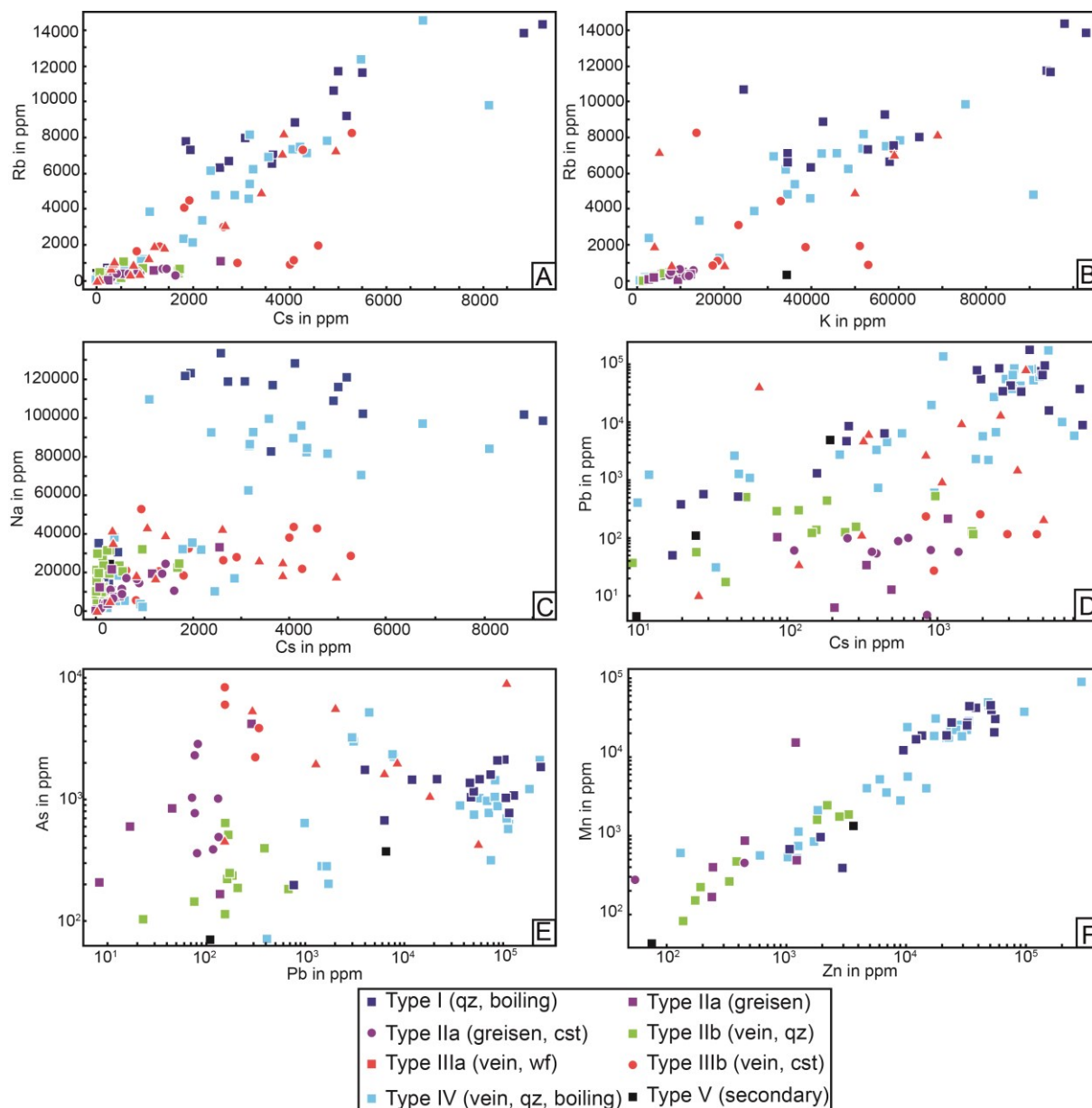


Fig. 2-7 Chemical variations of Rb vs. Cs (A), Rb vs. K (B), Na vs. Cs (C), Pb vs. Cs (D), As vs. Pb (E) and Mn vs. Zn (F) showing near-linear trends (A, B, F) suggesting a common source fluid as well as an association of type IIa fluids (Greisen quartz and cassiterite) with type IIb fluids from vein quartz and an association of type III fluids (Vein wolframite and cassiterite) with brine end-members from boiling assemblages of type I and IV inclusions in vein quartz

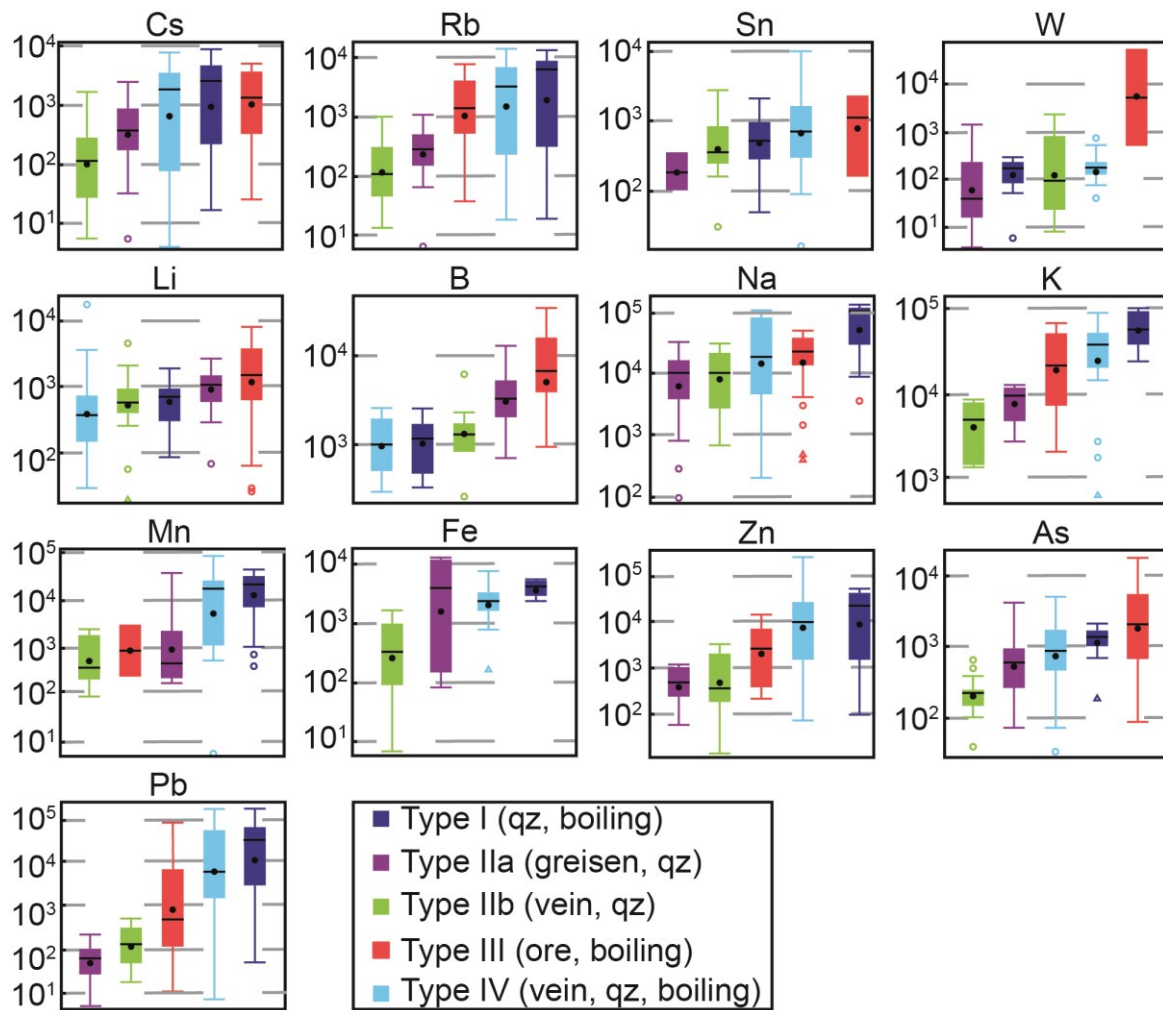


Fig. 2-8 Chemical variations of the main elements, sorted after increasing mean values (black circle), showing the similar contents of type III fluids (in red) with brine end-members from boiling assemblages of type I and IV inclusions in quartz (blueish). Black lines refer to the median, the bottom of the boxes represent the first quartile (25% of the data) and the top the third quartile (75% of the data), the whiskers are the extreme values that are not outliers, an outlier (circle) is further than $1.5 \times (Q3 - Q1)$ from the box, a far outlier is further than $3 \times (Q3 - Q1)$ from the box

3 Skarn-hosted Sn mineralization by unusually hot brines: insights from fluid inclusions in ore and gangue minerals from the polymetallic Hämmerlein deposit, Erzgebirge, Germany

Maximilian Korges¹, Philipp Weis¹, Volker Lüders¹, and Oscar Laurent²

¹*GFZ German Research Centre for Geosciences, Telegrafenberg, 14473 Potsdam, Germany*

²*ETH Zurich, Institute of Geochemistry and Petrology, 8092 Zurich, Switzerland*

Submitted to *Mineralium Deposita* and currently under revision after positive reviews. The readers must be aware of potential differences between the future publication and this chapter.

Abstract

Skarn-hosted deposits can be important high-grade resources for a variety of metals, but Sn skarns are still of subordinate importance for global mining because of their complex evolution. As part of recent exploration efforts, the economic potential of the Sn-Zn-(In) mineralization at the Hämmerlein skarn-hosted deposit is currently being re-evaluated. However, the temporal and spatial evolution of the ore-forming hydrothermal system is still debated. We analyzed fluid inclusion assemblages (FIA) in ore and gangue minerals using conventional and infrared-microthermometry and LA-ICP-MS. We further estimated alteration temperatures with chlorite thermometry and compared the fluid inclusion (FI) record at Hämmerlein with a mineralized greisen sample of the nearby Eibenstock granite.

Cassiterite in skarn forms the major mineralization at Hämmerlein during stage I and host fluid inclusions showing homogenization temperatures of up to 500°C and salinities in the range between 30 and 47 wt% NaCl eq. Cassiterite from schists and greisen from later stage II show lower homogenization temperatures (350 - 400 °C) and considerably lower salinities varying from 1.9 to 6 wt% NaCl eq. However, LA-ICP-MS data of fluid inclusions hosted in both generations of cassiterite show that both cassiterite in skarn and schist and greisen have a common source. The gangue minerals mainly contain low temperature FIA (max. 330°C and 2 - 9 wt% NaCl eq.) and form during further cooling of the system in stage III. Geothermometry of intergrown chlorite yield similar temperatures of around 260 °C and is thus also related to stage III. FIA in sphalerite homogenize around 200°C with salinities between 2 and 6.7 wt% NaCl eq. and show decreasing trace element contents despite having the same salinity range as the gangue minerals, indicating dilution of the ore-fluid during stage IV as a possible precipitation mechanism.

Stage I inclusions are solely hosted in cassiterite from skarn, which shows the importance of fluid inclusion analyses in ore minerals, and record remarkable high mineralization temperatures, exceeding the typically temperature range reported in other studies by at least 100°C. Our results suggest that the main ore stage is related to the early expulsion of a high-salinity brine phase from an underlying magmatic intrusion at depths greater than 3 km, which likely is a relatively short-lived event within the evolution of the hydrothermal system.

3.1 Introduction

Economic Sn mineralization is typically associated with evolved silica-rich A- or S-type granites (Romer and Kroner 2016; Breiter 2012; Lehmann 2006) and hosted by greisen, magmatic-hydrothermal veins or skarn bodies. Even though skarns are important resources for metals like Pb, Cu, Fe, W and Zn (Meinert 2005; Meinert 1992; Einaudi and Burt 1982) and often reach particularly high ore grades, Sn skarns are currently only of subordinate importance for global Sn mining (Misra 2012).

Skarn formation typically results from metamorphic processes which overprint carbonate-bearing sedimentary host rocks and predates ore formation (Kwak 1987; Meinert 2005). Skarn Sn deposits often incorporate some Sn into silicate minerals, which can make them, despite having a valuable total tonnage, sub-economic for mining (Meinert 2005). Additionally, as a unique feature that is absent in other types of skarn mineralization, many Sn skarns have a greisen alteration overprinting the earlier skarn mineralogy (Meinert 2005; Kwak 1987). The complex evolution of skarn deposits with diverse mineral assemblages and various overprinting metamorphic and alteration stages is particularly challenging for the reconstruction of the mineralizing hydrothermal system and the evaluation of the resource. Fluid inclusions can provide direct insights into the properties and chemistry of the hydrothermal ore-forming fluid, but fluid inclusion studies on skarn mineralization being performed so far are rare, in particular for Sn skarns (Mei et al. 2015; Fu et al. 1993; Layne and Spooner 1991). Fluid inclusions studies of typical hydrothermal Sn mineralization document formation temperatures between 300 and 400°C (Naumov et al. 2011), e.g. the Mole granite, Australia (Eadington 1983), Zinnwald, Germany (Korges et al. 2018) and the polymetallic Quechisla district, Bolivia (Sugaki et al. 1984).

The Hämmerlein polymetallic skarn hosted-deposit in the Erzgebirge, Germany, is currently explored for Sn in cassiterite, as well as Zn and In in sphalerite (Treliver Minerals Limited 2015). Despite many years of historical mining and exploration activities, the formation of the skarn deposit and its relation to metamorphic, magmatic and hydrothermal events remains debated. Lefebvre et al. (2018) argue for skarn formation during regional metamorphism and a minor Sn occurrence prior ore formation. The main input of Sn and deposition of cassiterite is interpreted to be associated with a later hydrothermal fluid system (Lefebvre et al. 2018), which could be related to magmatic intrusions associated with the Eibenstock granite. Kern et al. (2018) also suggested that the mineralization is associated with the granitic intrusion and based on a statistical analysis of grain boundary contacts infer a

coeval precipitation of the main ore and gangue minerals, namely cassiterite, chlorite, fluorite, quartz and sulfides at a late stage retrograde epithermal event.

For this study, we analyzed the fluid inclusion record in the most important ore and gangue minerals, cassiterite, sphalerite, quartz, fluorite and garnet, to reconstruct the fluid evolution of the ore-forming hydrothermal system at the Hämmerlein deposit. The skarn formation itself cannot be analyzed with fluid inclusions due to its inclusion-rare mineralogy. The analyses rather investigate the differences between Sn ore occurrences in the skarn units and the surrounding schists as well as the relation to the Zn-(In) mineralization. Since the source for the ore-forming fluid is also unknown, we further analyzed a sample from the mineralized greisen parts of the nearby Eibenstock granite to compare its FI content with the one from Hämmerlein. Due to the lack of fluid inclusions in chlorite, we further analyzed their chemical composition for the use of chlorite thermometry.

3.2 The polymetallic Hämmerlein deposit

The Erzgebirge region at the German-Czech border is a historic mining district and estimated to still host resources of 0.2 to 0.5 Mt of Sn, which are currently re-evaluated by exploration projects (Lehmann 2006; Kern et al. 2018). The polymetallic Hämmerlein deposit is a major exploration target on the German side of the western Erzgebirge, which hosts a large number of voluminous S-type granites that intruded into the metamorphic nappes of the Saxo-Thuringian Zone of the Variscan orogeny (Kroner et al. 2007; Rötzler and Plessen 2010; Förster et al. 1999). These post-kinematic intrusions were derived from partial melting of the continental crust with subsequent emplacement in upper crustal levels at pressures below 2 kbar (Förster et al. 1999; Förster and Romer 2010). Depending on the lithological and geochemical signature of the crustal source rocks, there are two main types of granites in the Hämmerlein area (Förster et al. 1998; Sebastian 2013): (1) low F biotite granites (e.g. Kirchberg) and (2) high F, high P₂O₅ Li-mica granites, which are interpreted to be the main source for the major ore deposits of the region (Fig. 3-1).

The Eibenstock-Nejdek pluton is the most voluminous of these granitic intrusions (Fig. 3-1A), with the northern Eibenstock part covering an area of 25 x 22 km (Breiter 1993). It is hosted by various medium- to low-grade metamorphic rocks, predominantly phyllites, gneisses and schists (Schuppan and Hiller 2012). The granitic body was formed by several intrusive events between 320 Ma and 310 Ma (Förster et al. 1998; Kempe et al. 2004; Tichomirowa et al. 2016), resulting in small compositional differences, including lower F contents in its southern part with a geochemical signature that is closer to the composition of

the Kirchberg granite (Sebastian 2013). However, the main parts of the Eibenstock granite have a peraluminous, Si-rich composition with siderophyllite, protolithionite, zinnwaldite and muscovite as the main mica phases (Förster et al. 1999; Sebastian 2013). The granitic body has been interpreted to spread out under the surface and underlie the nearby Hämmerlein deposit (Schuppan and Hiller 2012). Greisenization has been documented in some rare drill cores at the endocontact of the granite under Hämmerlein (Schuppan and Hiller 2012).

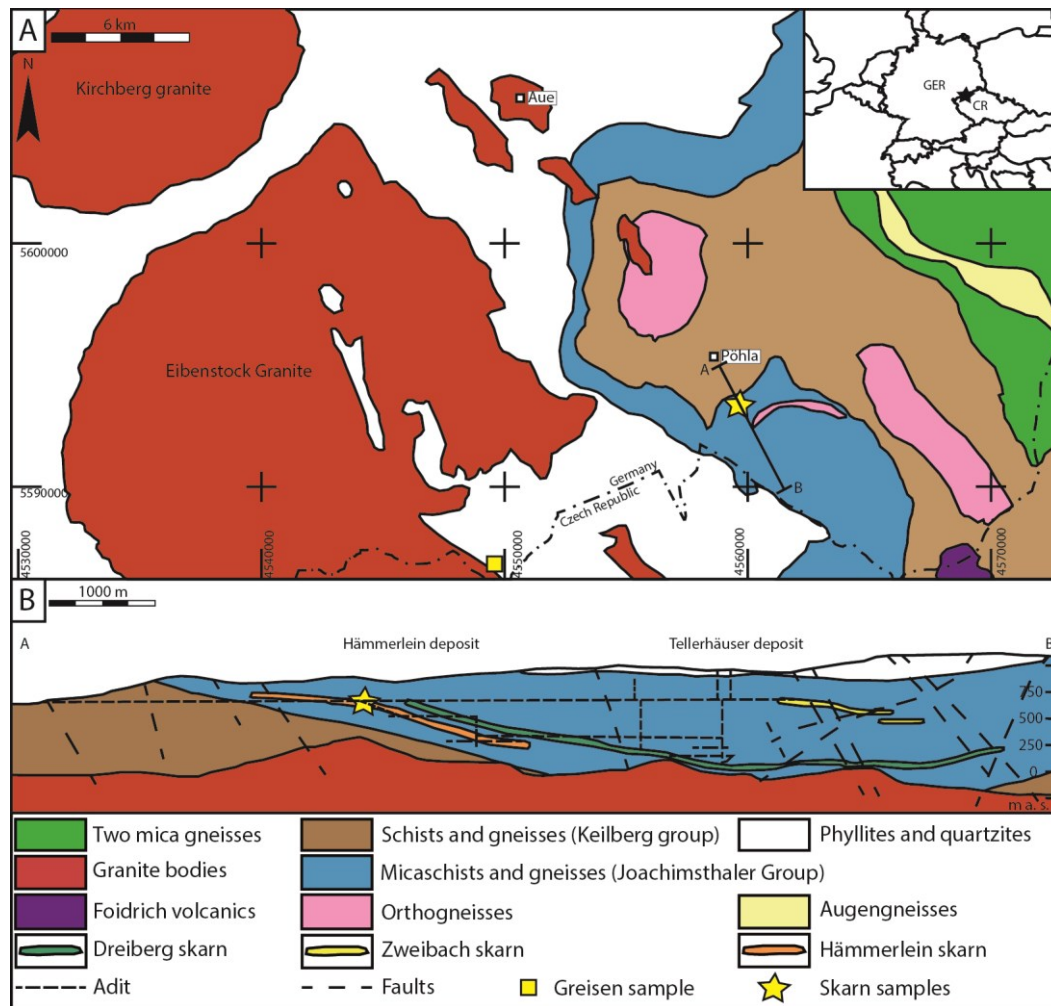


Fig. 3-1 A) Geological map of the Hämmerlein area (after Leonhardt et al. (1999); Leonhardt et al. (2004); Leonhardt et al. (2010)) showing sample locations of the Hämmerlein skarn (yellow star; 459952 (E), 5594367 (N)) and the greisen (yellow square; 4550845 (E), 5587207 (N)). B) Simplified NW-SE cross section through the Pöhla-Hämmerlein-Tellerhäuser region with indicated skarn-hosted mineralization (modified after Schuppan and Hiller (2012) and Anglo Saxony Mining (2015)). GER: Germany; CR: Czech Republic

The mineralized skarn units at Hämmerlein are embedded in the up to 1 km thick mica schists with layers of gneisses, quartzite-rich schists and carbon-rich schists (Shapenko and Smidel 1991) which are crosscut by the Eibenstock granite ca. 200 – 500 m below the deposit

(Schuppan and Hiller 2012; Kern et al. 2018). The main lithounits in Hämmerlein are the four different skarns - amphibole, magnetite, garnet, and pyroxene skarn - as well as the underlying schists. The thickness of the skarn package is 2 to 20 m, whereby the individual skarn units are distributed irregularly (Schuppan and Hiller 2012). Recent studies on the mineralization in Hämmerlein (Lefebvre et al. 2018) suggest that besides the main economic occurrence in cassiterite minerals, Sn is also notably incorporated in silicate minerals of the skarn, namely pyroxene and garnets (Mulligan and Jambor 1968; Butler 1978). Sphalerite occurrences can be locally enriched in In, making Zn as well as In possible by-products of prospected Sn mining at Hämmerlein (Bauer et al. 2017).

The entire Hämmerlein-Tellerhäuser-Breitenbrunn mining district is crosscut by later pitchblende-bearing quartz veins that used to be the main target for the historical U mining in the Tellerhäuser area (Fig. 3-1B). The region was extensively explored since 1946 due to its high U content (Schuppan and Hiller 2012), which lead to a total production of 1200 t uranium whereas tin was just experimentally mined between 1975 and 1979 (200 t extracted). The current exploration focuses on cassiterite and sphalerite and estimates 28,900 tons of indicated Sn with further 72,600 tons inferred, together with 2000 tons of inferred In and 200,000 inferred tons of Zn (Treliver Minerals Limited 2015).

3.3 Samples

The Hämmerlein deposit is accessible underground through the historical mining galleries which are maintained by the visitor mine at Pöhla. Furthermore, the current exploration projects allowed sampling in areas closed to the public. We systematically sampled the different skarn lithologies as well as the underlying mica schist and aimed for locations with high contents of Sn (cassiterite), Zn and In (both sphalerite).

For this study, we focused on the amphibole and magnetite skarns as the main units hosting cassiterite mineralization (Fig. 3-2A), which occurs in small veins together with quartz, fluorite and chlorite as single crystals or bigger aggregates with sizes up to a few centimeters. Cassiterite can also be found in small irregular lenses (Fig. 3-2B). The dark green amphibole skarn consists of amphibole, pyroxene, quartz and rare feldspars, showing different degrees of alteration. In particular, the amphiboles are strongly chloritized. Magnetite skarn occurs as massive black to dark brown rock, mainly consisting of magnetite, arsenopyrite, pyrite and local sphalerite as well as some quartz veins (Fig. 3-2C). Sphalerite mostly occurs in the magnetite skarn and forms almost monomineralic layers with thicknesses up to many centimeters or unregularly shaped pods (Fig. 3-2D).

A further occurrence of cassiterite is located in the altered mica schists of the foot wall, which are composed of quartz, muscovite and biotite with accessory garnet, rutile and tourmaline (Fig. 3-2E). Samples from mica schist contained mineralized quartz veins with subordinate fluorite. Cassiterite mineralization varies in grain size between a few μm to some mm and is located predominantly at the margin and occasionally in the center of the vein (Fig. 3-2F).

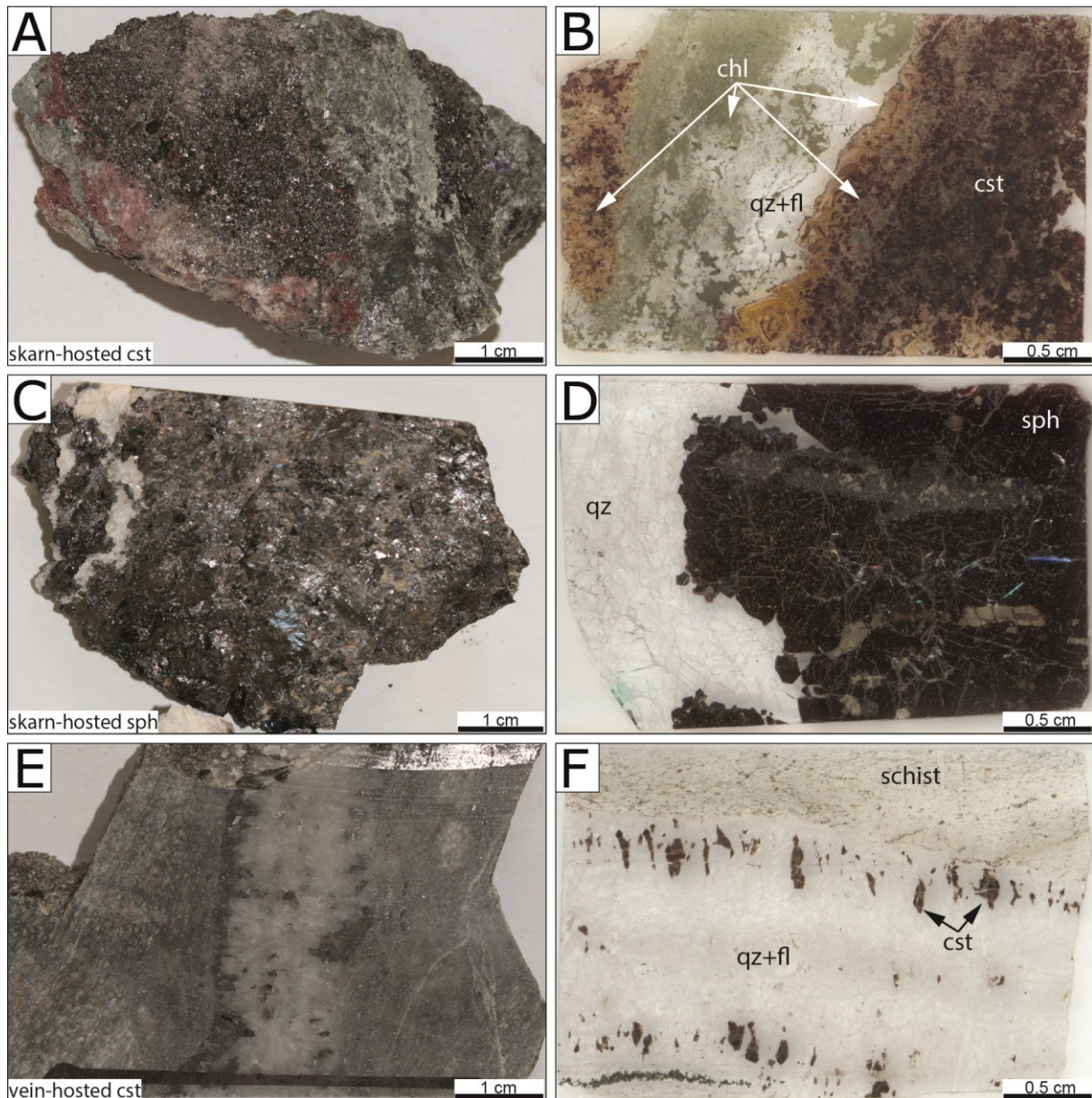


Fig. 3-2 Sampled lithologies with ore minerals at the Hämmerlein deposit: A-B) amphibole skarn (HAE 15) with lenses of cassiterite (cst) together with quartz (qz), fluorite (fl) and chlorite (chl). C-D) Magnetite skarn (HAE 2) with almost monomineralic occurrence of sphalerite close to a vein. E-F) Altered schist (HAE 8) with quartz (-fluorite) gangue and small cassiterite crystals mainly at the rim of the vein

Chlorite is a ubiquitous mineral in the skarn units and interpreted to be intimately related to mineralization (Malyshev et al. 1997; Kern et al. 2018). For the evaluation of the chlorite formation temperature, we selected one section (HAE 15) which hosts the most variable chlorite mineralogy (Fig. 3-3A and B). The sample contained four types of chlorite: (1) dense vein occurrences, (2) small veinlets in cassiterite with connections to the vein, (3) interstitial in cassiterite, and (4) overgrowing cassiterite at the rims of the veins.

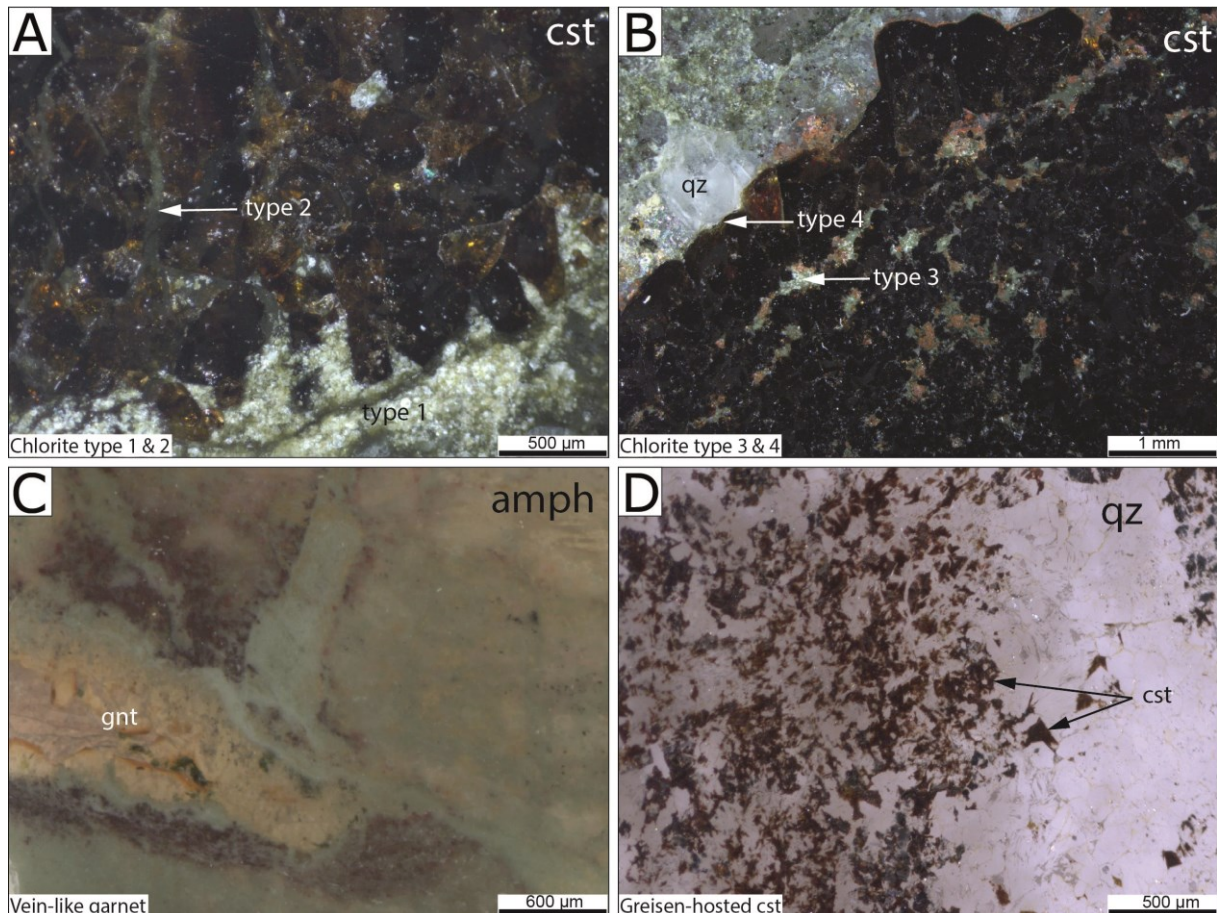


Fig. 3-3 Types of chlorite occurrences (HAE 15) as (A) vein chlorite (type 1) and chlorite-bearing veinlets in cassiterite (type 2), as well as (B) interstitial chlorite in cassiterite (type 3), and chlorite as thin overgrowth between cassiterite and vein (type 4). Vein-like garnet (HAE 3) occurrences in the amphibole skarn unit (C). Cassiterite-bearing greisen (JG 1) parts of the nearby Eibenstock granite (D)

Garnet is one of the main minerals in garnet and pyroxene skarn and may represent the original skarn formation, which is not the focus of this study and was thus not analyzed. However, garnet also occurs in vein-like structures (Fig. 3-3C) that likely postdate the skarn formation. Their relation to Sn and Zn mineralization is unclear and we analyzed their fluid inclusion content for comparison with fluid inclusions in other ore and gangue minerals.

The underlying granite and the contact zone to the mica schist are not exposed. However, we collected one sample from a mineralized greisen in direct association to the

Eibenstock granite at a distance of 12 km from the deposit as a reference for the greisenization of the granite underlying the Hämmerlein mineralization (Fig. 3-3D). In greisen, cassiterite occurs in the form of very small disseminated crystals with sizes below 1 mm, together with quartz, mica and rare tourmaline.

3.4 Methods

We collected a total of 40 samples, from which 23 were chosen for double-polished wafer preparation, with thickness of ca. 100 μm to ensure the transparency of the ore minerals in transmitted and near infrared (IR) light. The sections were petrographically investigated for fluid inclusion (FI) inventory. Fluid inclusions (FIs) hosted in studied minerals were classified as primary, pseudosecondary and secondary fluid inclusion assemblages (FIA) using the criteria proposed by Goldstein (2003) and Roedder (1984). FIs in transparent minerals (quartz, fluorite, garnet, and cassiterite in skarn) were studied using a FLUID INC. adapted USGS heating/freezing stage attached to an Olympus BX 50 microscope. FIs in sphalerite had to be analyzed using a Linkham THMS 600 system and a Olympus BHSM-IR microscope equipped with a QCam-IR camera because of its decreasing transparency upon heating (Lüders 2017). Some cassiterites in the greisen and schist samples showing highly variable transmittance were either studied in transmitted light or in near IR light. Both heating-freezing stages were calibrated using synesthetic FI standards provided by Synflinc. The measured T_m (ice) and T_m (halite) values were used for calculation of the corresponding salinity of aqueous FIs (Bodnar 1993). Because there is no microthermometric evidence for a significant presence of other gases beside H_2O , pressure estimates were calculated using the phase relations of the H_2O -NaCl system as described in Driesner and Heinrich (2007) and Driesner (2007).

LA-ICP-MS measurements were performed at ETH Zurich using the ETH-prototype GeoLas system equipped with a 193 nm ArF-Excimer Compex 102F laser ablation system (LambaPhysik-Coherent, Germany) coupled to a Nexion2000 (PerkinElmer, USA/Canada) fast-scanning quadrupole ICP mass spectrometer for multi-element analysis (see Günther et al. (1998) for a detailed description). In total, ten samples were analyzed in a ca. 5 cm^3 round glass cell. The gas blanks and system contamination were minimized following the cleaning and setup procedures described in Schläglova et al. (2017). The cell was fluxed with carrier gas consisting of high-purity (5.0 grade) He (1.1 Lmin^{-1}), to which H_2 was added (5 mLmin^{-1}) to enhance sensitivity for heavy elements (Guillong and Heinrich 2007). Sample gas consisting of 6.0 grade Ar (ca. 1 Lmin^{-1}) was admixed downstream of the ablation cell prior

to injection in the plasma. The ICP-MS was tuned for maximum sensitivity on the whole mass range and low oxide rate formation ($248\text{ThO}^+ / 232\text{Th}^+ < 0.5\%$). The glass standard NIST SRM 610 (Jochum et al. 2011) was used as the primary reference material (using conventional standard bracketing) except for Br, Cl and S for which the Sca-17 scapolite (Seo et al. 2011) was used. Both were analyzed with 40 μm pit size, repetition rates of 10 Hz and ca. 1 min measurement consisting of 30 s gas blank + 30 s ablation. FIs in quartz and fluorite were analyzed by slowly incrementing the spot size using an opening aperture (Gagnon et al. 2003). Repetition rates of 10 Hz with laser output energies between 170 and 190 mJ (corresponding to energy densities on sample of ca. 14 to 18 J cm^{-2}) were applied. Cassiterite and sphalerite were analyzed with a repetition rate of 10 Hz and output energies of 65 – 80 mJ (energy densities of ca. 5 to 7 J cm^{-2}). FIs in a few sphalerites and cassiterites could not be relocated directly with the given LA-ICP-MS setup and were therefore retrieved via a documentation of IR, coupled IR and reflected light, and reflected light photomicrographs. In total, we measured 35 elements: ^7Li , ^{11}B , ^{23}Na , ^{25}Mg , ^{27}Al , ^{29}Si , ^{34}S , ^{35}Cl , ^{39}K , ^{43}Ca , ^{55}Mn , ^{57}Fe , ^{62}Ni , ^{63}Cu , ^{66}Zn , ^{75}As , ^{78}Br , ^{85}Rb , ^{88}Sr , ^{93}Nb , ^{95}Mo , ^{107}Ag , ^{111}Cd , ^{115}In , ^{118}Sn , ^{121}Sb , ^{133}Cs , ^{138}Ba , ^{181}Ta , ^{182}W , ^{197}Au , ^{208}Pb , ^{209}Bi , ^{232}Th and ^{238}U . We subsequently reduced the data with the SILLS software (Guillong et al. 2008), using the salinity determined by microthermometry as internal standard.

The chemical compositions of cassiterite, sphalerite, garnet and chlorite were measured using a JEOL Hyperprobe JXA-8500F electron probe microanalyzer (EPMA) at GFZ Potsdam. All measurements used an accelerating voltage of 15 kV, a beam diameter of 20 μm and a current of 12nA. The EPMA analyses of cassiterite, sphalerite and garnet were used for internal calibration of the LA-ICP-MS data. The chlorite compositions were used to estimate the formation temperatures (T) according to Cathelineau (1988) as:

$$T = 321.98 \text{Al}^{\text{IV}} - 61.92. \quad (1)$$

We further compare these temperatures with formation temperature estimates according to Jowett (1991) and De Caritat et al. (1993), which adds the Fe and Mg contents:

$$T = 319 (\text{Al}^{\text{IV}} + 0.1 (\text{Fe}/(\text{Fe} + \text{Mg}))) - 69. \quad (2)$$

This modification is only applicable for $\text{Fe}/(\text{Fe} + \text{Mg}) < 0.6$, which is the case for all results of this study. Each type of chlorite occurrence (Fig. 3-3A and B) was measured at three different locations with two to four analyses.

3.5 Results

3.5.1 Fluid inclusion petrography and microthermometry

In the studied samples, five main types (I – V with decreasing homogenization temperature) and several subtypes of fluid inclusion assemblages (FIA) were distinguished depending on typical homogenization temperatures, salinities, lithologies, host minerals and petrographic observations. Cassiterite from the three sample lithologies host some primary and pseudosecondary FIA, which we categorize as type I (skarn) and type II (b: veins in schist; c: greisen) inclusions (Fig. 3-4). The measured FIs in gangue minerals (types IIa and III), namely in fluorite (IIa, IIIa), quartz (IIIb) and garnet (IIIc), occur in veins or disseminated in the different host lithologies and are mainly associated or intergrown with cassiterite (Fig. 3-5). FIA in sphalerite are restricted to samples from skarn (type IV). All quartz samples from the three lithologies contain secondary FIs (type V).

Type I: Cassiterite in skarn is made of euhedral crystals of light brown to whitish color with primary FIs decorating growth zones (Fig. 3-4A). The FIs vary in size between a few to 20-30 μm and consist of a liquid and a vapor phase as well as one or two solid phases (Fig. 3-4B-C). During heating, the salt crystals homogenize prior to the vapor bubble at T_m ranging from 150 to 390°C. Calculated salinities derived from halite dissolution temperatures (Driesner and Heinrich 2007) range between 30 and 47 wt.% NaCl eq. with mode salinity values of ca. 40 wt.% NaCl eq. (Fig. 3-6A). Homogenization of the vapor bubble occurs at temperatures between 470 and 500 °C. Type I inclusions were exclusively observed in cassiterite from skarn.

Type II: Some rare pseudosecondary FIA in fluorite (Fig. 3-5A) hosted by schist show T_h of around 450°C and salinities between 11 and 14 wt.% NaCl eq. (Fig. 3-6A). Type IIa fluorite crystal shows no direct relation to the quartz vein but is overgrown at its rim by quartz and thus seems to represent an earlier stage. Vein cassiterites hosted by schist have elongated grains and show brown to black color, which is challenging for microthermometry. However, we could analyze primary FIA in some rare growth zones (type IIb; Fig. 3-4D-E). The FIs contain a liquid and vapor phase and are smaller than those in cassiterites from the skarn (type I), with maximum sizes of ca. 20 μm . Type IIb FIs homogenize by vapor disappearance at around 390°C (Fig. 3-6A). The salinity of type IIb inclusions mainly lies between 2.5 and 6 wt.% NaCl eq. Cassiterites in greisen have small grain sizes of about 50-300 μm and show brown to black color. Both features are limiting FIs microthermometry and therefore, only a small number of FIs measurements of two-phase (L + V) inclusions (type IIc) could have been performed. The salinity and homogenization temperatures of type IIc inclusions (Fig. 3-

4F) are in a similar range compared to those of FIs in cassiterite hosted by schist (1.9-3.4 wt.% NaCl; 350 – 400°C; Fig. 3-6A).

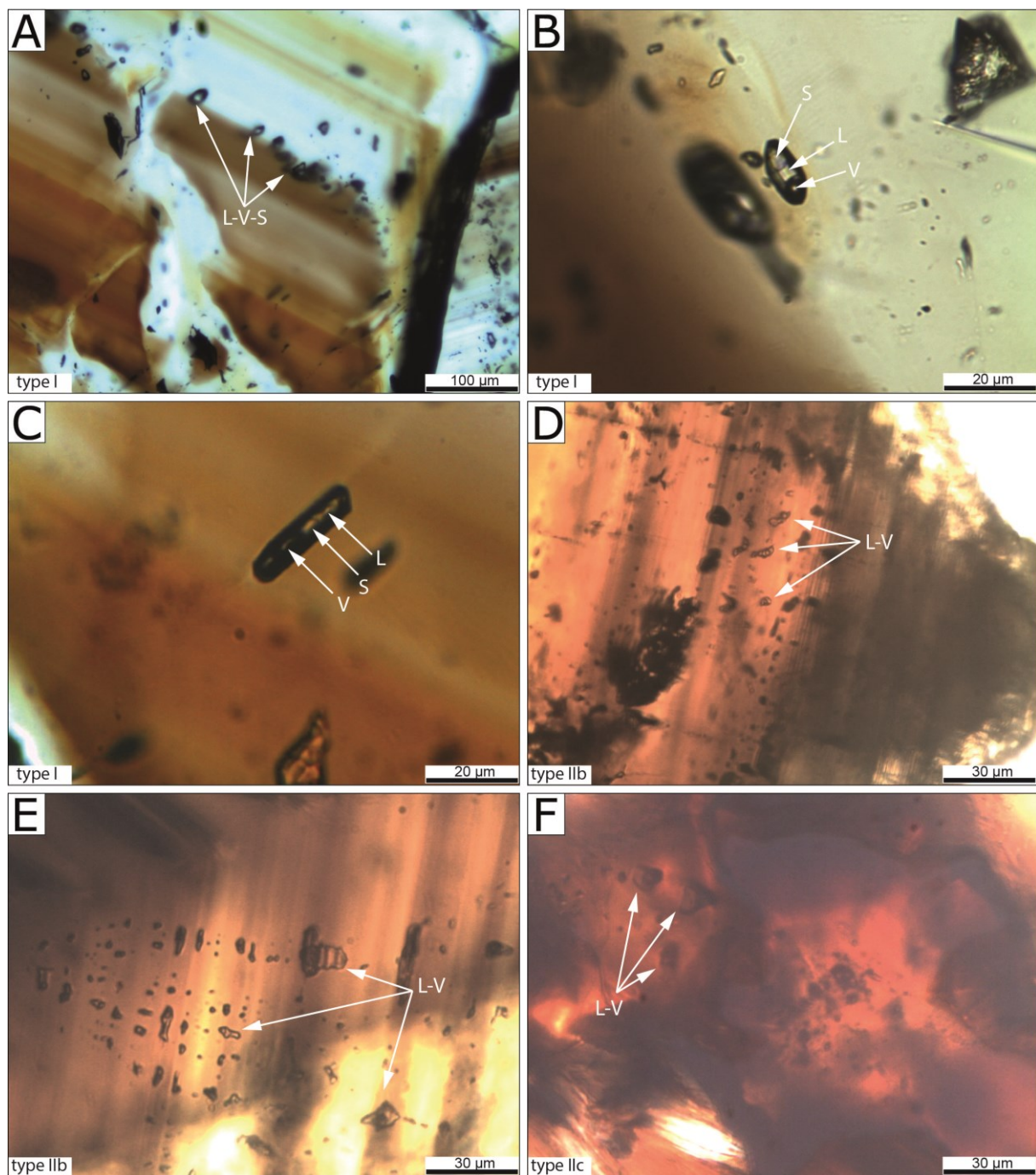


Fig. 3-4 Fluid inclusions types in cassiterite: A-C) Type I inclusions in growth zones of skarn cassiterite (HAE 15), typically containing two salt crystals. D-E) Two-phase type IIb inclusions in cassiterite of a vein in schist (HAE 7). F) Rare two-phase type IIc inclusions in cassiterite crystals of the greisen mineralization (JG 2)

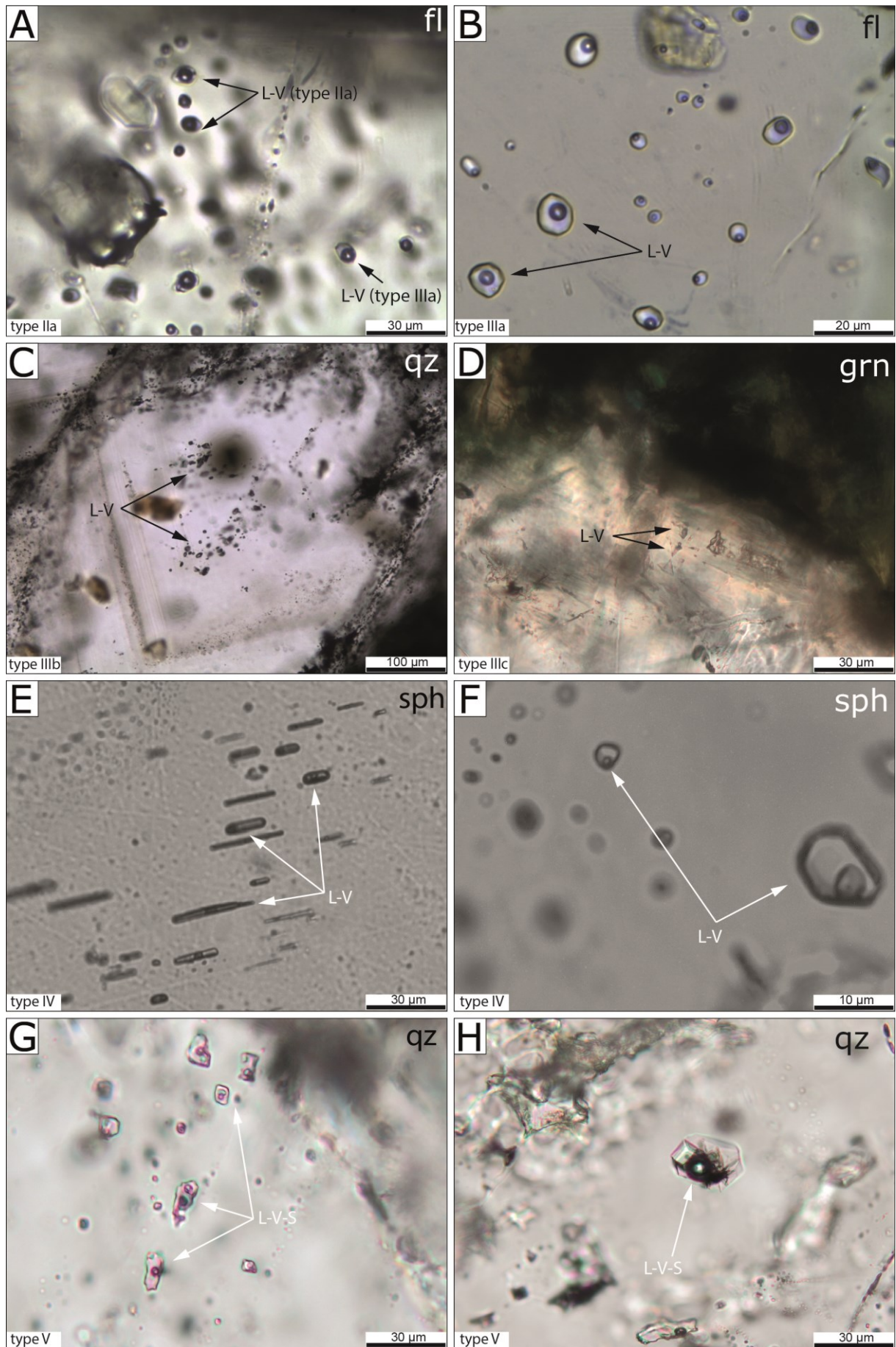


Fig. 3-5 (previous page) Fluid inclusions in various gangue minerals and sphalerite: A) Fluorite with pseudosecondary type IIa trails (HAE 9) but also containing secondary IIIa FI trails. B) Clouds of type IIIa inclusions in fluorite (HAE 15). C) Type IIIb inclusions in the wake of a growth zone in quartz (HAE 8). D) Rare Type IIIc inclusions in garnet (HAE 3). E-F) Stacked images of clouds of two-phase type IV inclusion in sphalerite (E: HAE 40, F: HAE 30). G-H) High-salinity type V inclusions in quartz (HAE 9)

Type III: This category contains all primary and pseudosecondary FIA in the gangue minerals fluorite (type IIIa), quartz (type IIIb) and garnet (type IIIc) besides the type IIa inclusions in fluorite (due to their higher temperature and salinity). FIs in gangue minerals are always aqueous-two phase and show vapor bubble disappearance during heating runs. T_h values and salinity of type III FIs show a similar distribution and are partially overlapping with the fluid inclusion data of cassiterite hosted by schist and greisen (types IIb and IIc). Fluorite was found in skarn and schist (type IIIa) and shows the widest T_h and salinity range of all gangue minerals (Fig. 3-5B). Type IIIa inclusions are forming pseudosecondary trails or clouds and homogenize between 210 and 320 °C with salinities from 2-9 wt.% NaCl eq. (Fig. 3-6A). The size of the inclusions is highly variable, from a few μm up to 40 μm in some rare FIA in skarn. Quartz is the most abundant gangue mineral and occurs in all units and highly intergrown with fluorite (except type IIa hosting fluorite) and chlorite. Quartz-hosted FIs are shown as type IIIb in Fig. 3-6A. Their homogenization temperatures vary from 230 to 330 °C and the salinities are between 3 and 7 wt.% NaCl eq. Variations of salinity and homogenization temperatures of the IIIb FIs are not related to the lithology that hosted the studied quartz samples. Fluid inclusions in the wake of growth zones had maximum sizes of 10 μm but were up to 20 μm in diameter in pseudosecondary trails or in isolated clouds (Fig. 3-5C). Garnet with measurable inclusions only occurs in one skarn sample (type IIIc), where it has a brownish to whitish color and grossular-andradite composition. Type IIIc inclusions are located in growth zones or occur as clouds and have an angular shape with sizes below 20 μm (Fig. 3-5D). They homogenize into the liquid phase at temperatures between 270-300 °C and have salinities ranging from 2 to 3.8 wt.% NaCl eq. (Fig. 3-6A).

Type IV: FIs in sphalerite were only observed as trails of aqueous two-phase (L+V) inclusions. These inclusions are the only detectable FIs in massive sphalerite which further lacks any distinct growth zones or crystal zonation (Fig. 3-5E-F). Thus, those inclusions are the presumed FIs which represent the sphalerite precipitating fluid. The shapes of the FI can be highly variable in different trails (round, elongated or angular) but are homogeneous within individual trails. Their sizes and shapes range from a few μm round FI to 30 μm long needles. The FI homogenize into the liquid phase at temperatures between 185 and 220 °C and have

salinities of 2-6.7 wt.% NaCl eq. (Fig. 3-6A). The FI in sphalerite contain the lowest T_h values of the entire data set but partly overlap with the lower limit of T_h analyzed in the gangue minerals (type III).

Type V: In addition to the primary and pseudosecondary FIA of types I to IV, quartz crystals hosted abundant FI of which few high saline measurable inclusions appeared as clouds or isolated occurrences (Fig. 3-5G-H). The vapor bubbles typically disappear at temperatures of ca. 170 °C and the FI eventually homogenize by salt disappearance at temperatures between 270 and 300 °C, resulting in a salinity of around 35 wt.% NaCl eq. (Fig. 3-6A). These inclusions are neither related to the other generations of FIs nor to any growth zone in the quartz and are thus considered to be secondary FIs that probably represent an event post-dating the main Sn-Zn-In mineralization.

3.5.2 Fluid compositions

Type I: The absolute trace element concentrations in type I inclusions are the highest in all measured inclusions (Fig. 3-6) with average Pb contents of 3500 ppm and Mn contents of 17,900 ppm. The highest absolute values in type I inclusions besides Na were contents of 33,000 ppm Zn (average: 22,700 ppm) and 125,000 ppm K (average: 66,000 ppm). K/Na ratios are typically close to one or slightly below, but can also reach values up to three in the FI (Fig.3-6D). Other abundant elements that were detectable throughout all measurements were Cs and Rb with average values of 2800 ppm and 680 ppm respectively.

Type II: The intermediate saline inclusions in fluorite of type IIa show element concentration of Cs and Rb between those of type I and type IIb/c with average values of 2960 ppm and 1290 ppm, respectively. Other elements which are abundant in cassiterite are below the detection limit in IIa inclusions, e.g. Mn or Pb. In general, the trace element content of FIs in types IIb and IIc is comparable, e.g. Pb (averages: 78 ppm in IIb, 156 ppm in type IIc) or Zn (averages: 824 ppm in IIb, 1790 ppm in type IIc) and notably is one to two orders of magnitude lower than in type I. Cs and Rb also have distinctly lower average values in IIb (Cs: 305 ppm, Rb: 126 ppm) and IIc (Cs: 460 ppm, Rb: 128 ppm) in comparison to type I.

Type III: The trace element concentrations of FIs in the gangue minerals (especially quartz) show similar ranges in comparison to the inclusions of type IIb and IIc. Cs contents vary mainly between average values of 1500 ppm in fluorite and 190 ppm in quartz (garnet: 109 ppm). Only few other elements were measurable throughout all the gangue minerals, e.g. Rb (averages: 195 ppm in fluorite, 76 ppm in quartz and 30 ppm in garnet) or K (averages: 5700 ppm in fluorite, 5200 ppm in quartz and 1900 ppm in garnet). In contrast to fluid

compositions in cassiterite, the base metal content (e.g. Zn, Pb) in the gangue minerals is only rarely above the detection limit. Paucity of signals above the detection limit can also be observed for Sn, which was only measurable in 20% of the analyses (with maximum contents of 1160 ppm).

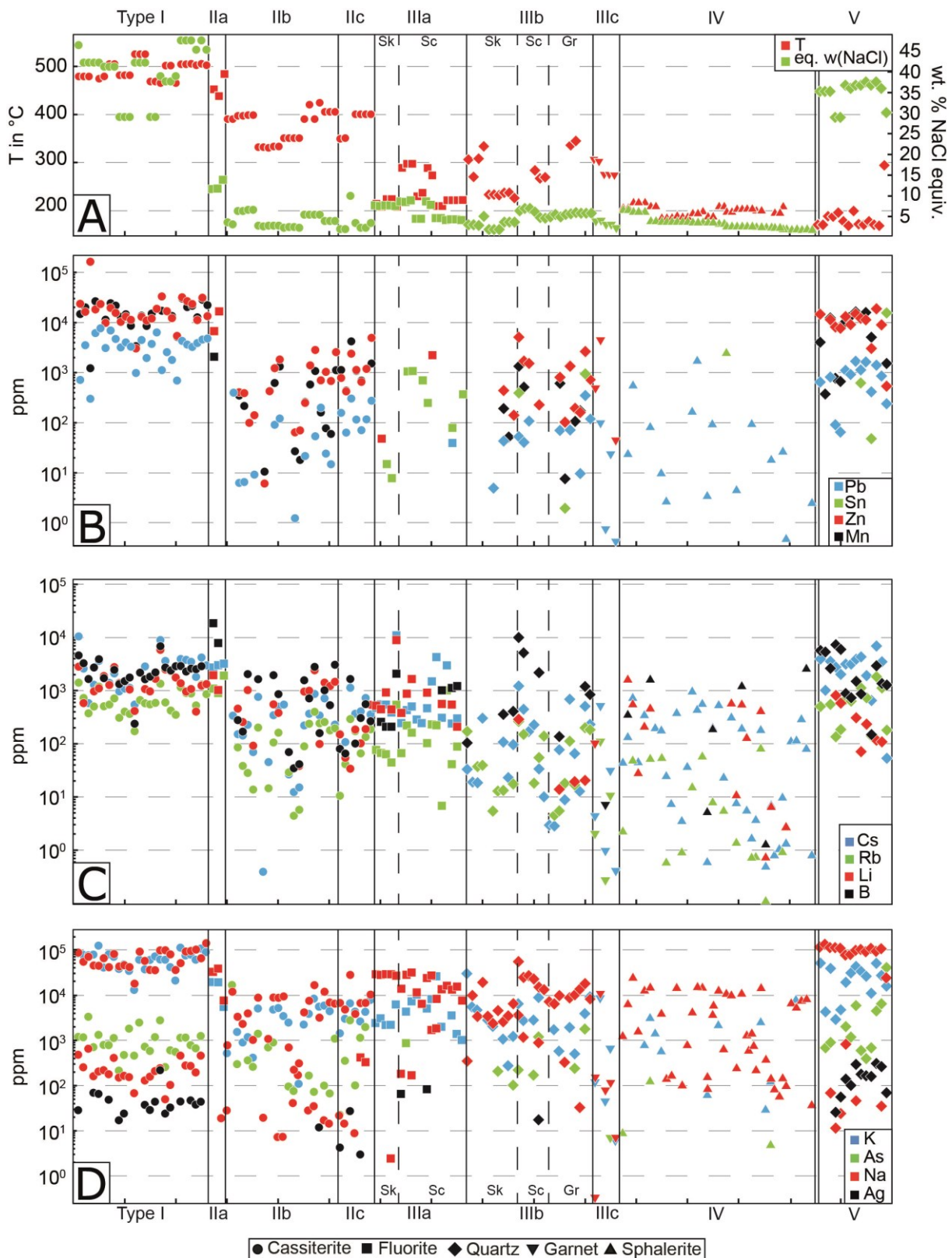


Fig. 3-6 (previous page) A) Homogenization temperatures and salinities of all types of fluid inclusion assemblages, with every data point representing one measured inclusion. B-D) Element contents (LA-ICP-MS analyses) in fluid inclusions hosted in cassiterite (circles), fluorite (squares), quartz (diamonds), garnet (downward triangles) and sphalerite (upward triangles). Sk: skarn, Sc: schist, Gr: greisen

Type IV: The chemistry of the FIs in sphalerite is characterized by generally lower concentrations than in the other minerals (e.g. Cs, Rb, Li, B and Pb) or values below the detection limit (e.g. Sn, Zn, Mn, As, Ag). In particular, the average contents of Cs (170 ppm) and Rb (20 ppm) are markedly lower than in other FI types at similar or slightly lower salinity.

Type V: The secondary high-salinity inclusions in quartz show high contents of various trace elements. The absolute values of Cs and Rb are similar to those measured in the high-salinity FI of type I with 2900 ppm and 710 ppm, respectively, but show a lower metal content, e.g. Pb (average: 840 ppm), Zn (average: 10300 ppm) or Mn (average: 9400 ppm). Furthermore, the K/Na ratios are lower, mainly ranging between 0.5 and 0.03 with an average of 0.3. The Na content of type V inclusions is relatively constant, whereas most trace element contents are highly variable.

3.5.3 Chlorite compositions

All four types of chlorite have relatively similar Al and Fe/(Fe+Mg) contents, with interstitial chlorite typically at the lower end and chlorite overgrowth at the upper end of the range (Fig. 3-7A). Calculated temperatures range from 227 to 276 °C after Cathelineau (1988) and are slightly higher, ranging from 232 to 282 °C, after Jowett (1991) (Fig. 3-7B). The maximum difference between the temperature estimates is about 6.5 °C. A few higher temperatures of chlorite overgrowing cassiterite relate to slightly higher Fe contents, which may also result from its strong intergrowth with some Fe-hydroxides. The average temperatures of the interstitial, vein and veinlet types range between 252 °C and 257 °C, while the overgrowth type shows slightly higher average temperatures of 266 °C and 272 °C.

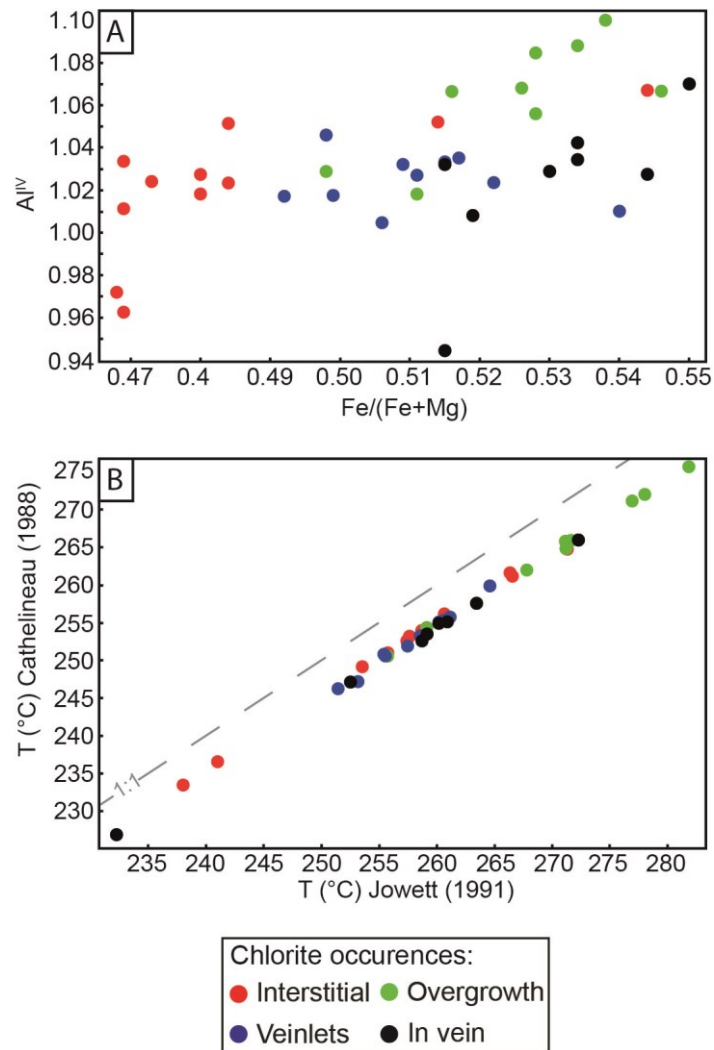


Fig. 3-7 Chlorite compositions and thermometry. A) Correlations of Al^{IV} vs. $Fe/(Fe+Mg)$, which are the main cations on which the thermometry calculations are based on. B) Chlorite formation temperature as calculated according to equations by Cathelineau (1988) and Jowett (1991)

3.6 Discussion

3.6.1 Variations in fluid compositions

The chemical compositions of the ore fluids obtained by LA-ICP-MS suggest that all cassiterite and gangue minerals precipitations (types I – III) can be traced back to a common fluid source. Variations in elemental abundances mainly depend on salinity. The selection of binary plots in Figure 8 documents this relation by near-constant element ratios in FI hosted in these minerals, such as a Zn:K ratio of about 4:1 for most of the data (Fig. 3-8A) and linear correlations of Pb vs. Mn (Fig. 3-8B), Na vs. Rb (Fig. 3-8C), and Pb vs. Cs (Fig. 3-8D). Conversely, the data from all inclusion types together define relatively tight clusters in Na-normalized binary plots, which eliminate the strong influence of salinity - such as the K/Na vs. Mn/Na (Fig. 3-8E) and Cs/Na vs. Rb/Na (Fig. 3-8F) ratio plots.

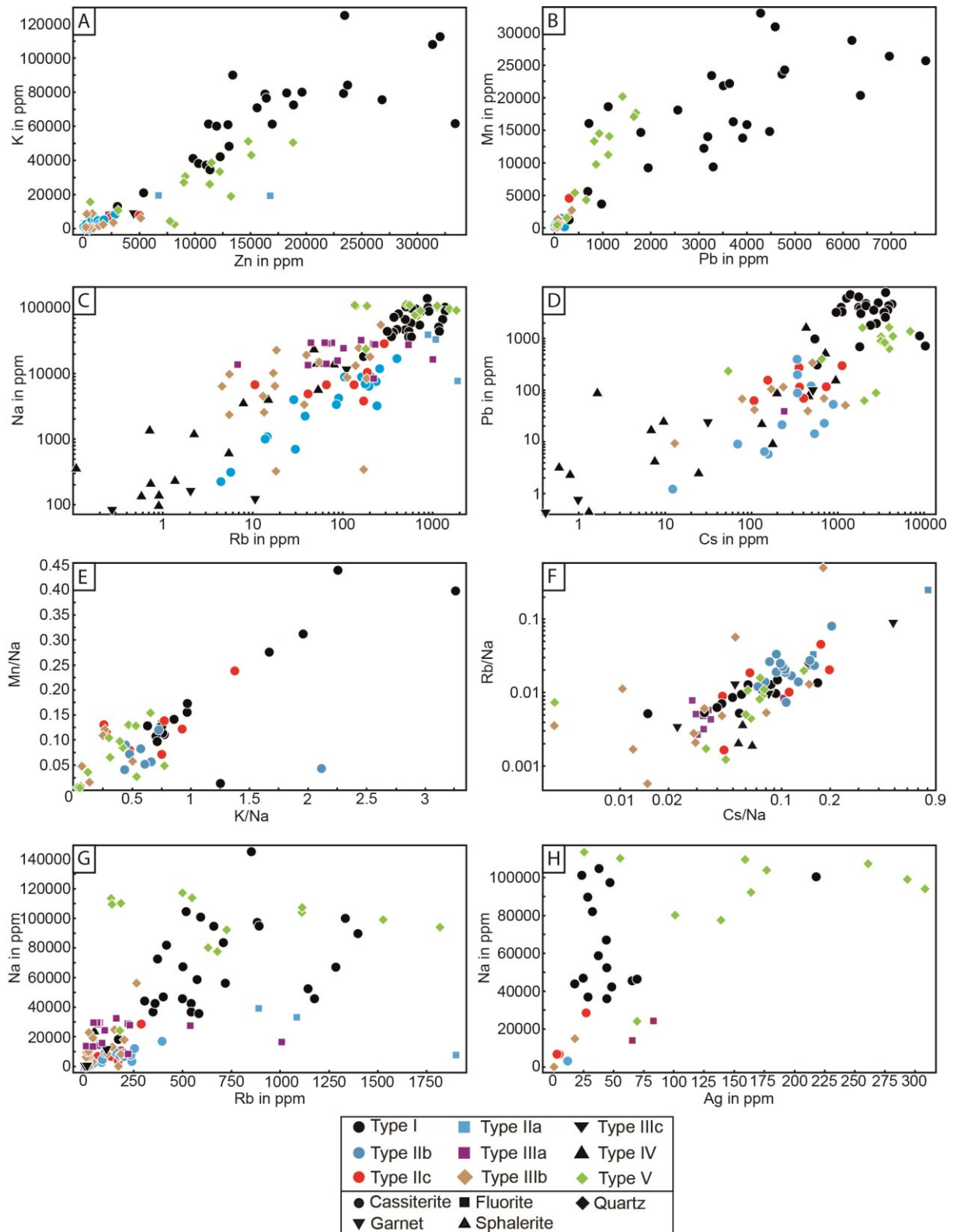


Fig.3-8 Variations in fluid compositions of absolute concentrations of Zn vs. K (A) and Pb vs. Mn (B) showing the good correlation of the FI types I to IV, as well as logarithmically plotted concentrations of Rb vs. Na (C) and Cs vs. Pb (D) illustrating the low trace element content in the sphalerite type IV FIs. Na-normalized Element ratios of K/Na vs. Mn/Na (E) and logarithmically plotted Cs/Na vs. Rb/Na (F) subtracting the influence of the salinity. Absolute concentrations of Rb vs. Na (G) and Ag vs. Na (H) showing the near-constant Na contents of the secondary type V inclusions while the Rb and Ag contents are highly variable. Type V FIs also show slightly different trends in A-D, indicating that they represent an independent later event

A good correlation can further be found by comparison of the chemical composition of FIs in greisen and schist within the same mineral, respectively (type IIb with type IIc FIs in cassiterite and inclusions within type IIIb in quartz). The similar inclusion properties and trace element contents are possible evidences that the fluid responsible for greisenization at the Eibenstock granite is comparable to the fluid forming the mineralization in the schist of the Hämmerlein deposit and the coeval gangue minerals, therefore suggesting that the underlying granite below Hämmerlein is associated to the Eibenstock granite and a potential source for the ore-forming fluids.

Type IIIc FIs in garnets from vein-like structures within the skarn units also show similar compositions as the other type I-III FIs, suggesting that the measured FIAs could represent a similar hydrothermal fluid. However, the FI content of garnet is very limited and represents the lower limit of the temperature range in the gangue minerals.

The low trace element contents of type IV FIs in sphalerite (Fig. 3-8C-D) compared to FIs from other types (type IIb, IIc, IIIa-c) suggests a process of dilution of the hydrothermal fluid which can take place by mixing of two chemically contrasting fluids, such as hydrothermal fluids and meteoric waters.

Only type V FI from secondary FIA seem to have a unique chemical signature. The variable trace element contents despite constant salinities are not visible in any other FI generation. Thus, we interpret the type V inclusions to correspond to a later stage which is unrelated to mineralizing event (Fig. 3-8G-H).

3.6.2 Fluid evolution

We interpret the fluid evolution at the Hämmerlein deposit by using petrographic observations and inferring a general trend from an early high-temperature stage followed by gradual cooling towards a waning stage (Fig. 3-9). The relative timing of FI types could not be reconstructed from petrographic observations in individual crystals, partially because the results show a remarkable clustering of FI types that are exclusively tied to specific mineral occurrences and/or settings. The FIA in fluorite show the widest range in temperatures and salinities, indicating that FI types I to IV form a continuous evolution of different stages (I – IV) of a cooling hydrothermal system, while FI type V remains separate as a late overprinting stage V.

Stage I: Skarn-hosted cassiterite exclusively and solely hosts type I FIs, representing an early hot, high-salinity stage within the hydrothermal evolution. This main ore stage occurs at unusually high temperatures of about 500 °C, which stands in contrast to typically reported

Sn-ore formation temperatures below 400°C (Heinrich 1990; Korges et al. 2018; Audétat et al. 2000). Similar high temperatures were only detected in gangue minerals (e.g. tourmaline) and have so far not been documented in cassiterite (Sugaki et al. 1988). The measured high temperatures narrow the temperature gap to an inferred granite solidus temperature of ~650°C (Johannes 1984). High-salinity brines can form by phase separation of a single-phase input fluid, which in this case would require pressures of approximately 50 MPa, based on phase relations in the H₂O-NaCl system (Driesner and Heinrich 2007). However, the calculated intrusion depth of 3 – 6 km of the Eibenstock granite based on melt inclusions (Thomas and Klemm 1997; Bankwitz and Bankwitz 2004) suggests that pressures were higher by some 50 to 150 MPa. Also, there is no evidence for a coexisting vapor-rich phase in the FIA that could be indicative for phase separation. High-salinity brines can also directly exsolve from granitic intrusions at this depth range, either as part of a two-phase fluid or as an early high-salinity brine phase as proposed by Cline and Bodnar (1991). An early high-salinity brine phase would also have a great capacity to fractionate large amounts of Sn from the melt to the hydrothermal systems (Yardley 2005). Despite their high density, fluid expulsion under lithostatically pressured conditions can lead to upward transport of the brines through the overlying host rock. During stage I, cassiterite precipitation was probably restricted to the skarn horizon due to favorable conditions for fluid-rock interaction (Schmidt 2018). The reactions with carbonate minerals of the inferred original lithology or with previously formed skarn silicates by metamorphism could both serve as potential triggers for ore formation.

Stage II: Rare occurrence of pseudosecondary trails in fluorite (type IIa) preserve inclusions with entrapment conditions between type I and IIb FIs. These erratic inclusions seem to represent the late veining phase of stage I and/or the beginning of stage II, indicating a gradual transition to lower-salinity input fluids as proposed by Cline and Bodnar (1991). Vein cassiterites hosted by schists exclusively contain type IIb FIs that were trapped at considerably lower temperatures from lower salinity fluids than type I FIs in skarn cassiterite. The good correlation with FI hosted in greisen cassiterite (type IIc) indicates that this stage may be coeval with typical greisenization of the apical parts of the underlying granite. Fluid rock interaction is also the main process of cassiterite formation in schist and greisen (Lefebvre et al. 2018; Stemprok 1987; Schmidt 2018). The documented types of inclusions cover the typical range of formation temperatures for Sn deposits (Heinrich 1990), but form only the smaller part of the Hämmerlein mineralization (Schuppan and Hiller 2012).

Stage III: The FI record in gangue minerals mainly comprises the stage after further cooling of the hydrothermal system, partly overlapping with the low-temperature end of cassiterite mineralization and the high-temperature end of sphalerite mineralization. The subordinate amount of Sn in type III inclusions can be a sign of an already less Sn-loaded hydrothermal fluid with only 20% of the measurements above the detection limit and therein an average Sn concentration of 480 ppm. The estimated formation temperatures of chlorite occurrences in skarn fall within the range of stage III, indicating that chlorite forms together with fluorite and quartz but post-dates the main mass of cassiterite in skarn. The FI content of garnets in vein-like structures in skarn are compatible with other stage III occurrences.

Stage IV: Skarn sphalerite exclusively and solely hosts type IV FI, which shows a further decrease in temperature and a dilution trend in chemical compositions. The solubility of Zn is highly temperature-dependent (Yardley 2005) and cooling is often inferred as a precipitation processes for massive sulfide deposits (Monecke et al. 2014). We suggest that stage IV may be related to the influx of meteoric waters into the waning hydrothermal system although a cooler, exhausting, late stage hydrothermal fluid may show equal properties. Mixing processes have also been proposed for late sulfide stage mineralizations of the Huangang Fe-Sn skarn (Mei et al. 2015) and sphalerite precipitation by slow mixing can lead to a lack of measurable primary fluid inclusions (Watanabe 1987; Bodnar 2003). The lack of coexisting gangue quartz supports this interpretation, because the meteoric water component would be on a heating path and may thus not precipitate but rather dissolve quartz due to the positive temperature dependence of quartz solubility (Fekete et al. 2016).

Stage V: Despite their spatial distance of about 12 km, the late type V FIs can be found in all three settings, skarn, schist and greisen. This generation of high-salinity brines homogenize by halite disappearance, suggesting that the fluids may have been salt saturated. The high salinity is accompanied by high metal contents, which are comparable to the ore-stage fluids of the Hämmerlein deposit and could indicate a potential remobilization or later post-Variscan mineralization event (Baumann and Werner 1968; Behr and Gerler 1987; Behr et al. 1987). However, even though type V FI have higher Ag contents than the other FI types and the district is known to host significant U mineralization post-dating the Sn mineralization, our results provide no constraints on the timing, significance or source of this event.

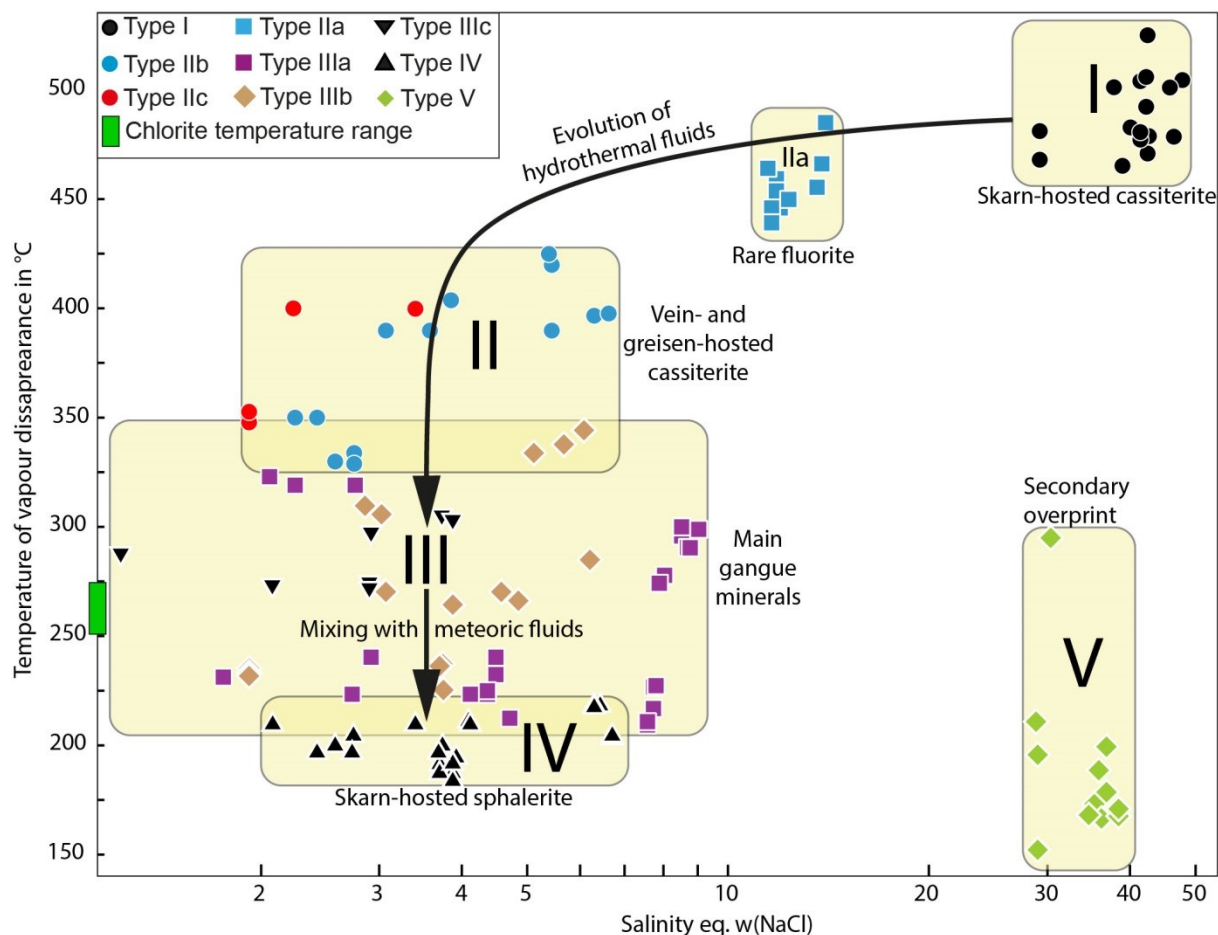


Fig. 3-9 Temperature-Salinity plot summarizing the FI data of types I to V, showing the evolution of the hydrothermal fluid

3.6.3 Implications

We have studied FIs in five different types of ore and gangue minerals (cassiterite, sphalerite, quartz, fluorite and garnet) and the results show that primary FIs and/or inclusions forming FIA in ore minerals are not contained in coexisting gangue minerals. In particular, type I FIs in the main cassiterite phase show much higher temperatures and salinities, i.e. the main ore-forming event is only captured in the actual ore mineral, highlighting the value of fluid inclusion analyses in ore minerals (Lüders 1996; Kouzmanov et al. 2010; Korges et al. 2018).

Combining FI data with chlorite thermometry further showed that there is a 200°C temperature gap between ore and gangue minerals. Chlorite thermometers can have a big scatter and should be used with care (Zimák 1999). However, our calculated chlorite formation temperatures only show small variations and suggest the same temperature range as the coexisting quartz and fluorite. Therefore, our results indicate that the analyzed veins rather document a later hydrothermal stage which overprints the original gangue minerals of the first

Sn mineralization. Kern et al. (2018) documented the statistical significance of the cassiterite-chlorite-fluorite-sulfide coexistence. Our fluid inclusion results support the interpretation of a common hydrothermal event, but suggest that precipitation was only partially coeval (indicated by the overlaps of type II – IV FI) but rather sequential during cooling of the hydrothermal fluids (Fig. 3-9). This interpretation is also supported by petrographic observations showing that chlorite typically occurs as overgrowths, veinlets and interstitial in massive skarn cassiterite (Fig. 3-2A, B; Fig. 3-3A, B), as well as the massive, almost mono-mineralic sphalerite occurrences (Fig. 3-2C, D).

Our results provide no direct constraints on the relative or absolute timing of skarn formation, Sn-Zn-In mineralization, granite emplacement and greisenization documented in the Hämmerlein district. However, the high temperatures of Sn skarn mineralization and the similarity to FIA in the greisen sample point towards a fluid source from an underlying intrusion related to the Eibenstock granite. The interpretation of the main Sn formation from the expulsion of an early high-salinity magmatic brine suggests a relatively short-termed event during the evolution of the magmatic province and its overlying hydrothermal system, which is able to concentrate the release of Sn in the fluid and focus its precipitation to a confined horizon that is particularly prone for reaction. This ideal chain of processes may explain why skarn horizons can represent such compact but high-grade ore deposits, which could become economically more important with improved mineral processing techniques (Buchmann et al. 2018).

3.7 Conclusions

Fluid inclusion assemblages in ore and gangue minerals from the Hämmerlein deposit provide direct insights into the fluid evolution during ore formation. We propose a sequential evolution that starts with the main cassiterite formation in the skarn horizon during stage I by the expulsion of an early high-salinity magmatic brine from a deep-seated intrusive body at unusually high temperatures of about 500°C compared to typically reported Sn mineralizations of 400°C and below. Vein cassiterite in schists precipitated from a cooler and less saline fluid from the same source during stage II. The similarity to FIs related to the greisenization of the nearby Eibenstock granite suggests a similar or common source. The FIs in gangue minerals and the results from chlorite thermometry show that most gangue minerals are related to this later fluid release and form simultaneously to the ore minerals in schist/greisen in stage II or later during further cooling in stage III. Influx of meteoric waters during the waning stage IV leads to the last ore-forming process by precipitating Zn and In in

sphalerite. Stage V marks a later overprint by high-salinity brines which is interpreted to be unrelated to the Sn-Zn-In mineralization of the Hämmerlein skarn deposit. The fluid inclusion record of the ore minerals was the key to reveal the difference between the three types of mineralization, in particular to identify the unusually hot brine as the main mineralizing fluid which has not been documented before, and emphasizes the importance of fluid inclusion analyses in ore minerals

4 Incremental magma chamber growth and its significance for ore precipitation in porphyry copper deposits

Maximilian Korges¹, Philipp Weis¹, Christine Andersen¹

¹*GFZ German Research Centre for Geosciences, Telegrafenberg, 14473 Potsdam, Germany*

In preparation for submission to *Earth and Planetary Sciences Letters* or *Geochemistry, Geophysics, Geosystems*. The readers must be aware of potential differences between the future publication and this chapter.

Abstract

Porphyry copper deposits are associated with magmatic fluids released from granitic to dioritic intrusions of batholithic dimensions. These plutons are inferred to have been incrementally built up by a series of injections of magmatic sills. Hence, magma chamber growth is mainly dependent on the magmatic volumetric injection rate but can also be influenced by hydrothermal convection and fluid release. However, the detailed interplay and impact of these various aspects is still debated. To quantify the interplay between magma chamber growth, fluid flow and ore formation, we implemented modelling capabilities that can simulate the injection of sills of various dimensions at different time intervals in concert with multi-phase fluid flow. In order for a magma chamber to be built up within a period of ca. 50 kyrs, an injection rate of at least $3.9 \times 10^{-4} \text{ km}^3/\text{y}$ is required, which constantly maintains a small region of melt. Higher magma influxes of ca $5 - 6.5 \times 10^{-4} \text{ km}^3/\text{y}$ are able to form magma chambers of 2 – 3 km in thickness and continuously produce fluids, which are precipitating a copper ore shell in the host rock ca 2 km above the injection location. The copper enrichment region associated to an incrementally growing magma chamber is more narrow and defined than the ones generated by an instantaneous emplacement of a voluminous magma chamber, due to a more constant production of magmatic fluids over time. The continuous flux of fluids is forming a stable fluid plume, precipitating a copper ore shell in a defined region, resulting in higher ore grades. Our simulation results suggest that magma chambers related to porphyry copper deposits form by rapid and episodic injection of magma. Slower magma chamber growth rates more likely result in barren plutonic rocks, although they are geochemically similar to porphyry hosting plutons.

4.1 Introduction

Porphyry copper systems form in volcanic arcs above subduction zones at convergent plate boundaries by hydrothermal fluids expelled from hydrous magmatic intrusions within the upper crust (Richards 2009; Sillitoe 2010). They provide most of the world's Cu and half of its Mo reserves and are important sources for Au, Ag, Re, Pb and Zn (Arndt et al. 2017). The mineralization is associated with intense stockwork veining and pervasive alterations formed by multiple cycles of magmatic-hydrothermal fluid influx into the host rock (Landtwing et al. 2005). Fluid inclusion data show that the magmatic fluids exsolved from the magma chamber have a salinity of 2 - 10 wt% NaCl and can contain several thousand ppm of base metals (Audétat et al. 2008; Landtwing et al. 2005; Sillitoe 2010). Upon ascent, this single-phase fluid can phase-separate during cooling and decompression into hypersaline brines with up to 70 wt% NaCl and a large volume of low-density vapor (Bodnar 1995; Fournier 1999; Roedder 1984). Cu precipitates during fluid cooling over a range of 550°C to 350°C, with typical values between 450°C and 350°C, assisted by fluid-rock interaction (Klemm et al. 2007; Redmond et al. 2004; Rusk et al. 2008; Sillitoe 2010). The mineralization is inferred to form on time scales of 50 to 100 kyrs, although the associated magmatic systems may be active over millions of years (Chelle-Michou et al. 2015; Gilmer et al. 2017; Von Quadt et al. 2011).

The underlying hydrous magmatic intrusion typically has a felsic composition, batholithic dimensions and is hosted by a long-lived magmatic complex which was incrementally built up by multiple intrusive events. These plutons can be the source for one deposit as well as for clusters of more deposits (Sillitoe 2010). However, the plutonic rocks themselves are only rarely exposed at the surface or by drill cores, e.g. Yerington district, Nevada (Dilles 1987), and are therefore difficult to be analyzed directly. Most numerical modelling studies of magmatic-hydrothermal systems assume an instantaneously emplaced magma chamber with hundreds of cubic kilometers of magma within a cold host rock (Cathles et al. 1997; Hayba and Ingebritsen 1997; Scott et al. 2017; Steinberger et al. 2013; Weis et al. 2012). However, geochemical data indicate that plutons of this size were emplaced over several million years (Coleman et al. 2004; Matzel et al. 2006) and that they are mostly forming by agglomeration of pulses of sills (Annen 2009; Menand 2008; Michel et al. 2008; Pasquarè and Tibaldi 2007). The magma influx rate has to be high enough to prevent older sills from complete solidification before the next sill arrives, but it should not be so high that the majority of magma erupts (Audétat et al. 2012; Bachmann et al. 2007). Volcanic eruptions are incompatible with simultaneous porphyry copper formation because the volatiles tend to

dissipate during the eruption rather than being preserved in the fluid plume (Cloos 2001; Pasteris 1996; Sillitoe 2010).

The thermal evolution during incremental magma emplacement has so far only been investigated by purely conductive numerical simulations (Chelle-Michou et al. 2017; Gelman et al. 2013; Schöpa et al. 2017). These studies provide first quantitative constraints for the relation between magma fluxes and porphyry copper mineralization, but do not consider the influences of expulsion of magmatic fluids and hydrothermal convection of ambient fluids. Constraining the magma flux rates that can build up a magma chamber that is sufficient to provide a fluid source capable of forming a porphyry copper deposit requires an approach which combines an incrementally growing, conductively cooling magma chamber with convective cooling by hydrothermal fluids circulating in the host rock and magmatic fluid expulsion.

4.2 Methods

In this study, we simultaneously simulate sill injection, heat transfer, release of metal-bearing magmatic fluids, multi-phase flow of saline hydrothermal fluids and dynamic permeability variations with a continuum porous medium approach using an implementation of the Complex System Modeling Platform (CSMP++), where mass and energy conservation are solved with a Control Volume Finite Element Method (Weis et al. 2014).

4.2.1 Sill injection and magmatic fluid production

So far, simulations of magmatic-hydrothermal systems using CSMP++ prescribed one large magmatic intrusion during model initialization. We developed a new functionality that enables sill injection as a hot horizontal sheet of magma at variable intervals and with adjustable sizes. For the bookkeeping of nodal variables during sill injection, we use a regular grid with a constant horizontal and vertical spacing ($dx=dy$) of 400 and 200 m between computational nodes. The triangular elements are arranged in a vertical fishbone pattern to avoid mesh effects due to a preferred diagonal orientation and to ensure that the node-centered control volumes along vertical transects have identical orientations and volumes (Fig. 4-1A). The width and thickness of the injected sill are set to be equal to or multiples of dx and dy , i.e. $a \times dx$ and $b \times dy$ with a and b being natural numbers. Sills are injected episodically after a specified time interval according to a time-integrated average magma flux. At the time of sill injection, the model creates space by downward movement of the rock mass below the sill. The mass and energy conserving variables of the control volumes within and

below the sill location are mapped downward to the respective control volumes located at a distance of $b \times dy$. Mass and energy stored in control volumes, which are moving out of the modelling domain are removed from the system, while the mass and energy of the new control volumes are initialized with properties representing the new magmatic sill.

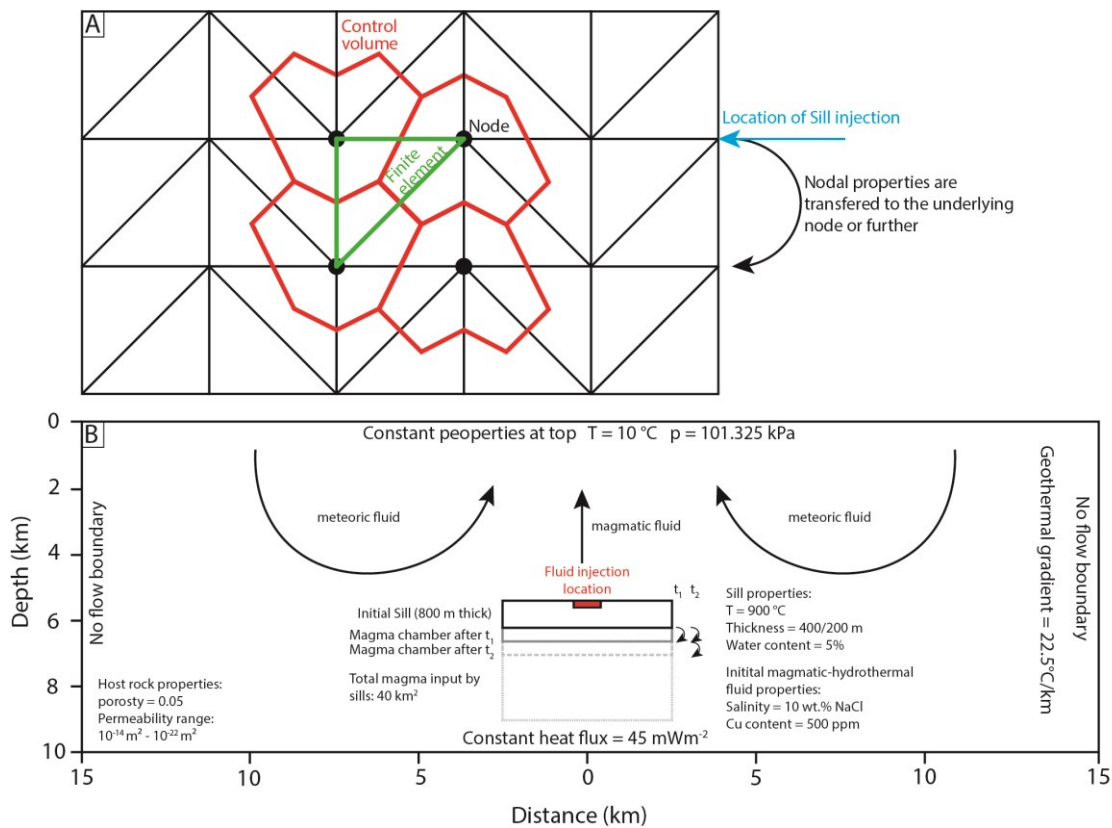


Fig.4-1 Mesh setup and initial conditions of the simulation. A: Fishbone mesh with indicated shift of node parameters by one row of nodes after sill injection. B: Initial condition of the simulation with outlined injection of sills

We assume that the hydrous silicic magma contains 5% of water ($C_{\text{water}} = 0.05$) which is linearly released during cooling between $T_{\text{liquidus}} = 750^\circ\text{C}$ and $T_{\text{solidus}} = 650^\circ\text{C}$. Injected sills can re-heat previously injected volumes, which have already released part of their water. To ensure mass balance, we therefore monitor the fluid volume released from a certain control volume and also map this information during sill injection. To this end, we modified the functionality of Weis (2015), which calculated the crystallized fraction of the elements below the solidus of 700°C , to a crystallized fraction of the control volumes. We further assume that the newly produced magmatic fluids are transported to the center region at the top of the magmatic intrusion by processes within the magma chamber unresolved by the model. The total mass of magmatic fluid injected at time t is calculated as

$$m_{fluid\ source}(t) = f_{2d} \cdot C_{water} \cdot \rho_{rock} \cdot \sum_{volumes} \left(f_{3d} \cdot V \cdot \frac{T(t-dt) - T(t)}{T_{liquidus} - T_{solidus}} \right) \quad (1)$$

with V as the volume and the density of the rock ρ_{rock} . Fluid accumulation from the 3rd dimension is taken into account by first scaling the 2-dimensional (2D) control volume to 3D using

$$f_{3d} = \pi dx_{center} w_y \quad (2)$$

where dx_{center} is the horizontal distance of the respective node to the assumed vertical center axis and w_y is the ratio of the horizontal dimensions in width and depth of the magma chamber ($w_y = 0.5$) resulting in a 3D cylindrical shape of every sill (for a detailed description see (Weis 2015)). The total fluid volume is then scaled back to a circular 2D cupola region with a radius $R=400$ m using

$$f_{2d} = \frac{2}{\pi \cdot R_{cupola}} \quad (3)$$

The total fluid mass is then equally distributed across the nodes representing the cupola.

4.2.2 Multi-phase fluid flow and dynamic permeability

We calculate the circulation of saline multi-phase hydrothermal fluids using the extended form of Darcy's law with the Darcy velocity of a fluid phase i (liquid (l) or vapor(v))

$$v_i = -k \frac{k_{r,i}}{\mu_i} (\nabla p - \rho_i g), \quad i = l, v \quad (4)$$

where k is the bulk rock permeability and $k_{r,i}$ the relative permeability, μ_i the dynamic viscosity and ρ_i the density of the indicated fluid phase i . The acceleration due to gravity is expressed by g and the total fluid pressure by p (Ingebritsen et al. 2006). Saline fluids can further precipitate a solid halite phase h . We apply a linear relative permeability with

$$k_{rv} + k_{rl} = 1 - S_h \quad (5)$$

where S_h is the volumetric saturation of the immobile halite phase. The liquid residual saturation is defined as $R_l = 0.3(1 - S_h)$ and the vapor residual saturation as $R_v = 0.0$. Conservation of fluid mass is calculated by

$$\frac{\partial(\phi(S_l\rho_l + S_v\rho_v + S_h\rho_h))}{\partial t} = -\nabla(v_l\rho_l) - \nabla(v_v\rho_v) + Q_{H_2O+NaCl} \quad (6)$$

where ϕ is the porosity, $Q_{H_2O+NaCl}$ refers to the source term of fluid mass and t is the time. The salt mass conservation is obtained by

$$\frac{\partial(\phi(S_l\rho_lX_l + S_v\rho_vX_v + S_h\rho_hX_h))}{\partial t} = -\nabla(v_l\rho_lX_l) - \nabla(v_v\rho_vX_v) + Q_{NaCl} \quad (7)$$

with Q_{NaCl} as the source term and X_i as the mass fraction of NaCl. Energy conservation includes heat advection by the fluid and heat conduction through the rock with a constant thermal conductivity K and is described by

$$\begin{aligned} \frac{\partial((1-\phi)(\rho_r h_r + \phi(S_l\rho_l h_l + S_v\rho_v h_v + S_h\rho_h h_h))}{\partial t} \\ = \nabla(K\nabla T) - \nabla(v_l\rho_l h_l) - \nabla(v_v\rho_v h_v) + Q_e \end{aligned} \quad (8)$$

where the rock is indicated by the subscript r and h_i refers to the specific enthalpy of the phase i . The heat source term is defined as Q_e , the thermal conductivity as K and the temperature as T . The total enthalpy is distributed over the rock and fluid within a control volume based on their thermodynamic properties. Properties of saline fluids are calculated based on the thermodynamic model for NaCl-H₂O by Driesner and Heinrich (2007) and Driesner (2007).

The permeability k is calculated as a dynamic element property (Weis et al. 2012; Weis 2015) and assumes (1) a depth-dependent background permeability profile, (2) a near-critically stressed brittle crust and a subsequent failure criterion for fractures at near-hydrostatic fluid pressure conditions, (3) an increasingly ductile behavior by heating, leading to decreased permeability and differential stress resulting in failure criteria at near-lithostatic fluid pressures (with the brittle-ductile transition starting at 360°C), (4) a pressure-dependent permeability increase counteracting the temperature-dependent permeability change, and (5) an incremental permeability increase due to hydraulic fracturing of up to two orders of magnitude if fluid pressures exceed the local stress-state dependent failure criterion. The details of the permeability model are described by Weis (2015) and have further been used by Coulon et al. (2017).

Copper is transported as a tracer in the fluid and distributed equally between the mobile fluid phases i (liquid (l) and vapor (v)) by the copper mass conservation equation

$$\frac{\partial(\phi(S_l\rho_l + S_v\rho_v + S_h\rho_h)C_{Cu})}{\partial t} = -\nabla(v_l\rho_l C_{Cu}) - \nabla(v_v\rho_v C_{Cu}) + Q_{Cu} \quad (9)$$

where C_{Cu} is the copper concentration in the fluid and the source term is defined as Q_{Cu} whereby $Q_{Cu} = C_{Cu}^{initial} Q_{H_2O+NaCl}$. Copper precipitation is calculated as a function of temperature, linked to an interval between 450°C to 350°C which is based on experimental and fluid inclusion studies of porphyry copper deposits (Hemley et al. 1992; Hezarkhani et al. 1999; Landtwing et al. 2005).

The copper enrichment potential within a control volume (V) is calculated by

$$\psi_{cu} = \frac{m_{Cu}}{C_{Cu}^{initial} C_{water} \rho_r V} \quad (10)$$

with the mass of precipitated copper m_{Cu} and the water content of the melt that is released during pluton cooling C_{water} . The copper enrichment potential relates the initial copper concentration of the fluid producing pluton to the copper enrichment in the rock and can be used as a rough estimate of the potential ore grade in wt%.

4.2.3 Simulation Setup

The model domain is a two-dimensional 30 km wide and 10 km high cross section with an initial sill emplaced at 5 km depth (Fig. 4-1B). A regular triangular mesh arranged in a vertical fishbone pattern (Fig. 4-1A) was used with element width and height of 400 or 200 m in the coarse mesh and fine mesh setup, respectively. No flow boundaries were applied at the bottom and sides. Fluids can leave or enter through the top boundaries, which keeps constant conditions with temperatures of 20°C and atmospheric pressure. We use a constant porosity of 0.05, thermal conductivity of 2 Wm⁻¹°C⁻¹ and heat capacity of 880 Jkg⁻¹°C⁻¹. The host rock is initially saturated with pure water along a thermal gradient of 22.5°C km⁻¹, which is maintained by a constant basal heat flux of 45 mWm⁻².

The initial sill has a width of 5 km and a thickness of 800 m. Additional sills intruded in the center of the initial magma chamber starting at 6 kyrs, 10 kyrs, 15 kyrs or 30 kyrs and were injected continuously at the same interval until the total volume of injected magma had reached 40 km³ (initial sill + 8 sills). The different intervals correspond to an average injection rate of ca. 6.5 x 10⁻⁴ km³/y, 3.9 x 10⁻⁴ km³/y, 2.6 x 10⁻⁴ km³/y and 1.3 x 10⁻⁴ km³/y, respectively. The frequency stays constant during simulation and the new sills have thicknesses of 400 or 200 m and a width of 5 km. Every sill has an initial temperature of 900°C. Magmatic fluids have a bulk salinity of 10 wt % NaCl and an initial copper

concentration of 500 ppm. They are released through the central part of the magma chamber which is ca. 800 m in width, with the exception of two sensitivity runs where fluids are released over the entire width or at the right side of the sill. The injected magma volume uses a doubled heat capacity during initialization which is reduced to the host rock value during crystallization to account for the release of latent heat (Hayba and Ingebritsen 1997).

4.3 Results

4.3.1 Magma chamber growth

At the time of 4kys after a magmatic influx of 20 km³, the highest injection rate of 6.5×10^{-4} km³/y results in a magma chamber of almost 2 km thickness and a width of 4 km, which slowly narrows towards the bottom (Fig. 4-2A). After an influx of 40 km³, the magma chamber has grown further and reaches a thickness of about 3 km whereby the edges are steep in the upper half of the chamber and narrow slowly towards the bottom (Fig. 4-2 B). Sill injections every 10 kyrs result in a less significant magma chamber which is mainly dominated by the last sill injection and only shows small amounts of preserved sill from previous injection events at the bottom of the pluton after injection of 20 km³ (Fig. 4-2C). After 40 km³, a magma chamber with a thickness of up to 1.5 km has formed, which narrows quickly to the bottom in areas where the influence of the last sill is insignificant (Fig. 4-2 D).

When a sill is injected every 15 kyrs, a magma chamber forms which is limited to the dimensions of the last intruded sill (Fig. 4-2E) and the lowest injection rate results in only a small amount of not fully crystallized magma (Fig. 4-2G). The two lowest sill injection frequencies result in a complete crystallization of the magma between sill injections due to rapid cooling caused by the cool host rock which was only slightly heated by the previous sills. The two setups with the lowest magma injection rate after 40 km³ of magma injected (Fig. 4-2F & H) are very similar to the results after 20 km³ of magma (Fig. 4-2E & G). They are dominated by the last injected sill and do not build up a significant magma chamber with dimensions bigger than the last intruded sill, even though the previous sills heated the host rock.

4.3.2 The influence of the hydrothermal system on magma chamber growth

Hydrothermal convection of ambient fluids and the rate and location of magmatic fluid release have a significant influence on the magma chamber evolution. In simulations of incremental growth of the magma chamber which are cooled by conduction only (Fig. 4-3A), the remaining magma chamber better preserves its horizontal dimensions.

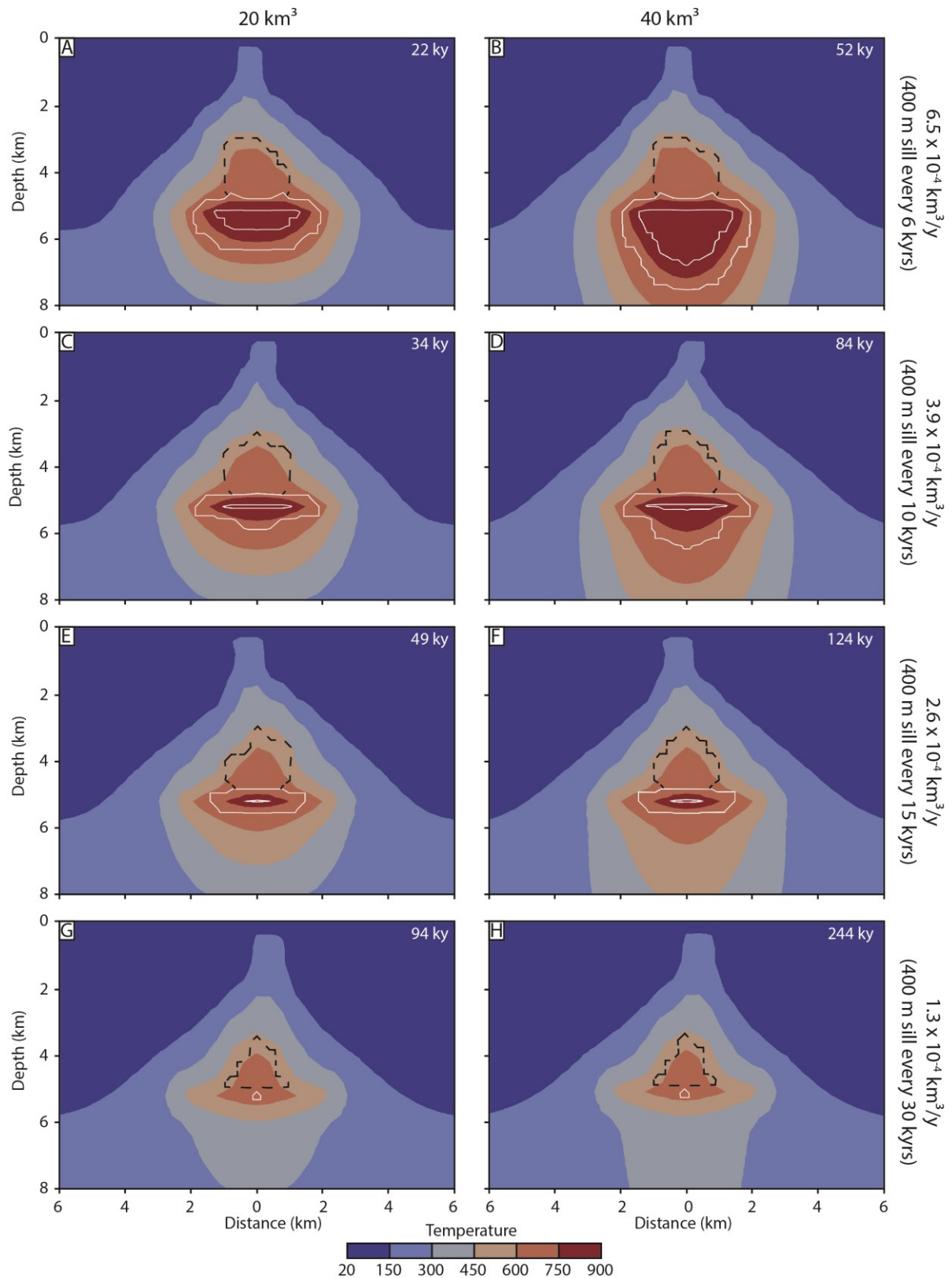


Fig. 4-2 Magma chamber dimensions after 20km³ and 40 km³ of magmatic input with decreasing injection rate from the top to the bottom. White lines correspond to the fraction of crystallization with displayed isolines of 0.1 and 0.9 from the inside to the outside of the magma chamber. The black-dashed lines show the pore fluid factor (fluid pressure divided by lithostatic pressure) with a value of 0.7 indicating the transition from near-hydrostatic fluid pressures to near-lithostatic fluid pressures

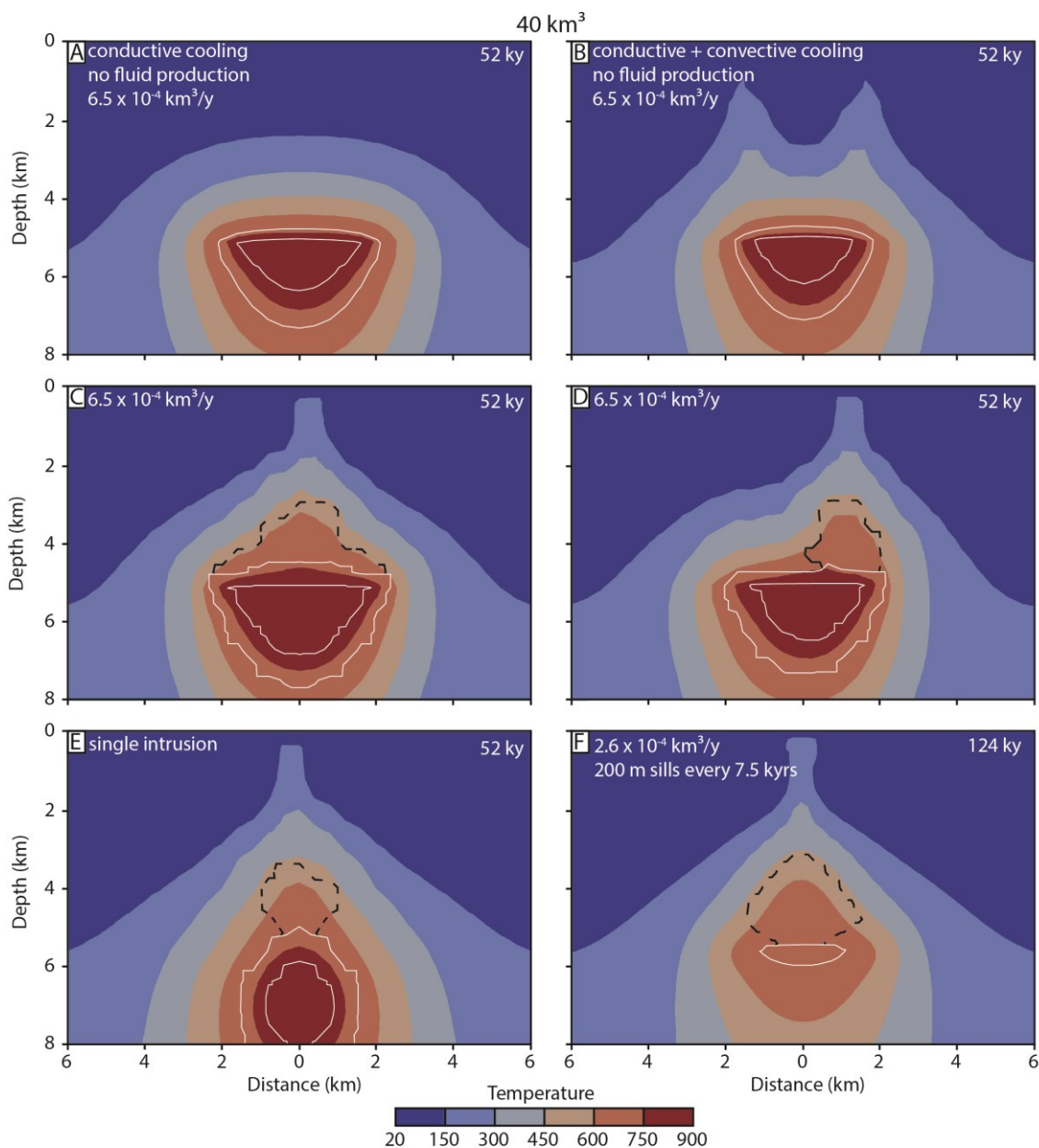


Fig. 4-3 Magma chamber dimensions after 40 km^3 magmatic inputs with various setups. A: conductive cooling and no fluid production, B: conductive and convective cooling and no fluid production, C: injection of the magmatic fluid over the entire top of the magma chamber, D: injection at the right side of the magma chamber, E: all magma was emplaced at the beginning of the simulation and F: injection by smaller 200 m sills. White lines correspond to the fraction of crystallization and the black-dashed lines show the pore fluid factor

In contrast, simulations with cooling by both conduction and meteoric fluid convection but no magmatic fluid production (Fig. 4-3B) demonstrate that the sills are cooled significantly at the rims. In comparison with the simulation including magmatic fluid production, the results show that high temperatures can only be maintained in a smaller area. This indicates that the fluid plume above the magma chamber can shield the magma chamber from cooling by

ambient fluids and further is mainly influenced by conductive cooling in the deeper parts of the chamber.

The magmatic fluids released during crystallization of the magma chamber below the solidus temperature, are focused by convecting ambient fluids. The region above the injection location is heated, resulting in an increased ductile behavior and decreased permeability. This leads to increased fluid pressure of the hydrothermal fluid which works against the temperature-dependent permeability decrease. If the fluid reaches the failure criterion the permeability reopens, resulting in overpressure-permeability waves that migrate from the injection location to the fluid plume (Weis 2015). As a result, the region above the injection location reaches higher temperatures as in the simulations without fluid production (Fig. 4-2B and 3B), which leads to a lower temperature gradient and slower heat loss by conduction.

This shielding effect by the fluid plume can be analyzed by varying the injection location of the exsolving fluids. Temperature distributions of setups with a central injection point result in a trapeze shape where the lateral temperature distribution narrows to the top and the bottom of the system (Fig. 4-2A-D). In contrast, injection of magmatic fluids over the entire length of the intruded sill culminates in a slightly bigger preserved pluton which narrows constantly towards the bottom (Fig. 4-3C). The release of the fluids at the right side of the sill over a width of 800 m shows only small influences on the overall shape of the magma chamber and is comparable to the simulations with central injection although the magma chamber is slightly tilted towards the injection side (Fig. 4-3D), which is reflected by steeper flanks at the right side of the magma chamber. The shielding effect seems to be most prominent at intermediate magmatic fluxes, where magma chamber growth only occurs along the width of the fluid plume (Fig. 4-2D).

All incremental growing setups simulated a total input of 40 km³ of magma by sill injection but the magma chamber never reached an equivalent size due to cooling between sill injections. An instantaneous input of the same magma volume of 40 km³ resulted in a circular pluton which narrows towards the bottom and the top and shows steep flanks (Fig. 4-3E). Using a finer mesh of 200 m resolution allows to add sills with smaller thicknesses of only 200 m in a frequency of 7.5 kyr resulting in a volumetric injection rate of about 2.6×10^{-4} km³/y. The initial sill thickness of 800 m was kept in order to allow the comparability with the coarse mesh setup at the same magma injection rate as displayed in Fig. 4-2E & F. Injection of smaller sills results in the formation of smaller magma chambers although the total magmatic input is the same. The smaller sills can be cooled more efficiently and therefore

preserve lower amounts of melt within the magma chamber as reflected by the crystallization fraction (Fig 2 & 3, white lines).

4.3.3 The influence of magma chamber growth on the hydrothermal system

Sill injection events and magma chamber growth control the release of magmatic fluids and thereby the evolution of the hydrothermal system associated with the intrusion. The influence of the magmatic-hydrothermal fluid above the magma chamber can be traced by the magmatic water fraction which indicates the proportion of magma-derived fluids to meteoric fluids. The fluid plumes and their shape as well as their location above the magma chamber are highly variable and mainly depend on the sill injection rate (Fig. 4-4). High magmatic influx results in a growing magma chamber and therefore leads to a constant fluid production. This continuous release of magmatic fluids results in a relatively stable fluid plume and locks it in space. The transition from a magmatic fluid-dominated system to a meteoric-dominated one occurs 2-3 km above the magma chamber. Only minor variations are visible during the simulation (Fig. 4-4A-C) and are (except for the beginning of the simulation) not directly related to the sill emplacement.

Intermediate magma influx rates ($3.9 \times 10^{-4} \text{ km}^3/\text{y}$) are also able to form a magma chamber although it is very limited in its dimension. Nevertheless, the steady exsolution of magmatic fluid also leads to the formation of a stable fluid plume above the injection location (Fig. 4-4D-F). However, the influence of the sill within this setup is distinct due to the small magma chamber, the cooling of the sill and the displacement of the magma chamber downwards in colder regions result in a short timed higher fluid production resulting in a bigger fluid plume (Fig. 4-4E). After consolidation, the fluid plume retracts to the previous location.

Slow magmatic emplacement rates ($2.6 \times 10^{-4} \text{ km}^3/\text{y}$) do not form a magma chamber after each sill injection (see above) resulting in a highly variable fluid plume (Fig. 4-4G-I). The dimensions of the fluid plume prior to sill injection are limited to 1 km above the injection location of the magmatic fluid (Fig. 4-4G). After sill injection, the rapid cooling and solidification results in a high fluid production leading to a fluid plume which reaches the top boundary of the modeling setup (Fig. 4-4H). However, the fluid production fades due to the gradually reduced magma volume and ends after the complete crystallization of the sill after a few thousand years leading to the collapse of the hydrothermal fluid plume followed by the influx of meteoric fluids.

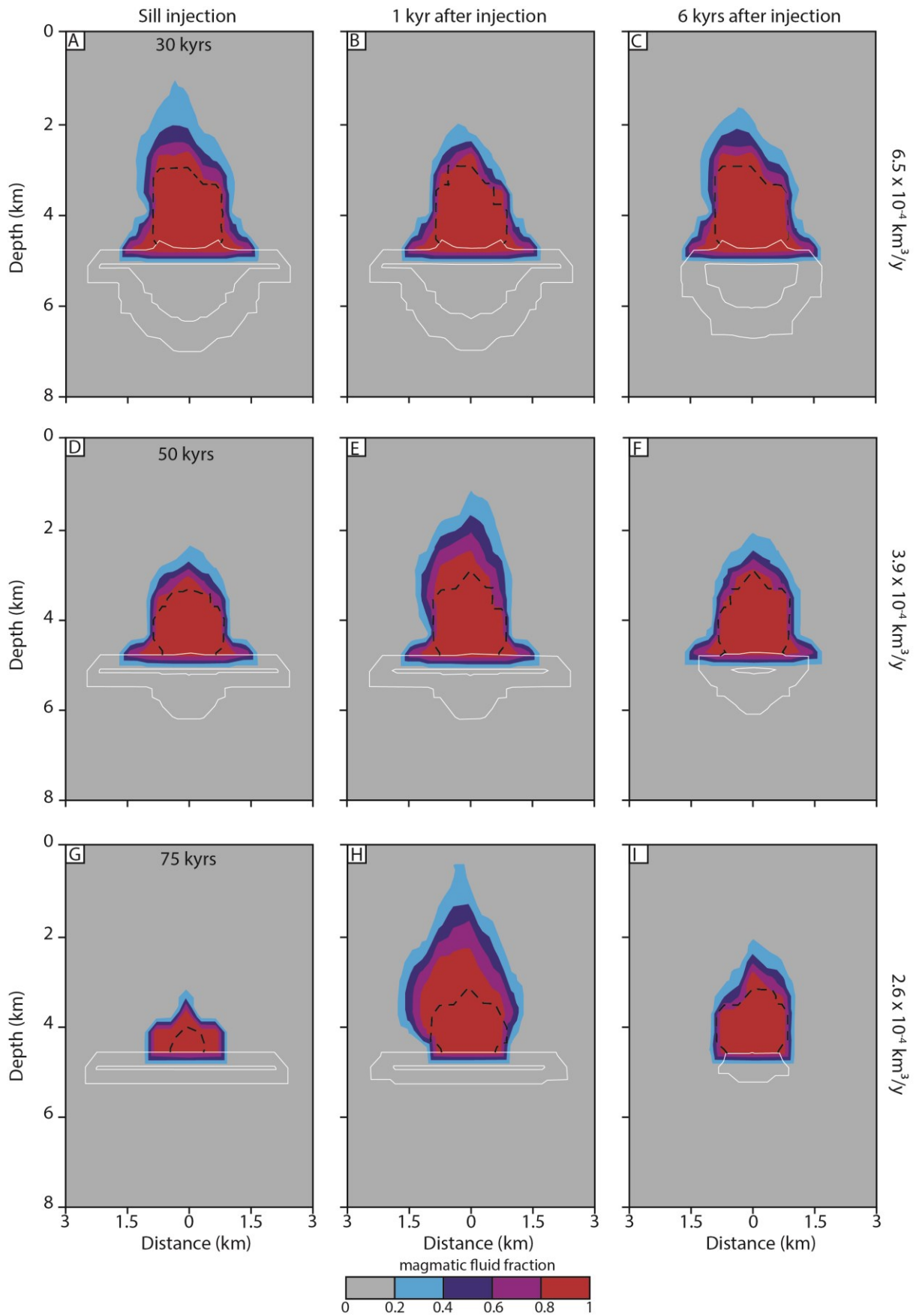


Fig.4-4 (previous page) Magma chamber dimensions, magmatic fluid fraction (magmatic fluid fraction = 1 means pure magmatic-hydrothermal fluid whereas 0 corresponds to pure meteoric water) and pore fluid factor with decreasing volumetric magmatic input from the top row to the bottom row. White lines correspond to the crystallization fraction and the black-dashed lines show the pore fluid factor. All setups correspond to an injection of 5 sills after the initial sill or 27.5 km³ total magma emplacement. The left column shows the condition before the sill starts to cool and produce fluid

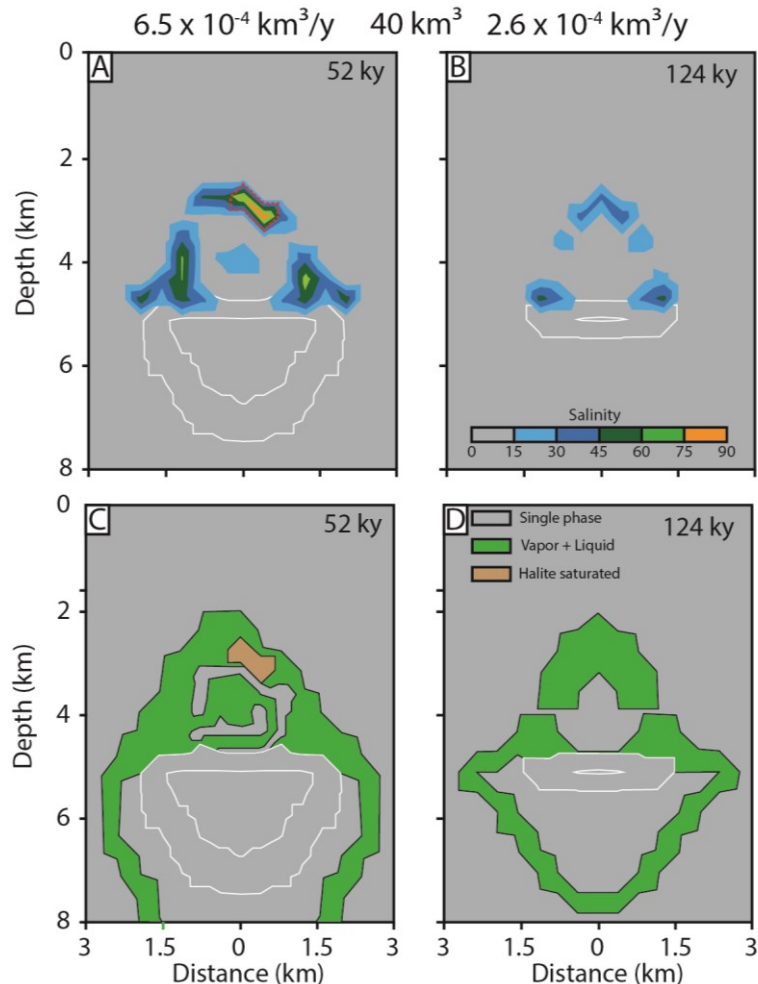


Fig.4-5 Salinity in the fluid plume of a fast (A) and a slow (B) setup after 40 km³ of magmatic input. Red pointed line refers to area of halite saturation. White lines correspond to the fraction of crystallization. C+D: Fluid states of the same setup with green areas show vapor-liquid coexistence and brown areas the halite saturation. High saline areas overlap with the two phase field and represent boiling regions

During cooling and pressure decrease the magmatic-hydrothermal fluids start to phase-separate in a low-density vapor phase and a higher-density, saline liquid phase (Fig. 4-5). The loss of fluid due to rapid ascend of vapor results in a salinity increase of the fluid which can in some cases even precipitate halite (Fig. 4-5). Higher magmatic influxes result in local salinities of up to 60-70 wt% NaCl, especially detectable at similar locations of the main decrease in magmatic fluid fraction (at the top of the fluid plume and at the flanks close to the

magma chamber). In setups with lower magma injection rates, the salinity reaches values between 40 and 50 wt% NaCl. The shape of the salinity shell is highly dependent on the availability of magmatic fluids and therefore on the magmatic fluid production and thus bigger in setups with more frequent sill injections. The salinity and the dimensions of the shells in the two setups with high magmatic injection rate remain relatively constant whereas the low magmatic influx setups undergo dilution processes due to the influx of meteoric waters resulting in lower salinities.

4.3.4 Copper enrichment

The accumulation of copper that precipitated from the cooling magmatic fluids leads to the formation of ore shells above the magma chamber which are typical for porphyry copper deposits (Fig. 4-6). The highest copper values are found on average 2 km above the roof of the magma chamber. The highest ore grades are mainly located within the uppermost part of the shell and copper enrichment potential decreases strongly within a range of 500 m from the highest values to barren areas (copper enrichment potential below 100). Although the total magmatic fluid production remains constant, the shape of the ore shells and their grades are highly variable between the different setups. The most confined ore body with values of up to 1000 in copper enrichment potential is located above magma chambers with the highest magmatic input (Fig. 4-6A, E, F). An ore shell with similar dimensions but slightly lower absolute copper potential values is hosted by the setup with intermediate magmatic influx (Fig. 4-6B) whereas the slowest magma emplacement rate results in a highly disseminated ore shell (Fig. 6C & D).

The shapes of the ore shells also depend on the injection location of the magmatic fluids. An injection over the entire chamber width results in copper enrichment above the entire magma chamber and the highest enrichment at the top of the fluid plume (Fig. 4-6E). Although fluid injection at the side of the pluton results in similar dimensions of the ore shell compared to the central injection setups, the absolute enrichment potential is higher (Fig. 4-6F). This is caused by the steeper temperature gradients at the flanks of the fluid plume. The comparison of incrementally grown magma chambers with a single large magma chamber shows higher values of copper enrichment potential in the sill setup as well as a slightly narrower copper shell although the large pluton already crystallized the same volume of magma (Fig. 4-6G). The intrusion of smaller sills results in a copper ore shell that is wider and located slightly closer to the injection location of the magmatic fluids (Fig. 4-6H). As smaller sills are cooling, they produce a more constant fluid release, but the fluid plume does

not reach the same heights as in simulations with larger sills due to the smaller magmatic input at each injection (Fig. 4-6C vs. 4-6H).

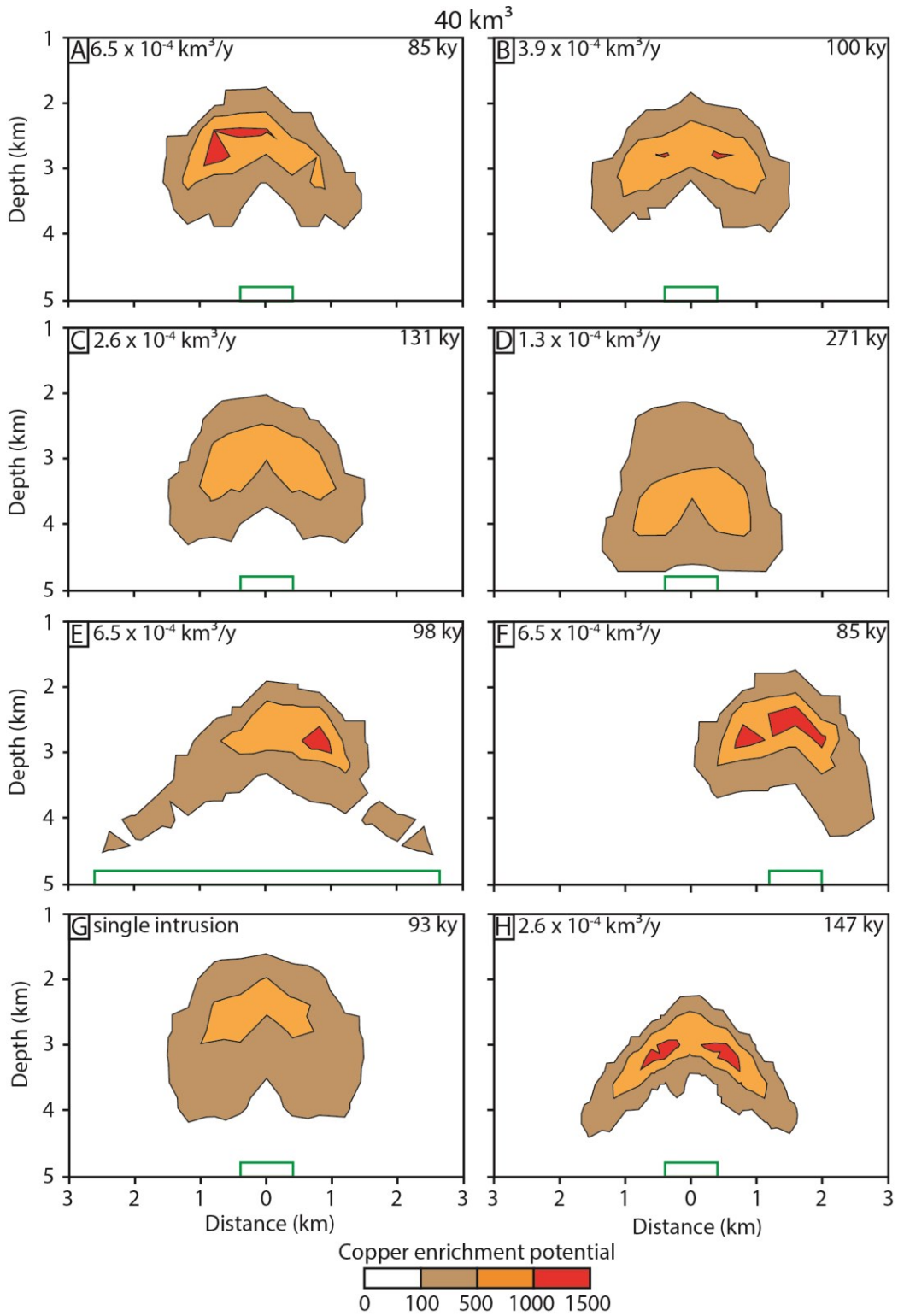


Fig 4-6 Copper ore shells of the various setups after total solidification of the magma chambers. Copper enrichment potential is displayed as colored areas. Green boxes refer to the injection location during each setup.

4.4 Discussion

The copper ore shells in our simulations show the characteristic bell-shaped outline and are located at 2 to 3 km depth, around 2 km above the top of the magma chamber where magmatic-hydrothermal fluids were injected, which is in line with natural porphyry copper deposits (Sillitoe 2010). Comparing the maximum copper enrichment and vertical extent of the simulated deposit suggests that the highest economic grades depend on an ideal window of injection rates and frequencies (Fig. 4-7) that are able to produce a constant fluid release rate.

During constant fluid production from high magmatic injection rates (Fig. 4-7A), the temperature range for copper precipitation (350°C to 450°C) has a fixed location within a stable fluid plume. This constant magmatic fluid flux confines the ore shell and results in a higher copper enrichment potential of up to 1000, corresponding to a maximum ore grade of about 2.5 weight percent (Weis et al. 2012). The ore shell becomes wider if fluids are injected over the entire width of the sill, but the absolute copper values in the top part of the mineralized region are unaffected, due to the focusing effect of the convecting meteoric fluids in the host rock. In contrast, fluid release at the flank of the magma chamber leads to ore shell dimensions similar to the ones from setup with centered injection, but the absolute copper grades are higher (Fig. 4-7B). Magmatic fluids forming at one side of the pluton get in contact with meteoric hydrothermal fluid from the entire lateral host rock domain where they are cooled within a more confined area and therefore produce the highest copper grades. Indeed, many economic ore deposits are associated with porphyry dikes injected at one side of the host pluton (Sillitoe 2010).

Higher magmatic injection rates, like the extreme end-member of an instantaneous intrusion of a large magma chamber at the start of the simulation creates an ore shell with lower copper enrichment and a larger vertical extent. The emplacement of a large, hot magma body in a cold host rock leads to high magmatic fluid production during the beginning of the simulation which then decreases whereas during slow magma chamber growth, the magmatic fluids form a stable outflow. Outflow from the single intrusion is not able to fix the temperature front at a certain location over time. Hence, very high magmatic injection rates may not be optimal for ore formation.

Low magmatic injection rates (below $3.9 \times 10^{-4} \text{ km}^3/\text{y}$) result in the total solidification of magma between the sill injections (see above). Every new sill is therefore injected in an environment which is already cooled down substantially, resulting in a rapid crystallization of every new sill. The magmatic fluid plume is therefore influenced by pulsing events of large

amounts of expelled fluids followed by the collapse of the plume after the last sill is completely cooled (Fig. 4-7A). Hence, low injection rates also seem to be less ideal for ore formation. However, this effect can be damped at the same injection rates but with more frequent injections of smaller sills, which can lead to higher ore grades in a more confined ore shell.

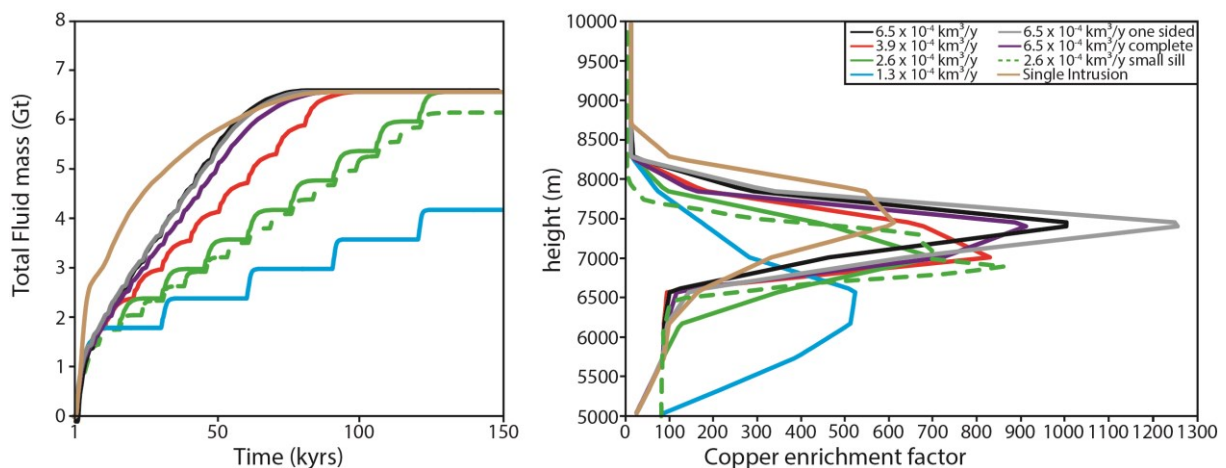


Fig 4-7 Total fluid production over time and copper distribution above the magma chamber. A: Total produced fluid mass showing the continuous outputs in the setups with high injections rates of fluids after sill intrusion. Single intrusion related fluid production is high in the beginning and fades after ca 50 kyrs. The slightly lower total fluid mass of the small sill can be explained by the finer mesh resolution at the rims of the setup, resulting in a slightly lower total volume. B: The various fluid productions result in different ore shells after the injection of 40 km³ of magmatic sill. Highest values with most confined location is associated to the highest magmatic emplacement rate whereas lower values result in lower copper enrichment factors and more disseminated ore shells. Single intrusions and the slowest injection rate correspond to the smallest values in copper and the broadest ore shells

Field observations at porphyry deposits worldwide indicate several fluid pulses during ore formation, which creates the stockwork veining and potassic alteration and a temporal association of veining and emplacements of porphyry dikes. This phase is followed by a gradual decrease in temperatures and decline of the fluid plume with time. According to our simulations, these observations are best matched with relatively fast sill injection rates. Lower frequencies would lead to multiple overprints of lower temperature alterations by new high-temperature events, which are typically not observed. Higher frequencies lead to a rapid build-up of a voluminous magma chamber, which can lead to more variable fluid production rates or may cause volcanic eruptions. Recent studies document that the same magmatic system may rapidly switch from subvolcanic ore formation to volcanism (Buret et al. 2017)

Our modelled input of 40 km³ injected magma is the minimum volume inferred from field observations and theoretical calculations and our new results show that an incrementally

growing magma chamber with a high sill intrusion frequency of 3.9 to 6×10^{-4} km^3/y can produce a confined ore shell with a high ore grade in less than 100 kyrs. Our required magma emplacement rates are lower than rates suggested from studies where magma chamber were emplaced continuously (Chelle-Michou et al. 2017; Schöpa et al. 2017). However, if pluton growth is even slower, the system would create similar granitoid plutons that are barren. Our calculated time scales are in line with the time ranges for porphyry copper mineralization between 50 kyrs and 100 kyrs as inferred by U/Pb zircon dating at various deposits, e.g. Bingham, Utah, Bajo de la Alumbrera, Argentina or Don Manuel, Chile (Chelle-Michou et al. 2015; Gilmer et al. 2017; Tapster et al. 2016; Von Quadt et al. 2011). Prolonging the period of sill injections or increasing the sill width would lead to higher ore grades and/or to higher magmatic fluid production rates that may lead to shallower depth levels of the deposit.

4.5 Conclusions

Our numerical simulations of an incrementally growing hydrous magma chamber which is cooled by conduction and hydrothermal convection in the host rock show that the formation of porphyry copper deposits requires volumetric magma emplacement rates of at least 3.9 to 6×10^{-4} km^3/y in order to form a magma chamber within the narrow geological time postulated for copper mineralization (Buret et al. 2017; Von Quadt et al. 2011). The periodic growth leads to the formation of up to 3 km thick magma chambers within a time range of 50 kyrs. Those values are in line with geological pluton growth rates (de Saint Blanquat et al. 2011; Menand et al. 2015) or otherwise would form eruptive setting (Gelman et al. 2013) and therefore suggesting that magma chambers of reasonable size for porphyry copper source rock form by rapid and episodic injection of magma. The injection location of the magmatic-hydrothermal fluid has a direct effect on the copper ore shell, with fluid release at one side of the pluton leading to particularly high ore grades. Copper precipitation is bound to a temperature decrease between 450°C and 350°C within the fluid plume, which occurs within a narrower zone if ambient convecting fluids in the host rock stabilize and cool the expelled magmatic hydrothermal fluid significantly resulting in maximized copper ore grades.

5 Thesis conclusion and outlook

This doctoral thesis presents new insights into the evolution of Sn (-W) and porphyry copper deposits. The mineralization in two deposits of the Erzgebirge was analyzed for fluid inclusion compositions in ore and gangue minerals. The results from analyses of ore mineral fluid inclusions helped to establish a more comprehensive understanding of the ore-formation processes. Numerical simulation obtained new constraints on the buildup of magma chambers connected to porphyry copper deposits, and the relevance of magma formation for the copper ore shells. The following chapter summarizes the individual investigations, and suggests themes of future research.

5.1 The magmatic-hydrothermal evolution of Sn deposits

The Zinnwald Sn-W deposit hosts mineralized veins and greisen bodies that contain significant amounts of cassiterite and wolframite. Fluid inclusion analyses show that the mineralization formed due to fluid-rock interaction resulting in the greisen bodies, especially in the Czech part of the deposit. In contrast, boiling played an important role in vein mineralization that has been mined in the German part of the deposit. However, the FIs and geological observations suggest that both precipitation mechanisms happened at approximately the same time, and within a similar temperature and pressure regime. Boiling itself is a process that was described as being of subordinate importance for Sn-W ore formation, which was thought mainly to be associated with fluid mixing and fluid rock interaction (Heinrich 1990). Phase separation is mainly associated to the opening of veins, resulting in a significant decrease from lithostatic to hydrostatic pressures. Fluid inclusion data cannot show if this vein opening is directly related to the over pressured fluid or bounded to opening of the veins by the local pressure regime. The change in the pressure regime can only occur in mineralization environments that are located in shallow crustal levels. Deep-seated intrusions may avoid boiling processes and therefore prevent the metals in the fluid from precipitating close to the exsolving granite bodies. This suggests that these fluids can migrate further into more distal parts of the host rock where they interact with the surrounding rock and form mineralization due to fluid rock interaction. Although the FI data within Zinnwald suggest this interpretation, detailed analysis of other shallow Sn-W mineralized granitic intrusions and their ore minerals should be examined in order to validate the impact of the emplacement depth for the deposits location.

The Hämmerlein deposit is host to cassiterite and sphalerite mineralization in a skarn horizon, as well as cassiterite mineralization in the underlying host rock schist. Fluid inclusion analysis shows that both ores are associated with a common magmatic-hydrothermal fluid.

Inclusions in cassiterite hosted by skarn also contain brine inclusions that formed at temperatures of up to 500°C, suggesting that exsolution during the cooling of the underlying granite body started with a high saline hot fluid. Further cooling led to the formation of intermediate to low saline fluids with temperatures of 300 to 400°C, which is responsible for the mineralization of cassiterite in the schist. Additional mixing processes with ambient fluids occurred during the formation of sphalerite. However, FIs cannot give further insights in the relationship of the mineralizing ore fluid to the skarn stage itself, and it is highly debated if both events are co-genetical or if the skarn formation is earlier (Lefebvre et al. 2018). Further investigations of the FI content in the skarn minerals, especially garnet, could help to investigate the link between mineralizing fluid and skarn formation. Furthermore, early high-salinity fluids are only rarely exposed in other tin mineralized environments (Naumov et al. 2011; Thomas 1982). Continuous fluid exsolution from the granite can re-equilibrate any early fluid inclusions in the ore and gangue minerals. This gives rise to the question if hot brines are of general importance for tin mineralization but not preserved in the FIs. Furthermore, the Hämmerlein is mainly explored for its tin content but there are extremely high concentrations of sphalerite, which are enriched in In. Although fluid mixing with meteoric fluid is an excellent method for metal precipitation (Xue et al. 2007), the detailed formation of the sulfide mineralization stage is still debated (Bauer et al. 2017).

5.2 IR-Microthermometry

Numerous studies have documented that closely intergrown ore minerals and gangue minerals may form at different time or even originate from different fluids (Campbell et al. 1988; Campbell and Panter 1990; Casanova et al. 2018; Kouzmanov et al. 2010; Lüders 1996; Wilkinson and Kesler 2009). This shows that only fluid inclusion analyses in both opaque and transparent gangue minerals are able to represent the fluid evolution in an ore deposit. Evaluation of the FI content in ore minerals via infrared microthermometry was the key for the understanding of the fluid evolution in Zinnwald and in Hämmerlein. In both deposits, the inclusion hosted unique temperature and salinity condition that were absent in the coexisting gangue minerals. Cassiterite and wolframite crystals from Zinnwald preserve the start of fluid boiling, which was responsible for their formation due to the separation of Cl⁻ into the vapor phase. Although boiling assemblages are also preserved in quartz minerals, the occurrence of them was very limited and further not directly related to the ore minerals. These boiling assemblages further did not preserve the same temperature and salinity condition as cassiterite and wolframite. Only both groups allowed the interpretation that vein opening resulted in a

pressure change from lithostatic to hydrostatic that was responsible for the mineralization. Cassiterite and sphalerite in Hämmerlein also preserved unique temperature and salinity ranges which were absent in the gangue minerals. Cassiterite in the skarn minerals preserved high temperatures and salinities, suggesting the early unmixing of such fluid from the magma whereas sphalerite inclusions preserved evidence of mixing from their geochemical composition. Although fluid inclusion in ore minerals can be a powerful tool for understanding of the ore-forming processes, it is only rarely used (a summary of literature can be found in Casanova et al. (2018)), as a result of several pre-analysis considerations. Radiative heating of the dark samples represent the biggest obstacle, which can result in a shift in temperatures of up to 40°C (Casanova et al. 2018). It is crucial that low intensity light is used, which requires a high sensitive IR-Camera. Additionally, the wavelengths of infra-red light are higher than visible light, which thus lowers the optical resolution of the microscope (Wilkinson 2001). This further leads to the dark appearance of the fluid inclusion rims, which is challenging because most homogenizing phases tend to move to the FI wall (Roedder 1984). LA-ICP-MS studies of FIs in opaque minerals are even less common as IR-cameras are not typically attached to LA-ICP-MS systems. This means a high degree of documentation is required for relocating the exact inclusion location (each FI required at least 15 photos via IR-microscopy, reflected light microscopy and binocular). However, FIs in ore minerals have a broad application in many mineralizing systems and record valuable information on the fluid evolution in those systems once the technical obstacles are eliminated.

5.3 Modeling

Numerical simulations about the formation of magma chambers responsible for porphyry copper mineralization provide new insights on the intrusion rate as well as the influence for the copper enrichment. We analyzed the incremental growth of plutons by injecting a magmatic sill into a defined interval, and showed that magma chambers do not form below an average volumetric magma influx of ca. $4 \times 10^{-4} \text{ km}^3/\text{y}$. Higher influx values produce magma chambers of several km thickness within a short geological time of few 10 kyrs, which is in line with geological observation (Buret et al. 2017). The accumulation of a high-grade ore can only be achieved by continuous magmatic-hydrothermal fluid exsolution out of the magma chamber, and is hampered if the fluid plume is too variable in its dimension. Furthermore, the simulation analyzed the influence of the injection location on the ore grade. It is shown that the highest copper concentration can be found in areas with the steepest temperature gradient in the range responsible for copper precipitation. These high gradients can be achieved in areas with higher input of cold ambient fluids, especially located at the

edges of the magma chamber. Numerical modeling of ore-related systems are a unique tool to find constraints for the formation of these systems, which are absent in the geological record and further allow the application on a wide spectra of deposits. The documented simulation can be extended and may be able to introduce new metals (e.g. Sn and W), reproduce the fluid evolution in a shallow intrusion (e.g. the depth of the Zinnwald granite) with the relevant boiling processes, or include a pressure and temperature dependent salinity of the exsolving fluid in order to simulate the early exsolution of high saline hot fluids (as in Hämmerlein).

Bibliography

- Anglo Saxony Mining (2015) Westerzgebirge project Hämmerlein-Tellerhäuser: long section through adit (<http://www.anglosaxony.com/projects/germany/tellerhauser>).
- Annen C (2009) From plutons to magma chambers: Thermal constraints on the accumulation of eruptible silicic magma in the upper crust. *Earth and Planetary Science Letters* 284:409-416.
- Arndt NT, Fontboté L, Hedenquist JW, Kesler SE, Thompson JF, Wood DG (2017) Future global mineral resources. *Geochemical Perspectives* 6:1-171.
- Audétat A, Günther D, Heinrich CA (2000) Causes for large-scale metal zonation around mineralized plutons: fluid inclusion LA-ICP-MS evidence from the Mole Granite, Australia. *Economic Geology* 95:1563-1581.
- Audétat A, Pettke T, Heinrich C, Bodnar R (2008) The composition of magmatic-hydrothermal fluids in barren and mineralized intrusions. *Economic Geology* 103:877-908.
- Audétat A, Simon AC, Hedenquist J, Harris M, Camus F (2012) Magmatic controls on porphyry copper genesis. *Geology and genesis of major copper deposits and districts of the world - A tribute to Richard H Sillitoe*:553-572.
- Bachmann O, Miller CF, De Silva S (2007) The volcanic–plutonic connection as a stage for understanding crustal magmatism. *Journal of Volcanology and Geothermal Research* 167:1-23.
- Bakker RJ (2016) Fluid Inclusions Short Course. Montan Universität, Leoben, pp 239.
- Bankwitz P, Bankwitz E (2004) The relationship of tilt and twist of fringe cracks in granite plutons. *Geological Society, London, Special Publications* 231:183-208.
- Bauer ME, Seifert T, Burisch M, Krause J, Richter N, Gutzmer J (2017) Indium-bearing sulfides from the Hämmerlein skarn deposit, Erzgebirge, Germany: evidence for late-stage diffusion of indium into sphalerite. *Mineralium Deposita*:1-18.
- Baumann L, Werner C-D (1968) Die Gangmineralisationen des Harzes und ihre Analogien zum Erzgebirge und zu Thüringen. *Ber deutsch Ges geol Wiss* 13:525-548.
- Behr H-J, Gerler J (1987) Inclusions of sedimentary brines in post-Variscan mineralizations in the Federal Republic of Germany—a study by neutron activation analysis. *Chemical Geology* 61:65-77.
- Behr H-J, Horn E, Frenzel-Beyme K, Reutel C (1987) Fluid inclusion characteristics of the Variscan and post-Variscan mineralizing fluids in the Federal Republic of Germany. *Chemical Geology* 61:273-285.
- Bischoff JL, Rosenbauer RJ, Fournier RO (1996) The generation of HCl in the system CaCl₂-H₂O: Vapor-liquid relations from 380–500 C. *Geochimica et Cosmochimica Acta* 60:7-16.
- Bodnar R (1993) Revised equation and table for determining the freezing point depression of H₂O-NaCl solutions. *Geochimica et Cosmochimica Acta* 57:683-684.

- Bodnar RJ (1995) Fluid-inclusion evidence for a magmatic source for metals in porphyry copper deposits. *Mineralogical Association of Canada Short Course Series* 23:139-152.
- Bodnar RJ (2003) Introduction to fluid inclusions In: Samson I, Anderson A, Marshall D (eds) *Fluid inclusions: Analysis and interpretation*. Mineralogical Association of Canada, Vancouver, pp 1-8.
- Bons PD, Elburg MA, Gomez-Rivas E (2012) A review of the formation of tectonic veins and their microstructures. *Journal of Structural Geology* 43:33-62.
- Breiter K (1993) The Nejdeč pluton—discussion of granite evolution and Sn-W mineralization. *Z geol Wissenschaft* 21:2-36.
- Breiter K, Forster HJ, Seltnann R (1999) Variscan silicic magmatism and related tin-tungsten mineralization in the Erzgebirge-Slavkovsky les metallogenic province. *Mineralium Deposita* 34:505-521.
- Breiter K (2012) Nearly contemporaneous evolution of the A-and S-type fractionated granites in the Krušné hory/Erzgebirge Mts., Central Europe. *Lithos* 151:105-121.
- Breiter K, Škoda R (2012) Vertical zonality of fractionated granite plutons reflected in zircon chemistry: the Cínovec A-type versus the Beauvoir S-type suite. *Geologica Carpathica* 63:383-398.
- Breiter K, Ďurišová J, Hrstka T, Korbelová Z, Vaňková M, Galiová MV, Kanický V, Rambousek P, Knésl I, Dobeš P (2017) Assessment of magmatic vs. metasomatic processes in rare-metal granites: A case study of the Cínovec/Zinnwald Sn-W-Li deposit, Central Europe. *Lithos* 292-293:198-217.
- Buchmann M, Schach E, Tolosana-Delgado R, Leißner T, Astoveza J, Kern M, Möckel R, Ebert D, Rudolph M, van den Boogaart K (2018) Evaluation of Magnetic Separation Efficiency on a Cassiterite-Bearing Skarn Ore by Means of Integrative SEM-Based Image and XRF–XRD Data Analysis. *Minerals* 8:390.
- Buret Y, Wotzlaw J-F, Roozen S, Guillong M, von Quadt A, Heinrich CA (2017) Zircon petrochronological evidence for a plutonic-volcanic connection in porphyry copper deposits. *Geology* 45:623-626.
- Burnham CW, Ohmoto H (1980) Late-stage processes of felsic magmatism. *Soc Mining Geol Jpn* 8:1-11.
- Butler B (1978) Tin-rich garnet, pyroxene, and spinel from a slag. *Mineralogical Magazine* 42:487-492.
- Campbell A, Robinson-Cook S, Amindyas C (1988) Observation of fluid inclusions in wolframite from Panasqueira, Portugal. *Bulletin de minéralogie* 111:251-256.
- Campbell AR, Panter KS (1990) Comparison of fluid inclusions in coexisting (cogenetic?) wolframite, cassiterite, and quartz from St. Michael's Mount and Cligga Head, Cornwall, England. *Geochimica et Cosmochimica Acta* 54:673-681.
- Casanova V, Kouzmanov K, Audétat A, Wälle M, Ubrig N, Ortelli M, Fontboté L (2018) Fluid Inclusion Studies in Opaque Ore Minerals: II. A Comparative Study of Syngenetic

Synthetic Fluid Inclusions Hosted in Quartz and Opaque Minerals. *Economic Geology* 113:1861-1883.

Cathelineau M (1988) Cation site occupancy in chlorites and illites as function of temperature. *Clay minerals* 23:471-485.

Cathles LM, Erendi A, Barrie T (1997) How long can a hydrothermal system be sustained by a single intrusive event? *Economic Geology* 92:766-771.

Chelle-Michou C, Chiaradia M, Selby D, Ovtcharova M, Spikings RA (2015) High-resolution geochronology of the Corocochuayco porphyry-skarn deposit, Peru: A rapid product of the Incaic Orogeny. *Economic Geology* 110:423-443.

Chelle-Michou C, Rottier B, Caricchi L, Simpson G (2017) Tempo of magma degassing and the genesis of porphyry copper deposits. *Scientific reports* 7:40566.

Chiaradia M, Caricchi L (2017) Stochastic modelling of deep magmatic controls on porphyry copper deposit endowment. *Scientific reports* 7:44523.

Clark JR, Williams-Jones AE (1990) Analogues of epithermal gold–silver deposition in geothermal well scales. *Nature* 346:644-645.

Cline JS, Bodnar RJ (1991) Can economic porphyry copper mineralization be generated by a typical calc-alkaline melt? *Journal of Geophysical Research: Solid Earth* 96:8113-8126.

Cloos M (2001) Bubbling magma chambers, cupolas, and porphyry copper deposits. *International Geology Review* 43:285-311.

Cocherie A, Johan V, Rossi P, Stempok M (1991) Trace element variations and lanthanide tetrad effect studied in a Variscan lithium albite granite: case of the Cínovec granite (Czechoslovakia). In: Pagel M, Leroy JL (eds) *Source, Transport and Deposition of Metals*. Rotterdam, pp 745-749.

Coleman DS, Gray W, Glazner AF (2004) Rethinking the emplacement and evolution of zoned plutons: Geochronologic evidence for incremental assembly of the Tuolumne Intrusive Suite, California. *Geology* 32:433-436.

Coulon CA, Hsieh PA, White R, Lowenstern JB, Ingebritsen SE (2017) Causes of distal volcano-tectonic seismicity inferred from hydrothermal modeling. *Journal of Volcanology and Geothermal Research* 345:98-108.

De Caritat P, Hutcheon I, Walshe J (1993) Chlorite geothermometry: a review. *Clays and Clay Minerals* 41:219-239.

de Saint Blanquat M, Horsman E, Habert G, Morgan S, Vanderhaeghe O, Law R, Tikoff B (2011) Multiscale magmatic cyclicality, duration of pluton construction, and the paradoxical relationship between tectonism and plutonism in continental arcs. *Tectonophysics* 500:20-33.

Dilles JH (1987) Petrology of the Yerington Batholith, Nevada; evidence for evolution of porphyry copper ore fluids. *Economic Geology* 82:1750-1789.

Dilles JH, Proffett J (1995) Metallogensis of the Yerington batholith, Nevada. *Arizona Geological Society Digest* 20:306-315.

- Dolejš D, Stembrok M (2001) Magmatic and hydrothermal evolution of Li-F granites: Cínovec and Krásnointrusions, Krušné hory batholith, Czech Republic. *Bulletin of Czech Geological Survey* 76:77-99.
- Driesner T (2007) The system H₂O–NaCl. Part II: Correlations for molar volume, enthalpy, and isobaric heat capacity from 0 to 1000 °C, 1 to 5000 bar, and 0 to 1 XNaCl. *Geochimica et Cosmochimica Acta* 71:4902-4919.
- Driesner T, Heinrich CA (2007) The system H₂O–NaCl. Part I: Correlation formulae for phase relations in temperature–pressure–composition space from 0 to 1000°C, 0 to 5000bar, and 0 to 1 XNaCl. *Geochimica et Cosmochimica Acta* 71:4880-4901.
- Durisova J, Charoy B, Weisbrod A (1979) Fluid inclusion studies in minerals from tin and tungsten deposits in the Krušné Hory Mountains (Czechoslovakia). *Bulletin de Minéralogie* 102:665-675.
- Eadington P (1983) A fluid inclusion investigation of ore formation in a tin-mineralized granite, New England, New South Wales. *Economic Geology* 78:1204-1221.
- Edwards R (2012) *Ore deposit geology and its influence on mineral exploration*. Springer Science & Business Media.
- Einaudi MT, Burt DM (1982) Introduction; terminology, classification, and composition of skarn deposits. *Economic Geology* 77:745-754.
- Fekete S, Weis P, Driesner T, Bouvier A-S, Baumgartner L, Heinrich CA (2016) Contrasting hydrological processes of meteoric water incursion during magmatic–hydrothermal ore deposition: An oxygen isotope study by ion microprobe. *Earth and Planetary Science Letters* 451:263-271.
- Förster H-J (2012) Late–Variscan felsic magmatism in the western Erzgebirge–Vogtland In: Romer RL, Förster H-J, Kroner U, Müller A, Rößler R, Rötzler J, Seltmann R, Wenzel T (eds) *Granites of the Erzgebirge - relation of magmatism to the metamorphic and tectonic evolution of the Variscan Orogen* Scientific Technical Report 12/15,. GFZ German Research Centre for Geosciences.
- Forster HJ, Ondrejka M, Uher P (2011) Mineralogical responses to subsolidus alteration of granitic rocks by oxidizing As-bearing fluids: REE arsenates and As-rich silicates from the Zinnwald granite, Eastern Erzgebirge, Germany. *The Canadian Mineralogist* 49:913-930.
- Förster HJ, Tischendorf G, Seltmann R, Gottesmann B (1998) Die variszischen Granite des Erzgebirges: neue Aspekte aus stofflicher Sicht. *Z geol Wiss* 26:31-60.
- Förster HJ, Tischendorf G, Trumbull R, Gottesmann B (1999) Late-collisional granites in the Variscan Erzgebirge, Germany. *Journal of Petrology* 40:1613-1645.
- Förster HJ, Romer RL (2010) Carboniferous magmatism In: Linnemann U, Romer RL (eds) *Pre-Mesozoic Geology of Saxo-Thuringia–From the Cadomian Active Margin to the Variscan Orogen*. Schweizerbart, Stuttgart, pp 287-308.
- Fournier RO (1999) Hydrothermal processes related to movement of fluid from plastic into brittle rock in the magmatic-epithermal environment. *Economic Geology* 94:1193-1211.

- Foxford K, Nicholson R, Polya D, Hebblethwaite R (2000) Extensional failure and hydraulic valving at Minas da Panasqueira, Portugal: evidence from vein spatial distributions, displacements and geometries. *Journal of Structural Geology* 22:1065-1086.
- Fraser T, Stanley C, Nikic Z, Pesalj R, Gorc D, Schroeter T (1995) The Mount Polley alkalic porphyry copper-gold deposit, south-central British Columbia. *Canadian Institute of Mining and Metallurgy Special Volume* 46:609-622.
- Fu M, Kwak T, Mernagh T (1993) Fluid inclusion studies of zoning in the Dachang tin-polymetallic ore field, People's Republic of China. *Economic Geology* 88:283-300.
- Fuex A, Baker DR (1973) Stable carbon isotopes in selected granitic, mafic, and ultramafic igneous rocks. *Geochimica et Cosmochimica Acta* 37:2509-2521.
- Gagnon JE, Samson IM, Fryer BJ (2003) LA-ICP-MS Analysis of Fluid Inclusions In: Samson I, Anderson A, Marshall DD (eds) *Fluid Inclusions Analysis and Interpretation*. Mineral Association of Canada, Vancouver, pp 391-323.
- Gelman SE, Gutiérrez FJ, Bachmann O (2013) On the longevity of large upper crustal silicic magma reservoirs. *Geology* 41:759-762.
- Gerstenberger H (1989) Autometamorphic Rb enrichments in highly evolved granites causing lowered RbSr isochron intercepts. *Earth and Planetary Science Letters* 93:65-75.
- Gilmer AK, Sparks R, Rust AC, Tapster S, Webb AD, Barfod DN (2017) Geology of the Don Manuel igneous complex, central Chile: Implications for igneous processes in porphyry copper systems. *GSA Bulletin* 129:920-946.
- Goldstein RH (2003) Petrographic Analysis of Fluid Inclusions In: Samson I, Anderson A, Marshall D (eds) *Fluid inclusions: Analysis and interpretation*. Mineralogical Association of Canada, Vancouver, pp 9-53.
- Graupner T, Brätz H, Klemd R (2005) LA-ICP-MS micro-analysis of fluid inclusions in quartz using a commercial Merchantek 266 nm Nd: YAG laser. *European journal of mineralogy* 17:93-102.
- Guillong M, Heinrich CA (2007) Sensitivity enhancement in laser ablation ICP-MS using small amounts of hydrogen in the carrier gas. *Journal of Analytical Atomic Spectrometry* 22:1488-1494.
- Guillong M, Meier DL, Allan MM, Heinrich CA, Yardley BW (2008) Appendix A6: SILLS: A MATLAB-based program for the reduction of laser ablation ICP-MS data of homogeneous materials and inclusions. *Mineralogical Association of Canada Short Course* 40:328-333.
- Günther D, Audétat A, Frischknecht R, Heinrich CA (1998) Quantitative analysis of major, minor and trace elements in fluid inclusions using laser ablation–inductively coupled plasmamass spectrometry. *Journal of Analytical Atomic Spectrometry* 13:263-270.
- Halter WE, Williams-Jones AE, Kontak DJ (1998) Modeling fluid–rock interaction during greisenization at the East Kemptville tin deposit: implications for mineralization. *Chemical Geology* 150:1-17.

Hayba DO, Ingebritsen SE (1997) Multiphase groundwater flow near cooling plutons. *Journal of Geophysical Research: Solid Earth* 102:12235-12252.

Heinrich CA (1990) The Chemistry of Hydrothermal Tin(-Tungsten) Ore Deposition. *Economic geology* 85:457-481.

Heinrich CA, Günther D, Audétat A, Ulrich T, Frischknecht R (1999) Metal fractionation between magmatic brine and vapor, determined by microanalysis of fluid inclusions. *Geology* 27:755-758.

Hemley J, Cygan G, Fein J, Robinson G, d'Angelo W (1992) Hydrothermal ore-forming processes in the light of studies in rock-buffered systems; I, Iron-copper-zinc-lead sulfide solubility relations. *Economic Geology* 87:1-22.

Hezarkhani A, Williams-Jones A, Gammons C (1999) Factors controlling copper solubility and chalcopyrite deposition in the Sungun porphyry copper deposit, Iran. *Mineralium Deposita* 34:770-783.

Hoffmann U, Breitzkreuz C, Breiter K, Sergeev S, Stanek K, Tichomirowa M (2013) Carboniferous–Permian volcanic evolution in Central Europe—U/Pb ages of volcanic rocks in Saxony (Germany) and northern Bohemia (Czech Republic). *International Journal of Earth Sciences* 102:73-99.

Ingebritsen SE, Sanford WE, Neuzil C (2006) *Groundwater in geologic processes*, 2nd edn. Cambridge University Press, New York.

James R, MacNaughton M (1977) The adsorption of aqueous heavy metals on inorganic minerals. *Geochimica et Cosmochimica Acta* 41:1549-1555.

Jochum KP, Weis U, Stoll B, Kuzmin D, Yang Q, Raczek I, Jacob DE, Stracke A, Birbaum K, Frick DA (2011) Determination of reference values for NIST SRM 610–617 glasses following ISO guidelines. *Geostandards and Geoanalytical Research* 35:397-429.

Johan Z, Johan V (2004) Accessory minerals of the Cinovec (Zinnwald) granite cupola, Czech Republic: indicators of petrogenetic evolution. *Mineralogy and Petrology* 83:113-150.

Johan Z, Strnad L, Johan V (2012) Evolution of the Cinovec (Zinnwald) Granite Cupola, Czech Republic: Composition of Feldspars and Micas, a Clue to the Origin of W, Sn Mineralization. *The Canadian Mineralogist* 50:1131-1148.

Johannes W (1984) Beginning of melting in the granite system Qz-Or-Ab-An-H₂O. *Contributions to Mineralogy and Petrology* 86:264-273.

Jowett EC (1991) Fitting iron and magnesium into the hydrothermal chlorite geothermometer. GAC/MAC/SEG Joint Annual Meeting (Toronto, May 27-29, 1991), Program with Abstracts 16, A62.

Kelly WC, Rye RO (1979) Geologic, fluid inclusion, and stable isotope studies of the tin-tungsten deposits of Panasqueira, Portugal. *Economic Geology* 74:1721-1822.

Kempe U, Bombach K, Matukov D, Schlothauer T, Hutschenreuter J, Wolf D, Sergeev S (2004) Pb/Pb and U/Pb zircon dating of subvolcanic rhyolite as a time marker for Hercynian

granite magmatism and Sn mineralisation in the Eibenstock granite, Erzgebirge, Germany: Considering effects of zircon alteration. *Mineralium Deposita* 39:646-669.

Kern M, Kästner J, Tolosana-Delgado R, Jeske T, Gutzmer J (2018) The inherent link between ore formation and geometallurgy as documented by complex tin mineralization at the Hämmerlein deposit (Erzgebirge, Germany). *Mineralium Deposita*:1-16.

Klemm LM, Pettke T, Heinrich CA, Campos E (2007) Hydrothermal evolution of the El Teniente deposit, Chile: Porphyry Cu-Mo ore deposition from low-salinity magmatic fluids. *Economic Geology* 102:1021-1045.

Korges M, Weis P, Lüders V, Laurent O (2018) Depressurization and boiling of a single magmatic fluid as a mechanism for tin-tungsten deposit formation. *Geology* 46:75-78.

Kouzmanov K, Pettke T, Heinrich CA (2010) Direct analysis of ore-precipitating fluids: combined IR microscopy and LA-ICP-MS study of fluid inclusions in opaque ore minerals. *Economic Geology* 105:351-373.

Kroner U, Hahn T, Romer RL, Linnemann U (2007) The Variscan orogeny in the Saxo-Thuringian zone-heterogenous overprint of Cadomian/Paleozoic Peri-Gondwana crust. *Special Papers - Geological Society of America* 423:153-172.

Kwak TA (1987) *W-Sn Skarn Deposits and Related Metamorphic Skarns and Granitoids*. Elsevier.

Landis G, P., Rye R, O. (1974) Geologic, Fluid Inclusion, and Stable Isotope Studies of the Pasto Buena Tungsten-Base Metal Ore Deposit, Northern Peru. *Economic Geology* 69:1025-1059.

Landtwing MR, Pettke T, Halter WE, Heinrich CA, Redmond PB, Einaudi MT, Kunze K (2005) Copper deposition during quartz dissolution by cooling magmatic–hydrothermal fluids: the Bingham porphyry. *Earth and Planetary Science Letters* 235:229-243.

Layne GD, Spooner E (1991) The JC tin skarn deposit, southern Yukon Territory; I, Geology, paragenesis, and fluid inclusion microthermometry. *Economic Geology* 86:29-47.

Lecumberri-Sanchez P, Vieira R, Heinrich C, Pinto F, Wälle M (2017) Fluid-rock interaction is decisive for the formation of tungsten deposits. *Geology* 45:579-582.

Lefebvre MG, Romer RL, Glodny J, Kroner U, Roscher M (2018) The Hämmerlein skarn-hosted polymetallic deposit and the Eibenstock granite associated greisen, western Erzgebirge, Germany: two phases of mineralization—two Sn sources. *Mineralium Deposita*:1-24.

Lehmann B (2006) *Metallogeny of tin*. Springer.

Leonhardt D, Geißler E, Fritzsche H (1999) Geologische Karte des Freistaates Sachsen 1:25000. Blatt 5543 Oberwiesenthal. Sächsisches Landesamt für Umwelt und Geologie Abteilung Geologie.

Leonhardt D, Geißler E, Engelhardt-Sobe A, Baumgart G (2004) Geologische Karte des Freistaates Sachsen 1:25000. Blatt 5542 Johanngeorgenstadt. Sächsisches Landesamt für Umwelt und Geologie Abteilung Geologie.

Leonhardt D, Geißler E, Engelhardt A, Baumgart G (2010) Geologische Karte des Freistaates Sachsen 1:25000. Blatt 5541 Eibenstock. Sächsisches Landesamt für Umwelt und Geologie Abteilung Geologie.

Linnemann U, Romer RL (2010) Pre-Mesozoic geology of Saxo-Thuringia. Schweizerbart Science Publishers.

Lüders V (1996) Contribution of infrared microscopy to fluid inclusion studies in some opaque minerals (wolframite, stibnite, bournonite); metallogenic implications. *Economic Geology* 91:1462-1468.

Lüders V, Ziemann M (1999) Possibilities and limits of infrared light microthermometry applied to studies of pyrite-hosted fluid inclusions. *Chemical Geology* 154:169-178.

Lüders V, Plessen B, di Primio R (2012) Stable carbon isotopic ratios of CH₄-CO₂-bearing fluid inclusions in fracture-fill mineralization from the Lower Saxony Basin (Germany)—A tool for tracing gas sources and maturity. *Marine and Petroleum Geology* 30:174-183.

Lüders V (2017) Contribution of infrared microscopy to studies of fluid inclusions hosted in some opaque ore minerals: possibilities, limitations, and perspectives. *Mineralium Deposita* 52:663-673.

Malyshev B, Mironova O, Naumov V, Savel'eva N, Salazkin A, Volosov A (1997) Fluids of the Hemmerlein Skarn-Greisen Tin Deposit, Erzgebirge, Germany. *Geochemistry International* 35:146-154.

Matzel JE, Bowring SA, Miller RB (2006) Time scales of pluton construction at differing crustal levels: Examples from the Mount Stuart and Tenpeak intrusions, North Cascades, Washington. *Geological Society of America Bulletin* 118:1412-1430.

Mei W, Lü X, Cao X, Liu Z, Zhao Y, Ai Z, Tang R, Abfaua MM (2015) Ore genesis and hydrothermal evolution of the Huanggang skarn iron-tin polymetallic deposit, southern Great Xing'an Range: Evidence from fluid inclusions and isotope analyses. *Ore Geology Reviews* 64:239-252.

Meinert LD (1992) Skarns and skarn deposits. *Geoscience Canada* 19:147-156.

Meinert LD (2005) World skarn deposits. *Econ Geol* 100th Aniv Vol:299-336.

Menand T (2008) The mechanics and dynamics of sills in layered elastic rocks and their implications for the growth of laccoliths and other igneous complexes. *Earth and Planetary Science Letters* 267:93-99.

Menand T, Annen C, de Saint Blanquat M (2015) Rates of magma transfer in the crust: Insights into magma reservoir recharge and pluton growth. *Geology* 43:199-202.

Michel J, Baumgartner L, Putlitz B, Schaltegger U, Ovtcharova M (2008) Incremental growth of the Patagonian Torres del Paine laccolith over 90 ky. *Geology* 36:459-462.

Misra K (2012) Understanding mineral deposits. Springer Science & Business Media.

- Moncada D, Baker D, Bodnar RJ (2017) Mineralogical, petrographic and fluid inclusion evidence for the link between boiling and epithermal Ag-Au mineralization in the La Luz area, Guanajuato Mining District, México. *Ore Geology Reviews* 89:143-170.
- Monecke T, Dulski P, Kempe U (2007) Origin of convex tetrads in rare earth element patterns of hydrothermally altered siliceous igneous rocks from the Zinnwald Sn–W deposit, Germany. *Geochimica et Cosmochimica Acta* 71:335-353.
- Monecke T, Petersen S, Hannington MD (2014) Constraints on water depth of massive sulfide formation: evidence from modern seafloor hydrothermal systems in arc-related settings. *Economic Geology* 109:2079-2101.
- Müller A, Seltmann R (2012) The eastern Erzgebirge volcano-plutonic complex In: Romer RL, Förster H-J, Kroner U, Müller A, Rößler R, Rötzler J, Seltmann R, Wenzel T (eds) *Granites of the Erzgebirge - relation of magmatism to the metamorphic and tectonic evolution of the Variscan Orogen* Scientific Technical Report 12/15,. GFZ German Research Centre for Geosciences.
- Mulligan R, Jambor J (1968) Tin-bearing silicates from skarn in the Cassiar district, northern British Columbia. *The Canadian Mineralogist* 9:358-370.
- Naumov V, Dorofeev V, Mironova O (2011) Physicochemical parameters of the formation of hydrothermal deposits: a fluid inclusion study. I. Tin and tungsten deposits. *Geochemistry International* 49:1002.
- Neßler J, Helbig M, Kühn K, Bachmann T, Hartsch J, Henker J (2011) Zinnwald Lithium Project. Freiberg, pp 204.
- Neßler J, Seifert T, Gutzmer J, Müller A, Henker J, Kühn K (2014) New lithogeochemical and mineralogical exploration of Li-Sn greisen mineralisation in old mining adits of the Zinnwald deposit, Germany EGU General Assembly Conference Abstracts.
- Norton D, Knight J (1977) Transport phenomena in hydrothermal systems: cooling plutons. *Am J Sci* 277:937-981.
- Pasquarè F, Tibaldi A (2007) Structure of a sheet-laccolith system revealing the interplay between tectonic and magma stresses at Stardalur Volcano, Iceland. *Journal of Volcanology and Geothermal Research* 161:131-150.
- Pasteris JD (1996) Mount Pinatubo volcano and “negative” porphyry copper deposits. *Geology* 24:1075-1078.
- Pitfield P, Brown T, Gunn G, Rayner D (2011) Tungsten - Mineral Profile. British Geological Survey.
- Plessen B, Lüders V (2012) Simultaneous measurements of gas isotopic compositions of fluid inclusion gases (N₂, CH₄, CO₂) using continuous-flow isotope ratio mass spectrometry. *Rapid Communications in Mass Spectrometry* 26:1157-1161.
- Polya D (1989) Chemistry of the main-stage ore-forming fluids of the Panasqueira W-Cu (Ag)-Sn deposit, Portugal; implications for models of ore genesis. *Economic Geology* 84:1134-1152.

- Redmond P, Einaudi M, Inan E, Landtwing M, Heinrich C (2004) Copper deposition by fluid cooling in intrusion-centered systems: New insights from the Bingham porphyry ore deposit, Utah. *Geology* 32:217-220.
- Richards JP (2009) Postsubduction porphyry Cu-Au and epithermal Au deposits: Products of remelting of subduction-modified lithosphere. *Geology* 37:247-250.
- Ridley J (2013) *Ore deposit geology*. Cambridge University Press.
- Robb L (2004) *Introduction to ore-forming processes*. Blackwell publishing.
- Roedder E (1984) *Fluid inclusions*. Mineralogical Society of America
- Romer R, Kroner U (2015) Sediment and weathering control on the distribution of Paleozoic magmatic tin–tungsten mineralization. *Mineralium Deposita* 50:327-338.
- Romer RL, Förster H-J, Kroner U, Müller A, Rößler R, Rötzler J, Seltmann R, Wenzel T (2012) Granites of the Erzgebirge - relation of magmatism to the metamorphic and tectonic evolution of the Variscan Orogen. Scientific Technical Report 12/15., GFZ German Research Centre for Geosciences.
- Romer RL, Kroner U (2016) Phanerozoic tin and tungsten mineralization—Tectonic controls on the distribution of enriched protoliths and heat sources for crustal melting. *Gondwana Research* 31:60-95.
- Rötzler K, Plessen B (2010) The Erzgebirge: a pile of ultrahigh-to low-pressure nappes of Early Palaeozoic rocks and their Cadomian basement In: Linnemann U, Romer RL (eds) *Pre-Mesozoic Geology of Saxo-Thuringia—From the Cadomian Active Margin to the Variscan Orogen*. Schweizerbart, Stuttgart, pp 253-270.
- Rub AK, Stemprok M, Rub MG (1998) Tantalum mineralization in the apical part of the Cinovec (Zinnwald) granite stock. *Mineralogy and Petrology* 63:199-222.
- Rusk BG, Reed MH, Dilles JH (2008) Fluid inclusion evidence for magmatic-hydrothermal fluid evolution in the porphyry copper-molybdenum deposit at Butte, Montana. *Economic Geology* 103:307-334.
- Samson I, Anderson A, Marshall DD (2003) *Fluid inclusions: analysis and interpretation*. Mineralogical Association of Canada.
- Schlöglöva K, Wälle M, Heinrich CA (2017) LA-ICP-MS analysis of fluid inclusions: contamination effects challenging micro-analysis of elements close to their detection limit. *J Anal At Spectrom* 32:1052-1063.
- Schmidt C (2018) Formation of hydrothermal tin deposits: Raman spectroscopic evidence for an important role of aqueous Sn (IV) species. *Geochimica et Cosmochimica Acta* 220:499-511.
- Schöpa A, Annen C, Dilles JH, Sparks RSJ, Blundy JD (2017) Magma Emplacement Rates and Porphyry Copper Deposits: Thermal Modeling of the Yerington Batholith, Nevada. *Economic Geology* 112:1653-1672.

- Schuppan W, Hiller A (2012) Die Komplexlagerstätten Tellerhäuser und Hämmerlein. Freiberg.
- Scott S, Driesner T, Weis P (2017) Boiling and condensation of saline geothermal fluids above magmatic intrusions. *Geophysical Research Letters* 44:1696-1705.
- Sebastian U (2013) Die Geologie des Erzgebirges. Springer Spektrum.
- Seifert T, Atanasove P, Gutzmer J, Pfänder J (2011) Mineralogy, geochemistry and age of greisen mineralization in the Li–Rb–Cs–Sn–W deposit Zinnwald, Erzgebirge, Germany. *Mineral Mag* 75:1833.
- Seltmann R (1994) Sub-volcanic minor intrusions in the Altenberg Caldera and their Metallogeny In: Seltmann R, Kämpf H, Möller P (eds) *Metallogeny of collisional Orogens*. Czech Geological Survey, Prague.
- Seo JH, Guillong M, Aerts M, Zajacz Z, Heinrich CA (2011) Microanalysis of S, Cl, and Br in fluid inclusions by LA–ICP–MS. *Chemical Geology* 284:35-44.
- Shapenko VV, Smidel P (1991) Sn and W mineralization in skarn-greisen deposits at the northern margin of the Bohemian massif. *Geokhimiya* 5:724-732.
- Sillitoe RH (1973) The tops and bottoms of porphyry copper deposits. *Economic Geology* 68:799-815.
- Sillitoe RH (2010) Porphyry copper systems. *Economic geology* 105:3-41.
- Simonson J, Palmer DA (1993) Liquid-vapor partitioning of HCl (aq) to 350 C. *Geochimica et Cosmochimica Acta* 57:1-7.
- Steinberger I, Hinks D, Driesner T, Heinrich CA (2013) Source plutons driving porphyry copper ore formation: combining geomagnetic data, thermal constraints, and chemical mass balance to quantify the magma chamber beneath the Bingham Canyon deposit. *Economic Geology* 108:605-624.
- Stemprok M (1965) Petrology and the vertical extent of mineralization in the Cínovec (Zinnwald) granite cupola. *Sbor Geol Věd LG* 5:7-106.
- Stemprok M (1967) Genetische Probleme der Zinn, Wolfram-Vererzung im Erzgebirge. *Mineralium Deposita* 2:102-118.
- Stemprok M, Sulcek Z (1969) Geochemical profile through an ore-bearing Lithium Granite. *Economic Geology* 64:392-404.
- Stemprok M (1971) Petrochemical features of tin-bearing granites in the Krušné Hory Mts., Czechoslovakia. *Soc Mining Geol Japan, Special issue* 2:112-118.
- Stemprok M (1987) Greisenization (a review). *Geologische Rundschau* 76:169-175.
- Stemprok M, Novák JK, David J (1994) The association between granites and tin-tungsten mineralization in the eastern Krušné hory (Erzgebirge), Czech Republic. *Monograph Series on Mineral Deposits* 31:97-129.

Stemprok M, Hulob FV, Novák JK (2003) Multiple magmatic pulses of the Eastern Volcano-Plutonic Complex, Krušné hory/Erzgebirge batholith, and their phosphorus contents. *Journal of Geosciences* 78:277-296.

Stemprok M, Dolejš D, Holub FV (2014) Late Variscan calc-alkaline lamprophyres in the Krupka ore district, Eastern Krušné hory/Erzgebirge: their relationship to Sn-W mineralization. *Journal of Geosciences* 59:41-68.

Sugaki A, Ueno H, Shimada N, Kusachi I, Kitakaze A, Hayashi K, Kojima S, Sanjines O, Sachnes A, Veralde O (1984) Geological study on the polymetallic ore deposits in the Quechisla district, Bolivia. *Sci Rept Tohoku Univ* 3:35-129.

Sugaki A, Kojima S, Shimada N (1988) Fluid inclusion studies of the polymetallic hydrothermal ore deposits in Bolivia. *Mineralium Deposita* 23:9-15.

Tapster S, Condon D, Naden J, Noble S, Petterson M, Roberts N, Saunders A, Smith DJ (2016) Rapid thermal rejuvenation of high-crystallinity magma linked to porphyry copper deposit formation; evidence from the Koloula Porphyry Prospect, Solomon Islands. *Earth and Planetary Science Letters* 442:206-217.

Thomas R, Baumann L (1980) Ergebnisse von thermometrischen und kryometrischen Untersuchungen an Kassiteriten des Erzgebirges. *Zeitschrift für geologische Wissenschaften, Berlin* 10:1281-1299.

Thomas R (1982) Ergebnisse der thermobarogeochemischen Untersuchungen an Flüssigkeitseinschlüssen in Mineralen der postmagmatischen Zinn-Wolfram-Mineralisation des Erzgebirges. *Freiberger Forschungsheft R C C* 370:1-85.

Thomas R, Klemm W (1997) Microthermometric study of silicate melt inclusions in Variscan granites from SE Germany: volatile contents and entrapment conditions. *Journal of Petrology* 38:1753-1765.

Tichomirowa M, Hoffmann M, Schaltegger U, Sergeev S, von Quadt A, Whitehouse M (2016) The older and younger granites from the western Erzgebirge—comparison of different zircon dating methods. *Freib Online Geosci* 46:36-38.

Tischendorf G, Gottesmann B, Foerster H-J, Trumbull RB (1997) On Li-bearing micas: estimating Li from electron microprobe analyses and an improved diagram for graphical representation. *Mineralogical Magazine* 61:809-834.

Treliver Minerals Limited (2015) Press Release Tellerhäuser Project Resource Statement. pp 29.

Vallance J, Cathelineau M, Marignac C, Boiron M-C, Fourcade S, Martineau F, Fabre C (2001) Microfracturing and fluid mixing in granites: W-(Sn) ore deposition at Vaulry (NW French Massif Central). *Tectonophysics* 336:43-61.

Van den Kerkhof AM, Hein UF (2001) Fluid inclusion petrography. *Lithos* 55:27-47.

Von Quadt A, Erni M, Martinek K, Moll M, Peytcheva I, Heinrich CA (2011) Zircon crystallization and the lifetimes of ore-forming magmatic-hydrothermal systems. *Geology* 39:731-734.

- Watanabe K (1987) Inclusions in flux-grown crystals of corundum. *Crystal Research and Technology* 22:345-355.
- Webster J, Thomas R, Förster H-J, Seltmann R, Tappen C (2004) Geochemical evolution of halogen-enriched granite magmas and mineralizing fluids of the Zinnwald tin-tungsten mining district, Erzgebirge, Germany. *Mineralium Deposita* 39:452-472.
- Weis P, Driesner T, Heinrich C (2012) Porphyry-copper ore shells form at stable pressure-temperature fronts within dynamic fluid plumes. *Science* 338:1613-1616.
- Weis P, Driesner T, Coumou D, Geiger S (2014) Hydrothermal, multiphase convection of H₂O-NaCl fluids from ambient to magmatic temperatures: a new numerical scheme and benchmarks for code comparison. *Geofluids* 14:347-371.
- Weis P (2015) The dynamic interplay between saline fluid flow and rock permeability in magmatic-hydrothermal systems. *Geofluids* 15:350-371.
- Wilkinson BH, Kesler SE (2009) Quantitative identification of metallogenic epochs and provinces: Application to Phanerozoic porphyry copper deposits. *Economic Geology* 104:607-622.
- Wilkinson JJ (2001) Fluid inclusions in hydrothermal ore deposits. *Lithos* 55:229-272.
- Wilkinson JJ (2013) Triggers for the formation of porphyry ore deposits in magmatic arcs. *Nature Geoscience* 6:917.
- Xue C, Chi G, Chen Y, Zeng R, Gao Y, Qing H (2007) The fluid dynamic process of large-scale mineralization in the Lanping Basin, Yunnan, SW China: evidence from fluid inclusions and basin fluid modeling. *Earth Science Frontiers* 14:147-155.
- Yardley BW (2005) 100th Anniversary Special Paper: metal concentrations in crustal fluids and their relationship to ore formation. *Economic Geology* 100:613-632.
- Zimák J (1999) Application of chlorite compositional geothermometres to hydrothermal veins in the Variscan flysch sequences of the Nížký Jeseník Upland, to Alpine-type veins in the Sobotín region, and to the paragenesis with “strigovite” from Žulová massif and Strzegom-Sobótka massif. *AUPO, Fac Rer Nat, Geologica* 36:69-74.

Appendices

Data Zinnwald

The fluid inclusion of the Zinnwald samples can be found on the attached CD. The file comprises the salinity, homogenization temperature, the trace element data and additional statistical analysis.

Data Hämmerlein

The fluid inclusion of the Hämmerlein samples and the microprobe data of chlorite can be found on the attached CD. The fluid inclusion file comprises the salinity, homogenization temperature as well as the trace element data.

Curriculum Vitae

Maximilian Korges

Address: GFZ German Research Centre for Geosciences
Inorganic and Isotope Geochemistry
Telegrafenberg
14473 Potsdam - Germany
Tel: +49 331 288 27504
E-Mail: maximilian.korges@gfz-potsdam.de

Academic Education

- 06/2015 – 06/2019 *Ph.D. in Earth Sciences*
Helmholtz Centre Potsdam GFZ – German Research Centre for Geosciences
- Coursework: Ore geology, Geochemistry, Numerical Modeling
 - PhD thesis: “Constraining the hydrology of intrusion-related ore deposits with fluid inclusions and numerical modeling”
- 10/2012 – 02/2015 *Master of Science in Applied Geosciences*
Martin-Luther-University Halle-Wittenberg, Germany
- Coursework: Ore geology, Geochemistry, Mineralogy, Hydrogeology
 - Master thesis: “Supergene mobilization and redistribution of platinum-group elements in the Merensky Reef, Eastern Bushveld Complex, South Africa”
- 10/2009 – 08/2012 *Bachelor of Science in Applied Geosciences*
Martin-Luther-University Halle-Wittenberg, Germany
- Coursework: Ore geology, Environmental geology, Mineralogy, Hydrogeology, Geochemistry, Geodynamic
 - Bachelor thesis: “Characterization of the opaque minerals in the Saxon Saale, the Haselbach, the Großen Bach and the Radau in regard of their possible PGM contents”

Practical Experience

- 06/2015 – 05/2019 *Research Assistant*
Helmholtz Centre Potsdam GFZ – German Research Centre for Geosciences
- Sampling and analysis of the fluid inclusion content of Sn (-W) deposits in Germany and Portugal
 - Developed and implemented new functionalities for numerical simulations
 - Simulations of porphyry copper deposits
 - Publishing in peer-reviewed scientific journals
 - Teaching assistant at the University of Potsdam, Germany
 - Attendance at national and international conferences

- 08/2013 – 09/2014 *Student Research Assistant*
 Martin-Luther-University Halle-Wittenberg, Germany
- Analysis of PGM content in supergene ores of the Bushveld Complex
 - Sampling, core logging, ore microscopy, mineralogical and chemical analysis
 - Final project report
- 8/2011 – 9/2011 *Student Research Assistant*
 Federal Institute for Geosciences and Natural Resources (BGR), Germany
- Ore microscopy and chemical analysis of PGM
 - Final report: “Distribution of platinum-group elements and minerals in the UG-2 Reef, Farm Hoepakrantz, Eastern Bushveld Complex, South Africa“

Further Professional Experience

- Petrology and petrography of ore deposits (microscopy, ore microscopy, REM, EPMA)
- Fluid inclusions analysis (microthermometry, LA-ICP-MS)
- Experience in C++ programming
- Modeling software: CSMP++, Feflow, Modflow, PhreeqC, Hydrotherm
- Visualization software : ArcGis, IOGas, ParaView, QuantumGis, R geochemical software, Rhino, Surfer 10, Sills, X'Pert High Score Plus
- Further software: Adobe Illustrator, Corel Draw, Microsoft Office
- Field work and mapping experience: Germany, Southern Sweden, South Africa, Central Portugal

Publications and Conference Contributions

Published:

Korges, M.; Weis, P.; Lüders, V.; Laurent, O. (2018): Depressurization and boiling of a single magmatic fluid as a mechanism for tin-tungsten deposit formation. *Geology* 46:75-78.

Submitted (currently in Revision):

Korges, M.; Weis, P.; Lüders, V.; Laurent, O. (2019): Skarn-hosted Sn mineralization by unusually hot brines: insights from fluid inclusions in ore and gangue minerals from the polymetallic Hämmerlein deposit, Erzgebirge, Germany. *Mineralium Deposita*

In preparation:

Korges, M.; Weis, P.; Andersen, C. (2019): Incremental magma growth and its significance for the copper precipitation in porphyry Cu deposits. *Earth and Planetary Science Letters*

Conferences:

Korges, M.; Weis, P.; Lüders, V.; Laurent, O. (2018): Hydrothermal evolution of a Sn deposit in the Erzgebirge – insights from fluid inclusions in ore and gangue minerals. *GeoBonn (Germany)*

Korges, M.; Weis, P.; Lüders, V.; Laurent, O. (2018): Phase separation of a single magmatic fluid as a mechanism for the formation of tin-tungsten deposits (Poster). *Gordon Research Conference (USA)*

Korges, M.; Weis, P.; Lüders, V.; Laurent, O. (2017): Fluid evolution and ore formation in the Zinnwald Sn-W-Li deposit, Erzgebirge (Germany): insights from microthermometry and LA-ICP-MS of fluid inclusions. *GeoBremen (Germany)*

- Korges, M.**; Weis, P.; Lüders, V.; Laurent, O. (2017): Fluid evolution of the Zinnwald Sn-W-Li deposit, Erzgebirge: insights from fluid inclusions. Goldschmidt Conference (Paris, France)
- Korges, M.**; Weis, P.; Lüders, V.; Laurent, O. (2017): The magmatic-hydrothermal evolution of the ore-forming fluids of the Zinnwald Sn-W-Li deposit, Germany. Ecrofi (Nancy, France)
- Korges, M.**; Oberthür, T. & Borg, G. (2014): Re-distribution of Platinum-Group Elements during oxidation of the Merensky Reef, Eastern Bushveld Complex, South Africa. 12th International Platinum Symposium (Yekaterinburg, Russia).

Participated Short Courses

- | | |
|---------|--|
| 02/2017 | Fluid and Melt Inclusions Course (ETH Zürich) |
| 03/2016 | Fluid Inclusions- Critical Review, Applications, Computer Modeling (Montanuniversität Leoben) |
| 09/2015 | Process modeling of hydrothermal systems (GFZ Potsdam) |
| 09/2015 | Data – Research, Re-use, Publication, Sharing, Repository and Metadata (GFZ Potsdam) |
| 11/2013 | Possibilities and boundaries of hydrogeochemical modeling of hydrothermal and geothermal processes with PhreeqC (Martin-Luther-University Halle) |
| 05/2012 | GIS in practice (Martin-Luther-University Halle) |